Universidade de Aveiro Departamento de Física,
2010

Berta Maria Barbosa Neto

Técnicas alternativas para amplificação de Raman em telecomunicações

Universidade de Aveiro Departamento de Física,
2010

Berta Maria Barbosa Neto

Técnicas alternativas para amplificação de Raman em telecomunicações

"Sometimes, the reflection is far more present than the thing being reflected."

— Jim Jarsmusch
in The Limits of Control

Berta Maria Barbosa Neto

Técnicas alternativas para amplificação de Raman em telecomunicações

Dissertação apresentada à Universidade de Aveiro para cumprimento dos requesitos necessários à obtenção do grau de Doutor em Física, realizada sob a orientação científica de Paulo Sérgio de Brito André, Investigador auxiliar do Instituto de Telecomunicações (IT) e Professor auxiliar do Departamento de Física da Universidade de Aveiro .

Apoio financeiro da FCT e do FSE no âmbito do VI Quadro Comunitário de Apoio

o júri / the jury

presidente / president

Doutor João Manuel Nunes Torrão
Professor Catedrático da Universidade de Aveiro (por delegação da Reitora da Universidade de Aveiro)

vogais / examiners committee

Doutor João de Lemos Pinto
Professor Catedrático da Universidade de Aveiro

Doutor José Luís Campos de Oliveira Santos
Professor Professor Associado com Agregação da Faculdade de Ciências da Universidade do Porto

Doutor Hypolito José Kalinowsky
Professor Associado da Universidade Tecnológica Federal do Paraná, Brasil

Doutor Henrique José Almeida Silva
Professor Associado da Universidade de Coimbra

Doutor António Luís Jesus Teixeira
Professor Associado da Universidade de Aveiro

Doutor Paulo Sérgio de Brito André
Investigador auxiliar do Instituto de Telecomunicações (IT) e Professor Auxiliar da Universidade de Aveiro e (orientador)

agradecimentos

O trabalho desenvolvido no âmbito desta tese contou, felizmente, com as contribuições de pessoas e instituições , pelo que quero expressar a todos os meus mais sinceros agradecimentos.

Ao Doutor Paulo André, pela atitude diligente com que orientou esta tese, nomeadamente o apoio prestado em todas as fases do trabalho, a disponibilidade para esclarecimento de dúvidas, alguma liberdade de ação que muito contribuiu para o meu desenvolvimento pessoal, e finalmente o apoio na revisão dos vários capítulos desta tese.

À Fundação para a Ciência e Tecnologia (FCT) pelo suporte específico dado a este trabalho através da bolsa (SFRH/BD/28904/2006) e pelo financiamento providenciado através dos projectos ARPA (POSC/EEA-CPS/55781/2004), TECLAR (POSI/V.5/A0072/2005) e FEFOF (PTDC/EEA-TEL/72025/2006).

Ao Instituto de Telecomunicações (IT) por ter disponibilizado os recursos materiais que permitiram a realização desta dissertação.

Ao National Intitute of Information and Communications Technology (NICT), Tóquio, Japão, pelo acolhimento e disponibilização de recusos labororatoriais de topo no âmbito de um estágio de curta duração, ao Doutor Hideaki Furakawa pelo acompanhamento experimental e ao Doutor Nayoa Wada pela sua atenta supervisão.

Aos Doutores António Teixeira, Rogério Nogueira e Natasa Pavlovich, investigadores do IT e da Nokia Siemens Networks, pela pela interação, aprendizagem, por muitas e úteis informações que me ajudaram a perspectivar outros pontos de vista sobre o meu trabalho e pelos constantes incentivos e amizade.

Ao Mestre Claunir Pavan pela imprescindível ajuda e apoio com a edição da tese. Aos Mestres Ana Rocha, Donato Sperti, Cláudia Reis, Rogério Dionísio, Jacklyn Reis, Rui Morais, João Ferreira, Albano Baptista e Rodolfo Andrade, Engs. Pedro Teixeira, João Andrade, Andreas Klingler e José Pedro Girão, agradeço a colaboração no trabalho experimental e outras aprendizagens paralelas aos trabalhos desta tese.

Finalmente, aos meus colegas do grupo de comunicações óticas, pelo companheirismo e boa disposição com que engrandeceram o meu dia-a-dia.

Palavras Chave

Redes de acesso, amplificadores de Raman em fibra ótica, otimização do ganho, redes óticas de rajadas/pacotes, efeitos transitórios

Resumo

O presente trabalho centra-se no estudo dos amplificadores de Raman em fibra ótica e suas aplicações em sistemas modernos de comunicações óticas. Abordaram-se tópicos específicos como a simulação espacial do amplificador de Raman, a equalização e alargamento do ganho, o uso de abordagens híbridas de amplificação através da associação de amplificadores de Raman em fibra ótica com amplificadores de fibra dopada com Érbio (EDFA) e os efeitos transitórios no ganho dos amplificadores. As actividades realizadas basearam-se em modelos teóricos, sendo os resultados validados experimentalmente.

De entre as contribuições mais importantes desta tese, destaca-se (i) o desenvolvimento de um simulador eficiente para amplificadores de Raman que suporta arquitecturas de bombeamento contraprogantes e bidirecionais num contexto com multiplexagem no comprimento de onda (WDM); (ii) a implementação de um algoritmo de alocação de sinais de bombeamento usando a combinação do algoritmo genético com o método de Nelder-Mead; (iii) a apreciação de soluções de amplificação híbridas por associação dos amplificadores de Raman com EDFA em cenários de redes óticas passivas, nomeadamente WDM/TDM-PON com extensão a região espectral C+L; e (iv) a avaliação e caracterização de fenómenos transitórios em amplificadores para tráfego em rajadas/pacotes óticos e consequente desenvolvimento de soluções de mitigação baseadas em técnicas de clamping ótico.

Key words

Optical access networks, Raman fiber amplifiers, gain optimization, optical burst/packet switching networks, transient effect in optical amplifiers.

Abstract

The present work is based on Raman Fiber Amplifiers and their applications in modern fiber communication systems. Specific topics were approached, namely the spatial simulation of Raman fiber amplifiers, the gain enlargement and equalization the use of hybrid amplification approaches by association of Raman amplifiers with Erbium doped fiber amplifiers (EDFA) and the transient effect on optical amplifiers gain. The work is based on theoretical models, being the obtained results validated experimentally.

Among the main contributions, we remark: (i) the development of an efficient simulator for Raman fiber amplifiers that supports backward and bidirectional pumping architectures in a wavelength division multiplexing (WDM) context; (ii) the implementation of an algorithm to obtain enlargement and equalization of gain by allocation of pumps based on the association of the genetic algorithm with the Nelder-Mead method; (iii) the assessment of hybrid amplification solutions using Raman amplifiers and EDFA in the context of passive optical networks, namely WDM/TDM-PON with extension the C+L spectral bands; (iv) the assessment and characterization of transient effects on optical amplifiers with bursty/packeted traffic and the development of mitigation solutions based on optical clamping.

Contents

List of Acronyms

Notation	Description
APA	Average Power Analysis.
ASE	Amplifier Spontaneous Emission.
ATM	Asynchronous Transfer Mode.
AWG	Arrayed-Waveguide Grating.
BERT	Bit Error Rate Tester.
BPON	Broadband PON.
BVP	Boundary Value Problem.
CapEx	Capital Expenditures.
CO	Central Office.
CW	Continuous Wave.
CWDM	Coarse Wavelength Division Multiplexing.
DCF	Dispersion Compensating Fiber.
DFB	Distributed Feed-Back.
DS	Down-Stream.
DSF	Dispersion Shifted Fiber.
DWDM	Dense Wavelength Division Multiplexing.
EDF	Erbium Doped Fiber.
EDFA	Erbium Doped Fiber Amplifier.
EPON	Ethernet PON.
FBG	Fiber Bragg Grating.
FTTH/P	Fiber-to-the-Home/Premise.
FWM	Four-wave Mixing.
GA	Genetic Algorithm.
GPON	Gigabit PON.

Notation	Description
IP	Internet Protocol.
IVP	Initial Value Problem.
MPI	Multi Path interference.
MZI	Mach-Zehnder Interferometer.
ODE	Ordinary Differential equation.
OLT	Optical Line Terminal.
ONU	Optical Network Unit.
OpEx	Operational Expenditures.
OSNR	Optical Signal to Noise Ratio.
PON	Passive Optical Network.
PRBS	Pseudo Random Bit Sequence.
QoS	Quality-of-Service.
RFA	Raman Fiber Amplifier.
RN	Remote Node.
SARDANA	Scalable Advanced Ring-based passive Dense Access Network Architecture.
SOA	Semiconductor Optical Amplifier.
SRS	Stimulated Raman Scattering.
SSMF	Standard Single Mode Fiber.
TDM-PON	Time Division Multiplexing - Passive Optical Network.
US	Up-Stream.
VOA	Variable Optical Attenuator.
WDM	Wavelength Division Multiplexing.
WDM-PON	Wavelength Division Multiplexing - Passive Optical Network.
WDM/TDM-PON	Wavelength Division Multiplexing/Time Division Multiplexing - Passive Optical Network.

Notation	**Description**
YDFA	Ytterbium Doped Fiber Amplifier.

List of Symbols

Symbol	Description
h	Planck Constant.
c	Speed of the light in vaccum.
k_B	Boltzmann Constant.
P_P	Pump power.
P_s	Data signal power.
P_{ASE}	Amplified spontaneous emission power.
P_{SRB}	Single Rayleigh backscattering power.
P_{DRB}	Double Rayleigh backscattering power.
α_p	Fiber attenuation at the pump wavelength.
α_s	Fiber attenuation at the data signal wavelength.
g_R	Raman gain efficiency.
γ_R	Raman gain coefficient.
T_R	Raman time constant.
L_{eff}	Effective length.
$G_{on/off}$	On/off gain.
G_{net}	Net gain.
n_s	data signal number of photons.
n_p	pump number of photons.
T	Absolute temperature.
$\eta(T)$	Phonon occupancy factor.
NF	Noise figure.
NF_{eff}	Effective noise figure.
RIN	Relative intensity noise.
V	Group velocity.
J	Jacobi matrix.
n	Refractive index.
n_2	Nonlinear refractive index.
$\chi^{(3)}$	Third order nonlinear susceptibility.
τ	Fluorescence lifetime.
D	Relative inversion of population.

Symbol	Description
σ_{12}	Absorption cross section.
σ_{21}	Emission cross section.
S	Active area.
P^{IS}	Intrinsic saturation power.
τ_e	Characteristic decay time.
γ	Saturation factor.

List of Tables

List of Figures

Chapter 1

Introduction

1.1 Background and motivation

The unprecedented popularity of Internet and its derived new services such as video streaming delivery (HDTV, IPTV, etc) and file sharing applications (Peer-to-Peer for example) have pressed out the competition among providers in order to reduce the cost of the transmission systems.

In the 90s, the use of optical amplifiers brought a great development in the simplification of those systems by eliminating expensive and limitative optoelectronic regeneration. Thus substantial improvements have been brougth to transmission systems in terms of cost, flexibility design and capacity. Before them, the standard method to compensate the power loss in optical fiber was to use periodically spaced electronic regenerators along the transmission link.

In those expensive devices, the signal in the optical domain was converted to the electric domain using a photodetector, being processed, amplified and then reinjected into the optical fiber by a transmitter. One advantage of this technology is that the transmission impairments such as noise, dispersion and nonlinearities do not accumulate along the link, being compensated in each node. However, system upgrades, such as bit rates and modulation formats are expensive and difficult to implement because all the regenerators of the link have to be replaced. Besides that, the huge bandwidth of the optical fiber cannot be exploited properly.

The introduction of wavelength division multiplexing (WDM) is of great importance because it enabled the implementation of the actual high capacity optical fiber networks by fully exploiting the fiber bandwidth [1]. WDM exists in several frequency patterns which differ in the spacing of the wavelengths, number of channels, and the optical amplification ability. Conventional WDM systems provide up to 16 channels in the 3^{rd} transmission window (C-Band) of Silica fibers around 1550 nm, while dense wavelength division multiplexing (DWDM) uses the same transmission window but with denser channel spacing. Channel plans vary, but a typical system would use 40 channels at 100 GHz spacing or 80 channels with 50 GHz spacing. Some technologies are capable of 25 GHz spacing (sometimes called ultra dense WDM). These solutions are extensively used in long haul systems, sending as much information as possible. New amplification options (Raman amplification)

enable the extension of the usable wavelengths to the L-band by doubling these numbers [2]. Coarse wavelength division multiplexing (CWDM) uses increased channel spacing to reduce the network cost by the use of less sophisticated transceiver designs. Thus, to provide 16 channels on a standard single mode fiber (SSMF), CWDM uses the entire frequency band between the second and third transmission window (1310/1550 nm respectively) including both windows (minimum dispersion window and minimum attenuation window) but also the critical region where OH absorption may occur [3]. A representation of the ITU wavelength grid is depicted in Figure 1.1.

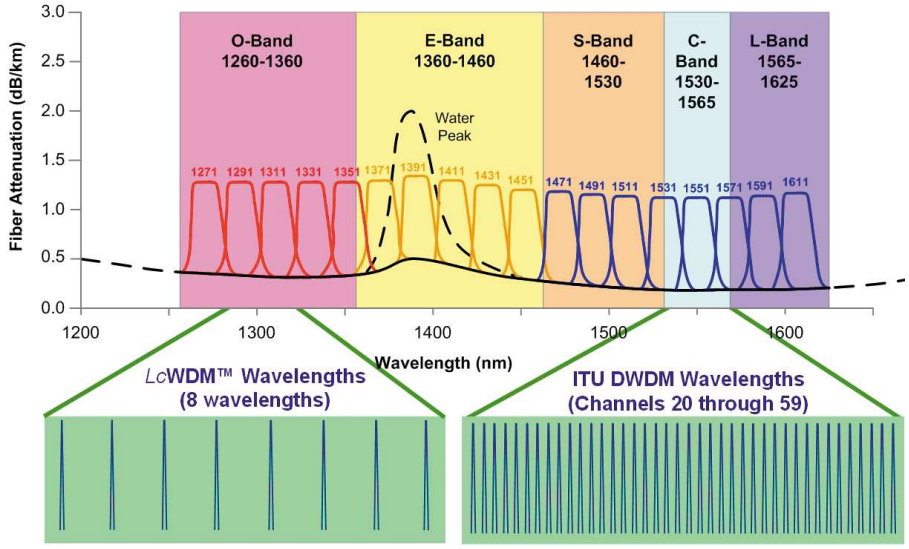

Figure 1.1: Representation of the ITU wavelength grid [4].

CWDM is a good solution whenever less information is transmitted over short distances in a less expensive way than DWDM. Their progressive introduction had become possible with the development of optical amplification, in particular, Erbium doped fiber amplifier (EDFA) which have revolutionized the field of optical communications due to the high deployed gain with relatively low power optical pumps. However, as the channels in CWDM systems are far apart, optical amplification is still a matter of concern because the EDFAs bandwidth ($20 - 40$ nm) cannot support the full band of CWDM channels [5].

Nevertheless, the EDFAs had undergown progressive improvements, and their initial bandwidth was enlarged from the C band to the L band, increasing the capacity of WDM systems. Besides that, new rare-earth fiber amplifiers had been implemented, namely Ytterbium doped fiber amplifier (YDFA), which presents high absorption/emission bands (from 850 nm to 1200 nm) [6]. Ytterbium can also be used together to Erbium as a co-dopant increasing the absorption because they can be pumped eith by the core or by the cladding [7], [8].

However, the EDFA bandwidth and its co-doped derivants was still must lower

than the transmission band of low loss fibers. Furthermore, EDFAs also have other disadvantages, such as the use of a lumped amplification scheme. In this scheme, a span of optical fiber is followed by a span of pumped Erbium doped fiber (EDF) at every 40-50 km. This distance is determined by the span loss and by the limit imposed from the maximum admissible power allowed in the fiber, without inducing nonlinear effects and the minimum acceptable power that avoids a large degradation of the optical signal-to-noise ratio (OSNR). The use of distributed amplification scheme could increase the transmission distance because it allows the the contention of the signal inside the limits imposed by the nonlinearities and of the signal-to-noise-ratio degradation resulting from higher span distances. This advantage of the distributed (Raman) over lumped amplification in containing the signal power is illustrated in Figure 1.2. The distributed amplification scheme can be used to cover very long span links or to increase the distance of ultra-long haul systems.

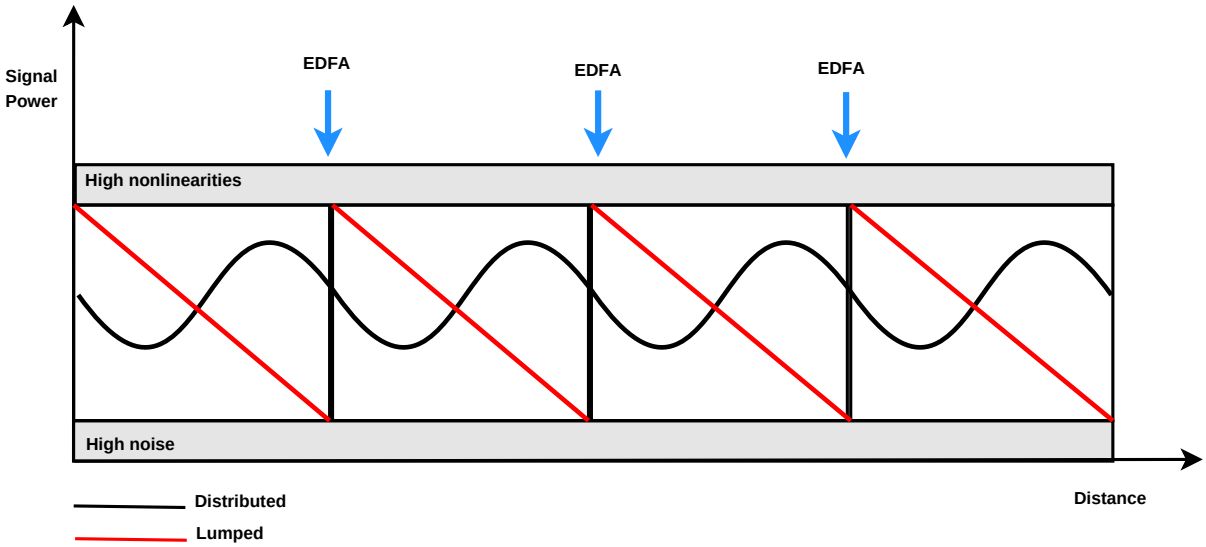

Figure 1.2: Optical signal power evolution in a distributed and in a lumped amplification scheme.

As a consequence, the interest on broad-band distributed amplifiers has been increasing, as depicted in Figure 1.3, where a number of optical amplifiers, (EDFA, Raman and SOA) citations in the IEEE database is plotted from 1975 to the present [9]. On looking at this plot, we notice that there is a research interest on Raman amplification since the 80s of the XX century. However, with the emergence of the EDFA in the 90s, the attention given to Raman amplification had decreased in that period. In the begging of the XXI century, the interest in Raman amplification was renewed, in part because the high power pump become available commercially at a reasonable cost and also because the bandwidth of the EDFA was already fully utilized, enabling the need for more optical channels and wider optical bandwidth.

The research interest in semiconductor optical amplifier (SOA) has also augmented

in last years. Given their relatively broad gain bandwidth, and applicability to all optical communication bands from 1300 through 1600 nm and beyond, SOAs are natural candidates for applications requiring a versatile, inexpensive broad-band amplifier [10], [11]. SOA are also becoming noticed due to other applications, such as optical switchers in optical packet networks [12] or integrated with Mach-Zehnder interferometer (MZI) to provide optical logic XOR gate for several kinds of all-optical device, such as comparators, adders and counters [13].

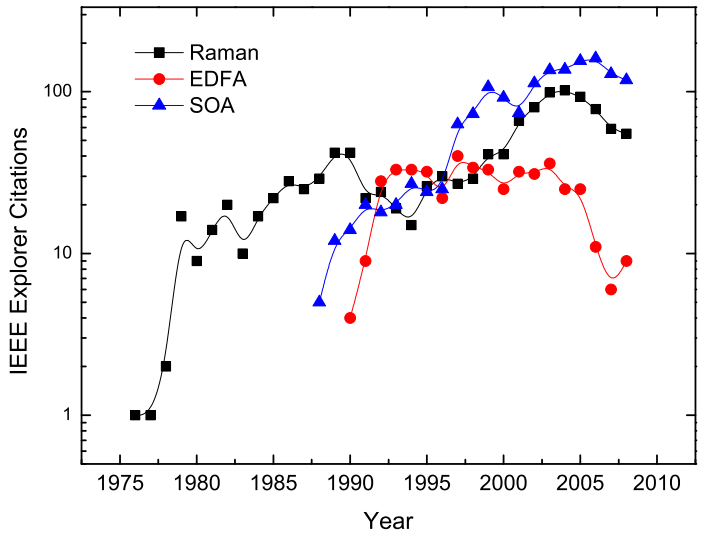

Figure 1.3: Number of citation in the IEEE database of optical amplifiers namely RFA, EDFA and SOA from 1975 to the present. Lines are visual guides for the eyes.

One possible solution for a near future amplification solution could rely on Raman fiber amplifiers, because they present flexible transmission band given the pumps frequencies. This behaviour is actually different from the rare-earth doped fiber amplifiers that depend on the energy bands of the dopants. Another benefit is that the transmission medium is also the gain medium (the amplification scheme is distributed not lumped). Hence, it allows the contention of the signal inside the limits imposed by the nonlinearities and by the OSNR degradation resulting from higher span distances. It must be stessed out that the distributed amplification scheme can be used to cover very long span links or to increase the distance of ultra-long haul systems. Besides the above mentioned merits, others advantages can be accounted for [14], [15], [16]:

- the gain depends only on the frequency separation between pump and signal and not absolute frequencies. Therefore, it is possible to obtain gain at any wavelength by choosing properly the pump frequency. The addition of

more pumping lasers enlarges the gain bandwidth necessary for broadband applications.

- the gain does not depend on the relative direction of propagation of a pump and signal.
- the noise performance is very good when compared to EDFA.
- the gain transience with burst traffic is negligible.

Besides that, Raman amplifiers have the merit of arbitrary gain band. The technique to shape the gain profile over a wide bandwidth is quite simple because it deals only with the optimization of pumping parameters, initial powers and wavelengths.

High bitrate optical networks with burst traffic are expected to be the next generation of photonic transmission systems. Optical burst switching (OBS) has been proposed as a technique to overcome issues related to WDM deployment, like lack of fine granularity in wavelength routing and electronic speed bottleneck in SONET/SDH. In these networks the traffic is, in a certain scale, uniform, due to the use of the protocol coding, which restricts the number of adjacent zero binary bits. However, the future optical networks can have packet traffic directly over the optical channels, imposing a lack of optical signal for a large period of time. This will lead to possible gain transients on the optical amplifiers. In fact one of the constrains for burst traffic in fiber networks arises from optical amplification, where the Erbium Dopped fiber amplifiers (EDFAs) present some limitations, ensuing from their long carrier lifetime [17]. The key point is, in fact, to enhance WDM technologies so that higher bit-rates per channel OBS traffic can be transmitted, moving them from the transport segment up to the Metro and Access segment [10]. It was unavoidable that the pursuit of such improvements in WDM technologies would narrow the margins of system design. For this reason, researchers have begun seeking alternative enabling technologies capable of mitigating system impairments, such as noise, transients, non-linear effects and handling wider bandwidths [1]. Raman amplification can be pointed out as a potential solution for the amplification of burst optical networks. Potentially, Raman amplifiers can overcome the EDFAs performance.

1.2 Raman amplification - state of the art

The fundamentals of Raman scattering was established on 1928 [18] but their application as optical amplifiers was only proposed in the 70s and 80s of the XX century [19], [20], with the discovery of stimulated Raman scattering (SRS) in 1962 [21]. Yet, since those initial amplifiers were not very competitive due to the

cost and lack of reliability of the needed high power pumping lasers, they had remained underestimated, especially after the invention of the EDFA. However, recent developments in the field of high power lasers had enabled the emergence of affordable devices and as a consequence, the interest on Raman fiber amplifier (RFA) was renewed [22].

Raman fiber amplifiers are based on the power transfer from pump(s) signal(s) to information carrying signals (usually described as probes) due to SRS which occurs when there is sufficient pump power within the fiber. Since the gain peak of this amplification is obtained for signals downshifted approximately by 13.2 THz (for Silica), relative to the pump signal frequency, to achieve gain at any wavelength we need to select a pump signal whose frequency complies with this relation. In this way, it is possible to optimize the number of pumps to obtain a wide and flat gain [23], [24], [25]. However, it is necessary to bear in mind that due to the pump-to-pump interaction, the shorter wavelength pumps demand more power to be effective [26], [27].

From a telecommunications point of view, the pump signals wavelengths must be placed around 1450 nm because the probe signal wavelengths used on the so called 3^{rd} transmission window are centered around 1550 nm and the maximum gain occurs for a Stokes frequency shift of 13.2 THz. Typically a high power laser for Raman amplification, provide an optical power of 300 mW, launched over an optical fiber, which for a SSMF is equivalent to a power density of $3.75\ GW/m^2$. This high power injected in to the fiber, especially when multi-pump lasers are utilized, imposes new concerns in terms of safety. One of the problems arising from the high powers is the fiber fuse effect, named due to the similarity with a burning fuse. This phenomenon can lead to the destruction of the optical fibers along kilometers. The fiber fuse is initiated by a local heating of an optical fiber, causing a strong light absorption that increases the temperature up to the Silica vaporization value. In this high temperature region the core of the fiber vaporizes emitting a visible radiation. Due to the heating transmitted to the neighboring regions the process propagates towards the high-power light sources [28], [29].

In terms of implemented systems, several architectures have been proposed, based in all Raman or hybrid Raman/EDFA amplification [30]. The use of bidirectional Raman amplification has also been reported for long reach access networks. Experimental results have shown the feasibility of systems with symmetric up-and-downstream signals with bitrates up to 10 Gb/s, supported by distributed Raman amplification over 80 km of fiber [31]. Field transmission experiments have been reported with 8×170 Gb/s over 210 km of single mode standard fiber, achieving spectral efficiency of 0.53 bit/s/Hz [32].

As said previously, RFA provide the feasibility of wide and flat spectral gain profiles with the combination of several pumping lasers operating at specific powers

and wavelengths. The composite amplification is determined from the mutual interactions among the pump and signal wavelengths. Gain spectra as large as 100 nm were obtained using multiple pumps. Emori *et al* [33] have presented an experimental Raman amplifier with a 100 nm bandwidth using a WDM laser diode unit with 12 wavelengths ranging from 1405 to 1510 nm, whose maximum total power was equal to 2.2 W. By this way, a gain equal to 2 dB is obtained over a 25 km SSMF link and a 6.5 dB gain using a 25 km dispersion shifted fiber (DSF) link, both with 0.5 dB of maximum ripple. Kidorf *et al* [26] provided a mathematical model to implement a 100 nm Raman amplifier using low power pumps with maximum power of each pump equal to 130 mW. They used 8 pumps from 1416 nm to 1502 nm along 45 km of SSMF, obtaining a gain around 4 dB with a maximum ripple equal to 1.1 dB.

Enlargement of the bandwidth of Raman amplifiers is also achieved using incoherent pumping instead of multi-pump schemes [34], [35], [36]. Vakhshoori *et al* proposed a high-power incoherent semiconductor pump prototype, that use a low-power seed optical signal, coupled into a long-cavity semiconductor amplifier, has achieved 400 mW of optical power over a 35 nm spectral window [37]. A 50 nm bandwidth amplifier was obtained with an on/off gain equal to 7 dB. It was also demonstrated that the use of six coherent pumps is less efficient, in terms of flatness, than the use of two incoherent pumps [4]. The signal wavelengths were comprised between 1530 nm and 1605 nm and the transmission occurs over 100 km of optical fiber. Another advantage of using incoherent pumping is the reducing of nonlinear effects, such as Brillouin scattering, four-wave mixing (FWM) induced by pump-pump, pump-signal and pump-noise interactions [38].

The growing maturity of high pump module technologies is providing competitive solutions based on Raman amplification and currently many alternative techniques are being developed to overcome the ordinary one pump and dual pumping methods [39]. In particular, two major techniques are highlighted. First, the use of low power pumping lasers provides gain comparable to the ordinary one pump Raman amplification. This technique is especially interesting for combining commercial and low cost lasers [40]. The second particular technique corresponds to an evolution of the cascaded Raman amplification. Actually, a sixth order cascade Raman amplifier was recently proposed [41]. In the cascade Raman amplification, the pump power is downshifted in frequency by using a pair of fiber Bragg gratings (FBGs) placed in spectral positions multiples of 13 THz, from the pump frequency. In a particular case, the generation of the fiber pump laser is obtained by using only one passive reflector element and distributed reflectors over the long optical fiber, establish by a nonlinear fiber intrinsic effect called Rayleigh backscattering.

1.3 Objectives and thesis organization

The goal of this thesis is to study the RFA in the scope of modern optical communication systems, accounting for their principal challenges [42]. Specific topics such as, the development of an efficient simulator for Raman amplified links, the gain enlargement and equalization, hybrid Raman/EDFA schemes and the effect of transients are important and thus addressed both theoretically and experimentally.

The work reported here was mainly performed in the facilities of the Instituto de Telecomunicações (IT) in Aveiro and had the advantage of being framed by both portuguese (TECLAR, ARPA, FEFOF, TOMAR-PON) and European projects (BONE, SARDANA and EURO-Fos). A short period training in the National Intitute of Information and Communications Technology (NICT) sitted in Tokyo, Japan, supervised by Professor Nayoa Wada, enabled the access to top laboratorial facilities and the accompliment of important work.

This thesis is organized in six chapters, in which several aspects of Raman amplification in telecommunications are studied.

Chapter 1 provides a background and a motivation for this work and an overview of Raman amplification within the frame of optical communications systems. Raman amplification principles of operation are introduced, being their pros and cons discussed. The most relevant challenges relating this topic are presented as well as state of the art work. Chapter 1 also presents a summary of results provided by a list of published work.

Chapter 2 presents the Raman amplification theory, namely SRS. A mathematical model for propagation in optical fibers is then introduced and the relevance of pumping shemes in optical communications analyzed. Since the computation of solutions is a cumbersone task, a relevant approximation, small-signal approximation, is presented, and its most important results discussed. The effect outside the approximation, pump depletion, is also discussed. An analysis of the noise behaviour of RFA is also presented, being their implications for communications systems discussed.

Chapter 3 is focused on modeling of RFA. Hence, a general mathematical model for multi-pump, multi-signal given by a system of nonlinear ordinary differential equation (ODE) is presented. Possible methodologies to solve the equations are presented and discussed. The latter, can be either numerical (shooting, collocation, etc) or semi-analytical. The use of average power analysis (APA) is introduced and their improvements in terms of accuracy and efficiency discussed. Other qualitative analytical approaches, such as the linearization in the vicinity of critical points or Lyapunov-second methods are also analyzed and applied to the problem of RFA.

Chapter 4 is devoted to the topic of gain enlargement and optimization by allocation of pumps, which is a very important application of RFA. A method based

on an hybrid Genetic Algorithm is introduced. This method uses a combination of an heuristic, GA, with a local search, Nelder-Mead. It is demonstrated that the proper configuration of this method allows a improvement of a factor of 2 in its efficiency. An experimental validation of the gain optimization and gain enlargement is also provided.

Chapter 5 regards the practical application of optical amplifiers in access networks. The work presented is mainly focused on amplifiers transients, RFA and EDFA, in the scope of optical bursty/packeted traffic. The latter were demonstrated to be more penalizing for EDFA, and experimental characterizations were carried on to assess the decays times. Two mitigation solutions based on optical gain clamping are proposed, one based on a feed-back ring and another based on enhanced bidirectional clamping with FBG. Their efficiency for WDM/TDM-PON is also discussed. This chapter also addresses the topic of hybrid Raman/EDFA amplification, namely for C+L band. Some practical situation are assessed, namely WDM ring in rural scenarios. The feasibility of this amplification schemes for normal and resilient modes is also discussed.

This thesis ends with chapter 6 where the main conclusions are summarized and directions for future work are pointed out.

1.4 Summary of results

The most important results accomplished from this thesis are:

- The development of an efficient and accurate simulator for Raman fiber amplifiers using average power analysis and its experimental validation .
- The implementation of a pump allocation algorithm for gain equalization using a combination of genetic algorithm and Nelder Mead method and its experimental validation.
- The assessment of extended and equalized gain in C+L transmission bands using hybrid Raman/EDFA for WDM/TDM PON solutions in rural scenarios.
- The assessment and charaterization of transients, Raman and EDFA and the combination of both in networks with bursty traffic.
- The implementation of mitigation solutions for EDFA transients based on optical gain clamping, suitable for metro and access networks.
- The evaluation of the above mentioned effect of transmission systems at 10 Gb/s.

The work accomplished within the period of this thesis resulted in 10 published papers in journals and another under peer revision, 26 conference proceedings and

also a chapter in a book. The work has also originated colaborations within other researchers in the optical communications group, which were also published. The publication are listed bellow .

1.4.1 List of publications

Chapters in books

1. J. Schlesinger, *Optical Fibers Research Advances*. Nova Science Pub Inc, 2007.

Papers in journals

1. **B. Neto**, A. Teixeira, N. Wada, and P. André, "Efficient use of hybrid genetic algorithms in the gain optimization of distributed raman amplifiers," *Optics Express*, vol. 15, no. 26, pp. 17 520–17 528, 2007.

2. D. Sperti, P. André, **B. Neto**, A. Rocha, A. Bononi, F. da Rocha, and M. Facão, "Experimental assessment of some Raman fiber amplifiers solutions for coarse wavelength division multiplexing applications," *Photonic Network Communications*, vol. 16, no. 3, pp. 195–202, 2008.

3. A. Rocha, **B. Neto**, M. Facao, and P. Andre, "Study of raman amplification with low cost incoherent pumps," *Microwave and Optical Technology Letters*, vol. 50, no. 2, pp. 301–303, 2008.

4. P. André, **B. Neto**, A. Teixeira, and N. Wada, "Raman amplification impact in packet base networks," *Microwave and Optical Technology Letters*, vol. 50, no. 12, pp. 3083–3085, 2008.

5. A. Rocha, **B. Neto**, M. Facao, and P. Andre, "Low cost incoherent pump solution for Raman fiber amplifier," *Optica Applicata*, vol. 39, no. 2, pp. 287–293, 2009.

6. J. Reis, **B. Neto**, P. André, and A. Teixeira, "WDM ring performance improvement by means of four-wave mixing crosstalk minimization algorithm," *Microwave and Optical Technology Letters*, vol. 51, no. 8, pp. 1949–1952, 2009.

7. **B. Neto**, J. Ferreira, N. Wada, A. Pinto, and P. André, "Evaluation of the effect of channel add/drop impact on power transients on the performance of a 10-GB/S DWDM transmission system with hybrid EDFA/Raman amplification,"*Microwave and Optical Technology Letters*, vol. 52, no. 6, pp.1225–1228, 2010.

8. M. T. M. R. Giraldi, A. M. Rocha, **B. Neto**, C. Correira, M. E. V. Segatto, M. J. Pontes, A. P. L. Barbero, J. C. W. Costa, M. A. G. Martinez, O. Frazão,

J. M. Baptista, H. M. Salgado, B. M. Marques, A. L. J. Teixeira, P. S. André, "Rayleigh assisted Brillouin effects in distributed Raman amplifiers under saturated conditions at 40 Gb/s,*Microwave and Optical Technology Letters*, vol. 52, no. 6, pp.1331–1335, 2010.

9. C. Reis, A. Maziotis, C. Kouloumentas, C. Stamatiadis, M. Bougioukos, N. Calabretta, P. Andre, R. Dionisio, **B. Neto**, H. Dorren, H. Avramopoulos, and A. Teixeira, "All optical synchronous SR flip-flop based on active interferometric devices", *Electronics Letters*, vol. 46, no. 10, pp. 709 –710, May 2010.

10. **B. Neto**, C. Reis, R. P. Dionísio, J. M. Ferreira, J. A. Lazaro, G. Tosi-Beleffi, A. N. Pinto, R. Nogueira, A. Teixeira, J. Prat, P. S. André "Assessment and mitigation of EDFA gain transients in hybrid WDM/TDM PON in the presence of packet based traffic, *Optoelectronics, IET*, to be published, 2010.

11. **B. Neto**, A. Klingler, C. Reis, R. P. Dionísio, R. N. Nogueira, A. Teixeira, P. S. André "Enhanced optical gain clamping for upstream packet based traffic on hybrid WDM/TDM-PON using Fiber Bragg Grating, *Journal of Optical Communications and Networking, OSA*, submitted, July 2010.

Papers in conference proceedings

1. P. Andre, A. Pinto, A. Teixeira, **B. Neto**, S. Junior, D. Sperti, F. da Rocha, M. Bernardo, M. Fujiwara, A. Rocha, and M. Facao, "Raman amplification using incoherent pump sources," in *Transparent Optical Networks, 2007. ICTON '07. 9th International Conference on*, vol. 1, July 2007, pp. 136–139.

2. P. André, A. Rocha, **B. Neto**, and M. Facão, "Improvement of Raman Amplification Gain Tilt Using Incoherent Pump Sources," *Laser Science*, 2007.

3. A. Teixeira, P. Teixeira, **B. Neto**, R. Nogueira, and P. Andre, "Automatic apodization profiling of super structured fiber Bragg gratings for OCDMA coding applications," in *Optical Fiber Conference OFC'08*, February 2008, pp. JThA29.

4. P. Teixeira, **B. Neto**, R. Nogueira, P. Andre, and A. Teixeira, "Code cardinality maximization using highly reflective SSFBG with optimum apodization profiles," in *10th Anniversary International Conference on Transparent Optical Networks, 2008. ICTON 2008*, 2008, pp. 55–57.

5. C. Reis, A. M. Rocha, **B. Neto**, N. Wada, P. Andre, "Raman amplification in high 10 Gbit/s and 40 Gbit/s packet optical networks," in *Mediterranean Winter, 2008. ICTON-MW 2008. 2nd ICTON.*, 11-13, pp. 1 –4.

6. J. Andrade, **B. Neto**, A. Rocha, C. Reis, A. Teixeira, and P. Andre, "Raman amplification in the context of next-generation passive optical networks," in *Mediterranean Winter, 2008. ICTON-MW 2008. 2nd ICTON*, 11-13 2008, pp. 1 –4.

7. J. Reis, **B. Neto**, P. Andre, and A. Teixeira, "WDM ring performance improvement by means of a nonlinear effects crosstalk minimization algorithm," in *Optical Fiber Communication - incudes post deadline papers, 2009. OFC 2009. Conference on*, 22-26 2009, pp. 1 –3.

8. A. Rocha, **B. Neto**, A. Martins, G. Incerti, D. Forin, G. Bellefi, M. Facao, J. Pinto, A. Teixeira, R. Nogueira, M. Lima, and P. Andre, "The effect of high power propagation in bended fibers," in *Telecommunications, 2009. ConTEL 2009. 10th International Conference on*, 8-10 2009, pp. 303 –304.

9. P. Coelho, J. Reis, **B. Neto**, P. Andre, and A. Teixeira, "Monitoring of fiber nonlinearities in wdm based passive optical networks," in *Telecommunications, 2009. ConTEL 2009. 10th International Conference on*, 8-10 2009, pp. 277 –281.

10. P. Andre, **B. Neto**, C. Reis, A. Rocha, N. Wada, G. Beleffi, and A. Teixeira, "Raman amplification challenges for next generation networks," in *Transparent Optical Networks, 2009. ICTON '09. 11th International Conference on*, june 2009, pp. 1 –2.

11. C. Reis, **B. Neto**, R. Dionisio, G. Incerti, G. Tosi-Beleffi, D. Forin, A. Rocha, A. Teixeira, and P. Andre, "Transience analysis of bursty traffic with erbium doped fiber amplifiers," in *Transparent Optical Networks, 2009. ICTON '09. 11th International Conference on*, june 2009, pp. 1 –3.

12. J. Reis, **B. Neto**, P. Andre, and A. Teixeira, "Optimization of passive optical networks by means of fiber nonlinearities interference reduction," in *Transparent Optical Networks, 2009. ICTON '09. 11th International Conference on*, june 2009, pp. 1 –4.

13. **B. Neto**, M. Rodrigues, E. Rocha, and P. Andre, "Stability analysis of raman propagation equations," in *Transparent Optical Networks, 2009. ICTON '09. 11th International Conference on*, june 2009, pp. 1 –4.

14. **B. Neto**, A. Klingler, C. Reis, J. Girao, A. Teixeira, and P. Andre, "EDFA transient assessment for bursty traffic," in *ICTON Mediterranean Winter Conference, 2009. ICTON MW 2009. 3rd*, 10-12 2009, pp. 1 –4.

15. **B. Neto**, C. Reis, A. Teixeira, P. André, and N. Wada, "Gain equalization technique for raman amplification systems based on the hybrid optimization algorithm," in *Microwave and Optoelectronics Conference (IMOC), 2009 SBMO/IEEE MTT-S International*, 3-6 2009, pp. 687 –689.

16. M. Rocco Giraldi, A. M. Rocha, **B. Neto**, C. Correia, M. Segatto, M. Pontes, A. Barbero, J. Costa, M. Martinez, O. Frazao, J. Baptista, H. Salgado, M. Marques, A. Teixeira, and P. Andre, "Brillouin effects in distributed raman amplifiers under saturated conditions," in *Microwave and Optoelectronics International Conference (IMOC), 2009 SBMO/IEEE MTT-S*, 3-6 2009, pp. 841 –845.

17. N. Pavlovic, A. Baptista, **B. Neto**, A. Rocha, P. Andre, D. Form, G. Beleffi, J. Lazaro, J. Prat, and A. Teixeira, "Demonstration of improved osnr in ring-based pons with remotely pumped amplification," in *OptoElectronics and Communications Conference, 2009. OECC 2009. 14th*, 13-17 2009, pp. 1 –2.

18. P. S. Andre, A. M. Rocha, **B. Neto**, A. Martins, M. Facao, J. L. Pinto, A. L. J. Teixeira, R. N. Nogueira, M. J. Lima, G. Incerti, D. Forin, G. T. Beleffi"Optical fiber bending limits for optical fiber infraestructures," in *AFRICON, 2009. AFRICON '09.*, 23-25, pp. 1 –3.

19. **B. Neto**, C. Reis, A. Rocha, J. P. Girão, R. P. Dionísio, , S. Chatzi, F. Bonada, J. Lazaro, J. A. and, and A. L. J. Teixeira, "Impact of transient response of optical amplifiers operating with burst traffic," in *7th Conference on Telecommunications, 2009. Conftele '09.*, vol. 1, May 2009, pp. —.

20. A. Martins, A. M. Rocha, **B. Neto**, A. Teixeira, M. Facão, R. N. Nogueira, M. Lima, P. S. André, "Modeling of Bend Losses in Single-Mode Optical Fibers," in *7th Conference on Telecommunications, 2009. Conftele '09.*, vol. 1, May 2009, pp.

21. **B. Neto**, C. Reis, A. Rocha, A. L. J. Teixeira, N. Wada, and P. S. André, "Transience response of traffic based on optical packets with optical amplifiers," in *Networks and Optical Communications, 2009. NOC '09. 14th European Conference on*, vol. 1, June 2009, pp. 545–550.

22. N. B. Pavlovic, A. Baptista, **B. Neto**, A. Rocha, D. Forin, J. A. Lazaro, J. Prat, and A. L. J. Teixeira, "Joint raman and remote add/drop amplification scheme for next generation pons," in *Networks and Optical Communications, 2009. NOC '09. 14th European Conference on*, vol. 1, June 2009, pp. 435–442.

23. C. Reis, R. Dionisio, **B. Neto**, A. Teixeira, and P. Andre, "All-optical XOR based on integrated MZI-SOA with co-and counter-propagation scheme," in *ICTON Mediterranean Winter Conference, 2009. ICTON-MW 2009. 3rd*. IEEE, 2010, pp. 1–4.

24. **B. Neto**, R. P. Dionísio, A. M. Rocha, C. Reis, S. Chatzi, F. Bonada, J. A. Lazaro, A. L. J. Teixeira, and P. S. André, "C+L band extended reach next generation access networks through raman amplification: assessment in rural scenario," in

OptoElectronics and Communications Conference, 2010. OECC 2010. 15th, 5-9 2010, pp. 1 –2.

25. **B. Neto**, A. Rocha, J. P. Girão, R. P. Dionísio, C. Reis, S. Chatzi, F. Bonada, J. A. Lazaro, A. L. J. Teixeira, and P. S. André, "C+L band gain equalization for extended reach wdm-ring pon using hybrid raman/in line edfa amplification," in *Transparent Optical Networks, 2010. ICTON '10. 12th International Conference on*, vol. 1, June 2010, pp. 136–139.

26. **B. Neto**, A. Rocha, J. P. Girão, R. P. Dionísio, C. Reis, S. Chatzi, F. Bonada, J. Lazaro, J. A. and, and A. L. J. Teixeira, and P. S. André, "Comparative analysis of hybrid in line edfa/raman with simple Raman amplification in WDM ring pon for C+L band," in *Networks and Optical Communications, 2010. NOC '10. 15th European Conference on*, vol. 1, June 2010, pp. —.

References

[1] J. Prat, *Next-Generation FTTH Passive Optical Networks: Research Towards Unlimited Bandwidth Access*. Springer Verlag, 2008.

[2] T. ITU, "694.2," *Spectral grids for WDM applications: CWDM wavelength grid (6.02)*.

[3] M. Bredol, D. Leers, L. Bosselaar, and M. Hutjens, "Improved model for OH absorption in optical fibers," *Lightwave Technology, Journal of*, vol. 8, no. 10, pp. 1536–1540, 1990.

[4] W. Mostert and D. Emms, "O band wdm," June 2008, `http://www.cable360.net/ct/sections/features/30007.html`.

[5] E. Desurvire, *Erbium-doped fiber amplifiers: principles and applications*. Wiley New York, 1994.

[6] M. Digonnet, *Rare-earth-doped fiber lasers and amplifiers*. CRC, 2001.

[7] M. Wright and G. Valley, "Yb-doped fiber amplifier for deep-space optical communications," *Journal of Lightwave Technology*, vol. 23, no. 3, p. 1369, 2005.

[8] G. Valley, "Modeling cladding-pumped Er/Yb fiber amplifiers," *Optical Fiber Technology*, vol. 7, no. 1, pp. 21–44, 2001.

[9] P. Andre, B. Neto, C. Reis, A. Rocha, N. Wada, G. Beleffi, and A. Teixeira, "Raman amplification challenges for next generation networks," in *Transparent Optical Networks, 2009. ICTON '09. 11th International Conference on*, june 2009, pp. 1 –2.

[10] D. Zimmerman and L. Spiekman, "Amplifiers for the masses: Edfa, edwa, and soa amplets for metro and access applications," *Lightwave Technology, Journal of*, vol. 22, no. 1, pp. 63 – 70, jan. 2004.

[11] K. C. Reichmann, P. P. Iannone, X. Zhou, N. J. Frigo, and B. R. Hemenway, "240-km CWDM Transmission Using Cascaded SOA Raman Hybrid Amplifiers With 70-nm Bandwidth," *Photonics Technology Letters, IEEE*, vol. 18, no. 2, pp. 328–330, 2006.

[12] S. Zsigmond, H. Furukawa, and N. Wada, "Scalability study of SOA based optical switch for optical packet networks," in *Photonics in Switching, 2009. PS'09. International Conference on*. IEEE, 2009, pp. 1–2.

[13] C. Reis, R. Dionisio, B. Neto, A. Teixeira, and P. Andre, "All-optical XOR based on integrated MZI-SOA with co-and counter-propagation scheme," in *ICTON Mediterranean Winter Conference, 2009. ICTON-MW 2009. 3rd*. IEEE, 2010, pp. 1–4.

[14] C. Headley and G. Agrawal, *Raman amplification in fiber optical communication systems*. Elsevier Academic Press, 2005.

[15] M. Yan, J. Chen, W. Jiang, J. Li, J. Chen, and X. Li, "Automatic design scheme for optical-fiber raman amplifiers backward-pumped with multiple laser diode pumps," *Photonics Technology Letters, IEEE*, vol. 13, no. 9, pp. 948–950, Sep 2001.

[16] J. Bromage, P. Winzer, and R. Essiambre, "Multiple path interference and its impact on system design," *Raman Amplifiers for Telecommunications 2*, pp. 491–568, 2004.

[17] Y. Awaji, H. Furukawa, N. Wada, E. Kong, P. Chan, and R. Man, "Guidelines for amplification of optical packets in WDM environment regarding impact of transient response of erbium-doped fiber amplifier," *Computer Networks*, vol. 52, no. 10, pp. 2087–2093, 2008.

[18] C. Raman and K. Krishnan, "A new type of secondary radiation," *Nature*, vol. 121, no. 3048, p. 501, 1928.

[19] R. Stolen and E. Ippen, "Raman gain in glass optical waveguides," *Applied Physics Letters*, vol. 22, p. 276, 1973.

[20] Y. Aoki, S. Kishida, K. Washio, and K. Minemura, "Bit error rate evaluation of optical signals amplified via stimulated Raman process in an optical fibre," *Electronics Letters*, vol. 21, p. 191, 1985.

[21] E. Woodbury and W. Ng, "Ruby laser operation in the near IR," *Proc. Ire*, vol. 50, no. 11, p. 2367, 1962.

[22] S. Namiki, K. Seo, N. Tsukiji, and S. Shikii, "Challenges of Raman amplification," *Proceedings of the IEEE*, vol. 94, no. 5, pp. 1024–1035, 2006.

[23] J. Hu, B. Marks, and C. Menyuk, "Flat-gain fiber raman amplifiers using equally spaced pumps," *Lightwave Technology, Journal of*, vol. 22, no. 6, pp. 1519 – 1522, june 2004.

[24] M. Giltrelli and M. Santagiustina, "Semianalytical approach to the gain ripple minimization in multiple pump fiber Raman amplifiers," *IEEE Photonics Technology Letters*, vol. 16, no. 11, pp. 2454–2456, 2004.

[25] S. Cui, J. Liu, and X. Ma, "A novel efficient optimal design method for gain-flattened multiwavelength pumped fiber raman amplifier," *Photonics Technology Letters, IEEE*, vol. 16, no. 11, pp. 2451 –2453, nov. 2004.

[26] H. Kidorf, K. Rottwitt, M. Nissov, M. Ma, E. Rabarijaona, T. Ltd, and N. Eatontown, "Pump interactions in a 100-nm bandwidth Raman amplifier," *IEEE Photonics Technology Letters*, vol. 11, no. 5, pp. 530–532, 1999.

[27] J. Bromage, "Raman amplification for fiber communications systems," *Journal of Lightwave Technology*, vol. 22, no. 1, p. 79, 2004.

[28] A. Rocha, B. Neto, A. Martins, G. Incerti, D. Forin, G. Bellefi, M. Facao, J. Pinto, A. Teixeira, R. Nogueira, M. Lima, and P. Andre, "The effect of high power propagation in bended fibers," in *Telecommunications, 2009. ConTEL 2009. 10th International Conference on*, 8-10 2009, pp. 303 –304.

[29] P. Andre, M. Facao, A. Rocha, P. Antunes, and A. Martins, "Evaluation of the fuse effect propagation in networks infrastructures with different types of fibers," in *Optical Fiber Communication (OFC), collocated National Fiber Optic Engineers Conference, 2010 Conference on (OFC/NFOEC)*, 21-25 2010, pp. 1 –3.

[30] D. Chen, T. Xia, G. Wellbrock, J. Peterson, D.L., S. Park, E. Thoen, C. Burton, J. Zyskind, S. Penticost, and P. Mamyshev, ""long span" 10 times;160 km 40 gb/s line side, oc-768c client side field trial using hybrid raman/edfa amplifiers," in *Optical Communication, 2005. ECOC 2005. 31st European Conference on*, 25-29 2005, pp. 15 – 16 vol.1.

[31] I. T. Monroy, R. Kjaer, B. Palsdottir, A. M. J. Koonen, and P. Jeppesen, "10 gb/s bidirectional single fibre long reach pon link with distributed raman amplification," in *Optical Communications, 2006. ECOC 2006. European Conference on*, 24-28 2006, pp. 1 –2.

[32] M. Schneiders, S. Vorbeck, R. Leppla, E. Lach, M. Schmidt, S. Papernyi, and K. Sanapi, "Field transmission of 8 times;170 gbit/s over high loss ssmf link using third order distributed raman amplification," in *Optical Fiber Communication Conference, 2005. Technical Digest. OFC/NFOEC*, vol. 6, 6-11 2005, p. 3 pp. Vol. 5.

[33] Y. Emori, K. Tanaka, and S. Namiki, "100 nm bandwidth flat-gain raman amplifiers pumped and gain-equalised by 12-wavelength-channel wdm laser diode unit," *Electronics Letters*, vol. 35, no. 16, pp. 1355–1356, 1999. [Online]. Available: http://link.aip.org/link/?ELL/35/1355/1

[34] B. Han, X. Zhang, G. Zhang, Z. Lu, and G. Yang, "Composite broad-band fiber raman amplifiers using incoherent pumping," *Opt. Express*, vol. 13, no. 16, pp. 6023–6032, 2005. [Online]. Available: http://www.opticsexpress.org/abstract.cfm?URI=oe-13-16-6023

[35] T. Zhang, X. Zhang, and G. Zhang, "Distributed fiber Raman amplifiers with incoherent pumping," *IEEE Photonics Technology Letters*, vol. 17, no. 6, pp. 1175–1177, 2005.

[36] S. Wen, "Design of the pump power spectrum for the distributed fiber Raman amplifiers using incoherent pumping," *Optics Express*, vol. 14, no. 9, pp. 3752–3762, 2006.

[37] D. Vakhshoori, M. Azimi, P. Chen, B. Han, M. Jiang, K. Knopp, C. Lu, Y. Shen, G. Rodes, S. Vote *et al.*, "Raman amplification using high-power incoherent semiconductor pump sources," in *Optical Fiber Communication Conference*, 2003.

[38] X. Zhou, M. Birk, and S. Woodward, "Pump-noise induced FWM effect and its reduction in a distributed Raman fiber amplifier," *IEEE Photonics Technology Letters*, vol. 14, no. 12, pp. 1686–1688, 2002.

[39] D. I. Chang, D. S. Lim, M. Y. Jeon, H. K. Lee, K. H. Kim, and T. Park, "Dual-wavelength cascaded raman fibre laser," *Electronics Letters*, vol. 36, no. 16, pp. 1356–1358, 2000. [Online]. Available: http://link.aip.org/link/?ELL/36/1356/1

[40] A. Teixeira, P. Andre, S. Stevan, T. Silveira, A. Tzanakaki, and I. Tomkos, "Raman Amplification based on Multiple Low-Power lasers," in *International Conference on Internet and Web Applications and Services/Advanced International Conference on Telecommunications, 2006. AICT-ICIW'06*, 2006, pp. 85–85.

[41] S. Papernyi, V. Ivanov, Y. Koyano, and H. Yamamoto, "Sixth-order cascaded Raman amplification," in *Optical Fiber Commun. Conf.(OFC), Anaheim, CA*, 2005.

[42] J. Schlesinger, *Optical Fibers Research Advances*. Nova Science Pub Inc, 2007.

Chapter 2

Raman amplification theory

2.1 Introduction

To understand the basics behind Raman amplification, it is necessary to understand the phenomenon that describes it, stimulated Raman scattering (SRS). A complete description of Raman amplification would approach thoroughly nonlinear optics and complex mathematics. We choose an intermediate approach that explains the physics of the amplifiers but keeping in mind an imediate application using a telecommunication perspective. Thus, the work described in four major references, Headley and Agrawal [1], J. Bromage [2]and Auyeung and Yariv [3], is followed in order to provide a description as as relevant as possible.

The theory is approached for the first time and a brief description of spontaneous and stimulated Raman scattering is provided in a quantum mechanical point of vue. The Raman gain coefficient is introduced analytically and the efficiency of Raman amplification is discussed for several types of fibers. Then, single pump amplification is approached and the pumping architecture is discussed. The physical model to predict the power evolution for data and pump signals is also presented. The model is mathematically described by a set of coupled nonlinear differential equations for which no analytical solution is available. Nevertheless, the topic of Raman amplifiers modeling will be discussed with more detail in chapter 3. However, to provide some physical insight, simplifications can be made, in particular, the one pump and one signal situation small-signal approximation. An analytical approach that follows the work developed by Auyeung and Yariv that considers pump depletion is presented, although this method is only valid for forward single pumping.

We proceed with a description of the performance limiting factors of Raman amplifiers, which are amplified spontaneous emission, single and double Rayleigh backscattering, also known as multipath interference (MPI) and pump noise transfer. Since amplified spontaneous emission is the dominant effect, it is examined with more detail and the related concept of noise figure and effective noise figure are approched, being their temperature dependence analysed for broadband amplifiers.

2.2 Theory

In a very simplified interpretation, Raman scattering can be understand as an inelastic scattering where light inicident on a medium is converted to a lower frequency. The process can be described by an excitation of the molecule of the medium up to a virtual level induced by the incident photon, followed by a de-excitation and emission of a lower frequency photon [4]. The difference in energy between incident and emitted photons is dissipated by molecular vibrations of the medium. In a solid-state quantum mechanical description, optical photons are inelastically scattered by quantized molecular vibrations called optical phonons [5], [2]. Photon energy is lost or gained, shifting the frequency of the light. The components of scattered light that are shifted to lower frequencies are called Stokes lines; those shifted to higher frequencies, anti-Stokes lines. This process differs from Rayleigh scattering, an elastic process in which the photon energy is conserved. These processes are depicted schematically in Figure 2.1. Since, the anti-Stokes process is typically orders of magnitude weaker than the Stokes process, it is irrelevant in the context of optical communications and will not be mentioned again in this thesis. Thus, from now on, when Raman scaterring is reffered, only the Stokes process is considered.

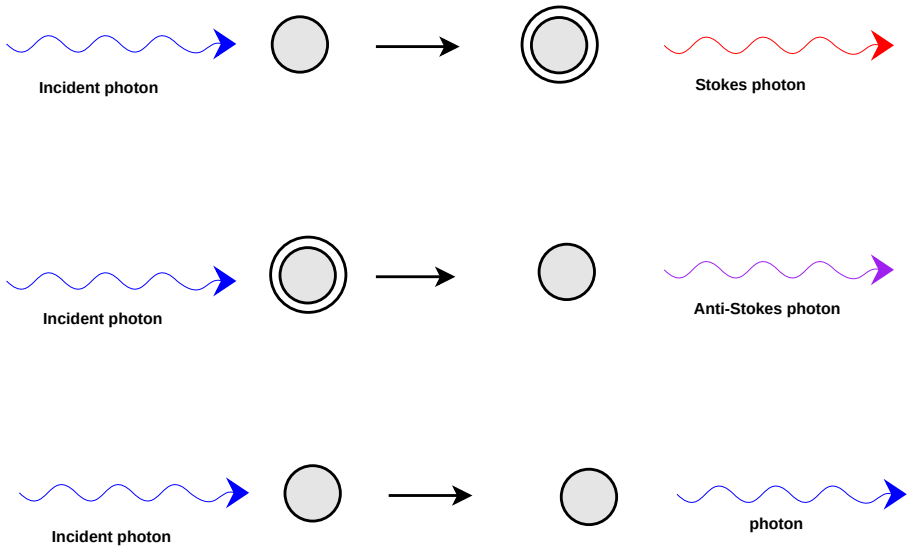

Figure 2.1: Sheme describing inelastic spontaneous Raman Scattering (top) with the Sokes radiation, (middle) anti-skokes radiation. (bottom) Elastic Rayleigh radiation.

Raman scattering can also be stimulated by signal light at an appropriate frequency shift from a pump, leading to stimulated Raman scattering. In this process, pump and signal light are coherently coupled. In a quantum mechanical interpretation, a pump photon is converted into a second signal photon that is an exact replica of the first, and the remaining energy produces an optical phonon. The initial signal photon

is therefore amplified, as schematized in Figure 2.2. For high enough pump power, the scattered light grows rapidly. This process is the gain mechanism behind Raman amplification. Some aspects of it are particularly relevant, namely, it can occur in any fiber, at any wavelength and in a very small timescale (tens of femtoseconds).

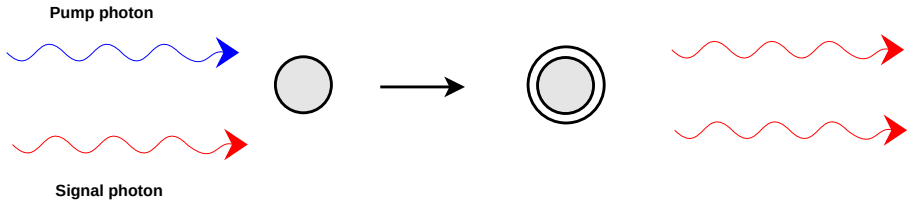

Figure 2.2: Sheme describing stimulated Raman scattering.

The most important parameter characterizing a Raman amplifiers is its gain coefficient, γ_R, since it described how the signal power grows through SRS. It is related to the imaginary part of the nonlinear third-order susceptibility, $\chi^{(3)}$ as [6], [7]:

$$\gamma_R(\Delta\omega) = \frac{4\pi\omega_0}{cn} Im\left[\chi^{(3)}(\Delta\omega)\right] \tag{2.1}$$

where ω_0 is the optical signal frequency, $\Delta\omega$ is the frequency shift between signals and n is the material refractive index.

An important quantity named Raman gain efficiency of the fiber, g_R, relates Raman gain coefficient with the effective area of the fiber, A_{eff}:

$$g_R = \frac{\gamma_R}{A_{eff}} \tag{2.2}$$

The efective area can be approximated to the core area as $A_{eff} \approx A_{core}$ when the field mode distribution is gaussian.

Due to the amorphous nature of Silica that allows a continuum of molecular vibrational frequencies, the Raman gain curve is fairly broad. Larger gain coefficient are obtained when the polarization states of the scattered light and the incident light are parallel, being smaller values obtained for perpendicula polarizations [2]. A peak is always observable for a frequency shift, $\Delta\Omega$, equal to 13.2 THz. When Silica is pumped by a 1450 nm wavelength pump, the Raman gain peak is at about a 100 nm shift (1550 nm). So a simple Raman amplifier can be built by choosing the signal at Stokes shift (1550 nm) and pumping the Silica fiber with a 1450 nm wavelength pump.In Figure 2.3, two Raman gain efficiency spectra are displayed, showing the different strengths of the Raman coupling of a SSMF and a dispersion compensating fiber (DCF), for a pump wavelength at 1450 nm. As a matter of fact, the small effective area of the DCF $(15\ \mu m^2)$ is determinant for its higher Raman gain efficiency when compared to the SSMF $(80\ \mu m^2)$ or when compared with DSF fibers $(50\ \mu m^2)$.

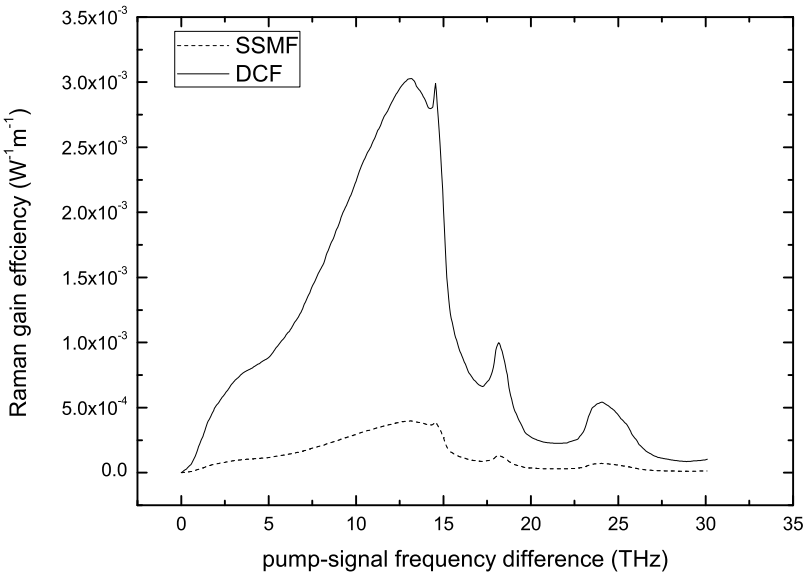

Figure 2.3: Raman gain coefficient spectra for two germanosilicate fibers: Standard Single Mode Fiber (SSMF) and Dispersion Compensating Fiber (DCF), for a pump wavelength of 1450 nm.

2.3 Single pump amplification

In the simplest situation, the amplification system is composed by a continuous wave (CW) pump that when launched into an optical fibre amplifies a CW signal. A basic scheme for a RFA architecture is displayed in Figure 2.4. The signal and pump waves are launched into the optical fiber (the gain medium) by a coupler, so, that stimulated Raman scattering can occur. Since this effect occurs uniformly for all the orientations between pumps and signals, Raman amplifiers can work both in forward and/or backward pumping configuration.

The model for power evolution in Raman amplifiers with a single pump and single signal assumes pump-to-signal and attenuation as the major interactions, stated in the set of equations 2.3 and 2.4.

$$\pm \frac{dP_s}{dz} = -\alpha_s P_s + g_R P_p P_s \tag{2.3}$$

$$\pm \frac{dP_p}{dz} = -\alpha_s P_p - \frac{\nu_p}{\nu_s} g_R P_p P_s \tag{2.4}$$

where $\alpha_{p,s}$ are the fiber attenuations measured at the pump and signal frequencies $\nu_{p,s}$. The term $\pm$ refers to co and counter propagating signals.

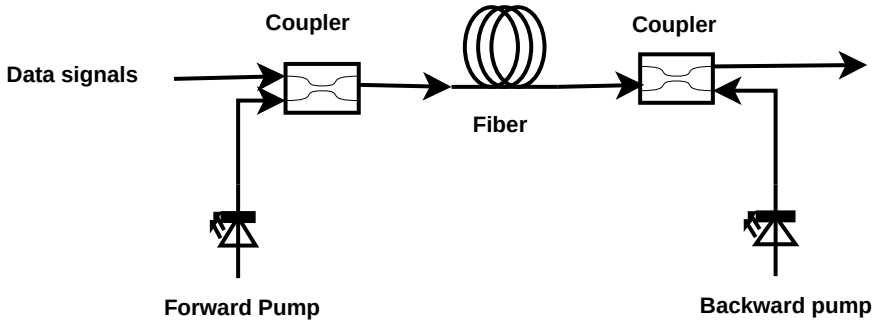

Figure 2.4: General scheme for a distributed Raman amplifier. For simplicity the optical isolators used to protect the pumps and signals sources, were omitted.

It is not easy to obtain an analytical solution for the set of equations 2.3 and 2.4 because it is nonlinear. However, some solutions obtained under specific simplifications are assessable which, although not general, can provide important information about the system behaviour.

In small signal appoximation, it is assumed that the pump depletion due to the transfer of power to the signal (second term in equation 2.4) is negligible. This assumption is valid whenever the signal power value is small in comparison to the pump power. In such situation, the second equation is no longer nonlinear and thus solvable analytically. The behaviour of the pump is an exponential decay due to its attenuation in the fiber, as stated in equations 2.5 and 2.6 in the co and counter propagating pumping respectively.

$$P_p(z) = P_0 \, exp(-\alpha_p z) \tag{2.5}$$

$$P_p(z) = P_0 \, exp[-\alpha_p (L - z)] \tag{2.6}$$

where P_0 is the input pump power and L is the fibre length.

The substitution of the equations above in the signal differential equation allows the derivation of an analytical solution for the signal, as follows.

$$P_s(z) = P_s(0) \, exp\left(g_R \int_0^z P_p(z')dz' - \alpha_s z \right) \tag{2.7}$$

Thus, the solutions at $z = L$ are given by:

$$P_s(L) = P_s(0) \, exp\left(g_R P_0 L_{eff} - \alpha_s L\right) \equiv G(L) \; P_s(0) \tag{2.8}$$

where $G(L)$ is the net gain computed at the end of the fibre. The quantity L_{eff} is designated by effective length and represents the length within which most of the amplification occurs.

$$L_{eff} = \frac{[1 - exp\,(-\alpha_p L)]}{\alpha_p} \tag{2.9}$$

Another important quantity often used is the on-off gain, G_{on-off}. It is defined as the signal power increase when the pump is turned on. Therefore, in the small signal limit, it is expressed by 2.10.

$$G_{on-off} = \frac{P_signal\,(z = L)\,with\ pumps\ on}{P_signal\,(z = L)\,with\ pumps\ off} \equiv exp\,(g_R P_0 L_{eff}) \tag{2.10}$$

It must be noted that in both co and counter pumping the signal reaches the end of the fibre with the same power, which means that, in terms of gain, the pumping schemes are equivalent.

To verify the validity of the small signal approximation, a practical situation with a pump and a travelling signal was implemented numerically. The pump is centered at 1450 nm and has an initial power of 500 mW while the signal is centered at 1530 nm. The numerical experiment follows a copropagating amplification scheme, being the gain medium a span of 40 km of SSMF. The implementation was carried out with different signal input powers (1, 10 and 50 mW) using the 4^{th} order Runge-Kutta method with adaptative stepsize and the small signal approximation given by equation 2.5. The implementations use values of 0.25 dB/km and 0.20 dB/km for the pump and signals attenuation. The Raman gain cofficients were obtained for germanosilicate fibers, using file data from the VPI software and an effective area of 80 μm^2 was considered. The calculated Raman gain efficiency was also multiplied by a factor of $1/2$ because the polarizations of pump and signal are completely scrambled along the propagation. The results are plotted on Figure 2.5.

On looking at the results, it is noticeable that the approximation stands valid when the signal is small (1 mW) and that the effect of pump depletion becomes more evident as the signal input power increases. The implementation of the signal power evolution also demonstrates the limitations of the small signal approximation, as shown on Figure 2.6, where the small signal approximation obtained with equation 2.7 was plotted together with the numerical one, for an input signal power equal to 10 mW. Indeed, in the numerical solution, the signal reaches the end of the optical fiber with more power due to the depletion exerted on the pump. However, the small signal approximation is useful when its applicability was previously verified.

In the bidirectional pumping, some modifications to the system of equations 2.3 and 2.4 have to be made, due to the addition of an extra pump. In this situation, the total inputted pump power is still P_0 but a fraction of it goes in each direction. Considering the small signal approximation, the equations are given by:

$$\frac{dP_p^+}{dz} = -\alpha_p P_p^+ \tag{2.11}$$

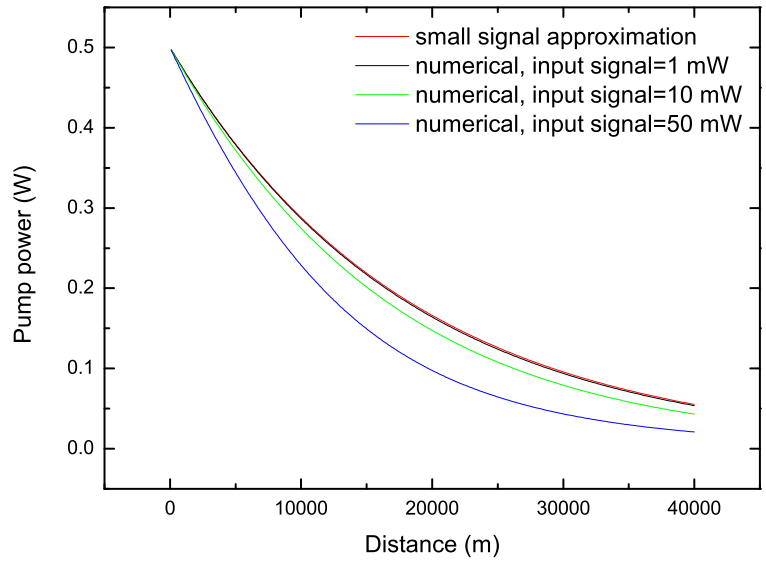

Figure 2.5: Pump power evolution along 40 km of SSMF in the small signal approximation and considering pump depletion for an input signal power equal to 1 mW, 10 mW and 50 mW.

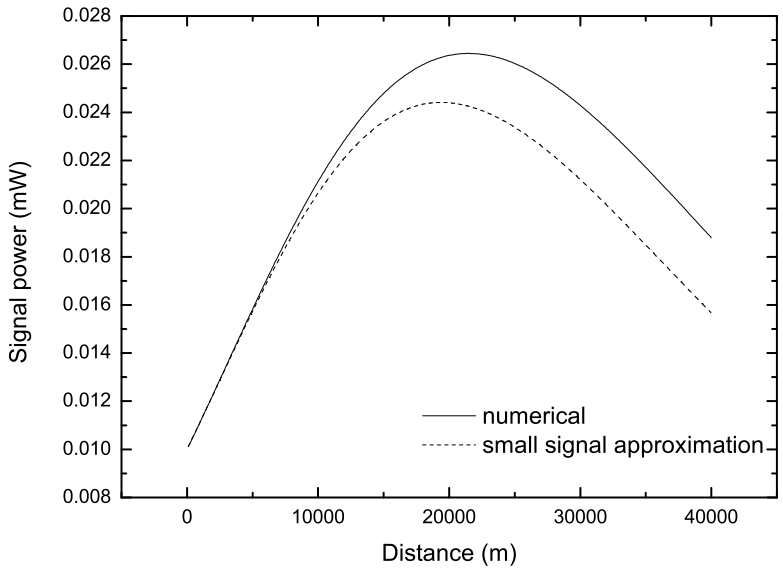

Figure 2.6: Signal power evolution along 40 km of SSMF in the small signal approximation and considering pump depletion. The initial pump power is equal to 500 mW.

$$\frac{dP_p^-}{dz} = \alpha_p P_p^- \tag{2.12}$$

$$P_p = P_p^+ + P_p^- \tag{2.13}$$

with $P_0^+ = r^+ P_0$ and $P_0^- = (1 - r^+) P_0$.

The solution of the system of equations 2.11, 2.12 and 2.13 for the total pumping

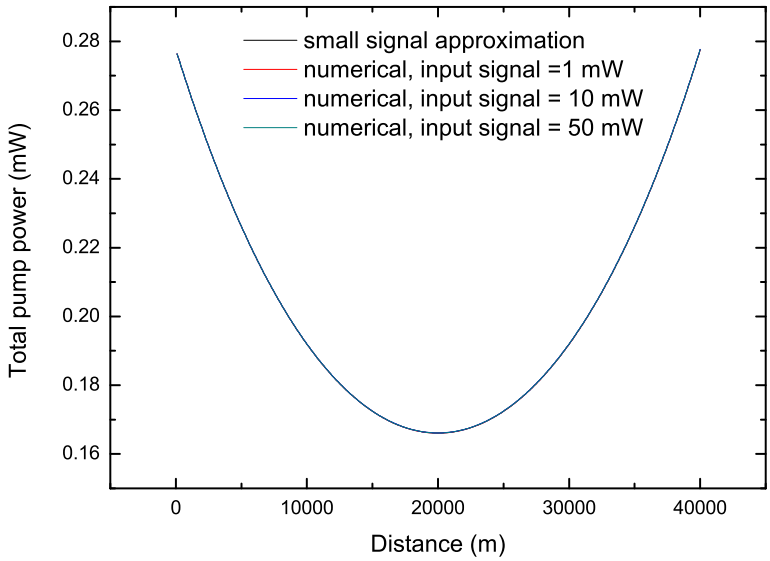

Figure 2.7: Pump power evolution along 40 km of SSMF in the small signal approximation and considering pump depletion for an input signal power equal to 1 mW, 10 mW and 50 mW.

power is given by a combination of the solutions in the co and counter-propagating directions, as follows:

$$P_p(z) = P_0 \left[r^+ exp\left(-\alpha_p z\right) + \left(1 - r^+\right) exp\left(-\alpha_p \left(L - z\right)\right) \right] \tag{2.14}$$

The substitution of equation 2.14 in equation of 2.3 yields to the solution of the signal for bidirectional pumping.

To verify the validity of the small signal approximation in the bidirectional scheme, the situation described above was implemented but two bidirectional pumps centered at 1450 nm were used instead of one. The total inputted pump power was still equal to 500 mW (250 mW in each end of the fiber) and a signal centered at 1550 nm was used. Once again, the initial signal powers were tested for 1 mW, 10 mW and 50 mW. The numerical implementation follows the APA method which will be presented more detailly in next chapter. The numerical results were compared with the ones obtained recurring to equations 2.11, 2.12 and 2.13 and plotted in Figure 2.7. On looking at the results, it is noticeable that unlike the co-propagated pumping situation the approximation stands valid for the three analyzed cases.

2.3.1 Pump depletion

The analytical results provided by the small signal approximation are based on the idea that the pump depletion is negligible, otherwise, the system of equations 2.3 and 2.4 is commonly solvable by numeric methods. However, in the co-propagated pumping architecture, the model developed by Auyeung *et al* [3] provides a suitable analytical solution and thus will be discussed in frame of this thesis.

As said above, Auyeung model for stimulated Raman scattering is valid for co-propagating single pump and multi-signal situation, however, only the single signal is analyzed here. It accounts for pump depletion and spontaneous scattering being its results broad enough to contemplate the small signal approximation presented above.

The system of equations 2.3 and 2.4 may be rewritten in terms of the pump and signal photon numbers n_p and n_s as [8]:

$$\frac{dn_s}{dz} = -\alpha_s n_s + \gamma_0 n_p n_s + \gamma_0 n_s \tag{2.15}$$

$$\frac{dn_p}{dz} = -\alpha_p n_p - \gamma_0 n_p n_s - \gamma_0 n_p \tag{2.16}$$

where γ_0 is the nonlinear Raman gain constant.

It must be noted that the last term in the pump and signal equations is related to the spontaneous scattering. The total number of photons, n_0, is conserved in this process, and may be computed recurring to the condition at $z = 0$, as:

$$n_0 = n_{p0} + n_{s0} \tag{2.17}$$

where n_{p0} and n_{s0} are the number of pump and signal photons at $z = 0$.

Making the approximation that pump and signal suffer the same attenuation α (this assumption is especially true in the infrared region where the attenuation is near its minimum and thus its variation with wavelength is small), the addition of equations 2.16 and 2.15 is given by:

$$\frac{d}{dz}(n_p + n_s) + \alpha(n_p + n_s) = 0 \tag{2.18}$$

Hence, the total number of photons varies as:

$$n_p + n_s = n_0 \exp(-\alpha z) \tag{2.19}$$

By replacing 2.19 in 2.15 and 2.16, the following is obtained:

$$\frac{dn_p}{dz} + n_p \left[\alpha + \gamma_0 + \gamma_0 n_0 \exp(-\alpha z)\right] = \gamma_0 n_p^2 \tag{2.20}$$

$$\frac{dn_s}{dz} + n_s\left[\alpha\gamma_0 - \gamma_0 n_0 \exp\left(-\alpha z\right)\right] = -\gamma_0 n_s^2 + \gamma_0 n_0 \exp\left(-\alpha z\right) \tag{2.21}$$

It must be noted that the system of equations 2.20 and 2.21 together with the initial conditions 2.17 is now solvable analytically because it is composed by first order exact differential equations. Thus, taking a change in the variable $n_p = 1/x$, the equation for the pump number of photons is converted into:

$$\frac{dx}{dz} - x\left[\alpha + \gamma_0 + n_0 \exp\left(-\alpha z\right)\right] = -\gamma_0 \tag{2.22}$$

Using the integrating factor $\exp\left[-\left(\alpha+\gamma_0\right) + \gamma_0 n_0/\alpha \exp\left(-\alpha z\right)\right])$], the equation takes the form:

$$\begin{aligned} x =& \exp\left[\left(\alpha+\gamma_0\right)z - \frac{\gamma_0 n_0}{\alpha}\exp\left(-\alpha z\right)\right] + \\ &+ \int_0^z \left[-\gamma_0 \exp\left(\left(\alpha+\gamma_0\right)z'\right) + \frac{\gamma_0 n_0}{\alpha}\exp\left(-\alpha z'\right)\right] dz' + C \end{aligned} \tag{2.23}$$

where C is a constant which will be determined by the initial conditions. Solving the integral with the integration by parts technique, the solution is given by:

$$\begin{aligned} x =& \frac{1}{n_0}\exp\left(\alpha z\right)\left\{1 - \gamma_0 \exp\left[\gamma_0 z - \frac{\gamma_0 n_0}{\alpha}\exp\left(-\alpha z\right)\right]\sum_{l=0}^{\infty}\frac{\left(\frac{\gamma_0 n_0}{\alpha}\right)^l \exp\left[-\left(l\alpha+\gamma_0\right)\right]}{\left(l\alpha-\gamma_0\right)!}\right\} + \\ &+ C\exp\left[\left(\alpha+\gamma_0 z\right) - \frac{\gamma_0 n_0}{\alpha}\exp\left(-\alpha z\right)\right] \end{aligned} \tag{2.24}$$

Finally, the pump photon number is given by the following:

$$n_p = \frac{n_0 \exp\left(-\alpha z\right)}{1+\eta+\xi} \tag{2.25}$$

where

$$\eta = \gamma_0 \exp\left[\gamma_0 z - \frac{\gamma_0 n_0}{\alpha}\exp\left(-\alpha z\right)\right]\sum_{l=0}^{\infty}\frac{\left(\frac{\gamma_0 n_0}{\alpha}\right)^l \exp\left[-\left(l\alpha+\gamma_0\right)\right]}{\left(l\alpha-\gamma_0\right)!} \tag{2.26}$$

$$\xi = \frac{n_{s0}}{n_{p0}}\exp\left\{\gamma_0 z + \frac{\gamma_0 n_0}{\alpha}\left[1 - \exp\left(-\alpha z\right)\right]\right\} \tag{2.27}$$

The determination of the photon signal equation is trivial taking into account equation 2.19 and can be expressed by:

$$n_s = n_0 \exp\left(-\alpha z\right)\frac{\eta+\xi}{1+\eta+\xi} \tag{2.28}$$

The solutions for the pump and signal photon numbers can be converted to pump and signal power according to:

$$P_p(z) = \frac{P_0 \exp(-\alpha z)}{1+\eta+\xi} \tag{2.29}$$

$$P_s(z) = \frac{\nu_s}{\nu_p} P_0 \exp(-\alpha z) \frac{\eta+\xi}{1+\eta+\xi} \tag{2.30}$$

$$\eta = \frac{\nu_p}{\nu_s} \frac{h\nu_s v_g}{P_0 L} \exp\left\{ \frac{g_R P_0}{\alpha A_{eff}} [1-\exp(-\alpha z\}] \right) \tag{2.31}$$

$$\xi = \frac{\nu_p}{\nu_s} \frac{P_{s0}}{P_{p0}} \exp\left\{ \frac{g_R P_0}{\alpha A_{eff}} [1-\exp(-\alpha z\}] \right) \tag{2.32}$$

The limiting situations are assessed taking the limits $\xi + \nu << 1$ and $\xi + \nu >> 1$. For the first situation, the pump power evolution is compliant with the small signal approximation, being the fiber attenuation the dominant effect. For the second situation, a full conversion of photons from pump to signal is achieved and thus the signal power evolution is given by:

$$P_s(z) \approx \frac{\nu_s}{\nu_p} P_0 \exp(-\alpha z) \tag{2.33}$$

2.4 Performance limiting factors

Although the benefits of Raman amplification are valuable and important in fiber optics communication systems, there are concerns to be aware of. The limitations on the performance of Raman amplifiers arise from three fundamental contributions: spontaneous Raman scattering, double Rayleigh backscattering and pump noise transfer. Other effects derived from polarization mode dispersion [9], [10] are also detrimental but will not be approached in the scope of this thesis.

Spontaneous Raman scattering and its subsequent amplification is dominant effect of noise in Raman amplification.

2.4.1 Amplified spontaneous emission (ASE)

The noise added from the spontaneous Raman scattering is ougthed to the random phases of the photons released in the process. The generation and amplification of ASE obeys:

$$\pm \frac{dP^{\pm}_{ASE}}{dz} = -\alpha_{ASE} P^{\pm}_{ASE} + g_R P_p P^{\pm}_{ASE} + g_R [1+\eta(T)] h\nu_{ASE} B_{ref} P_p \tag{2.34}$$

where $P_{ASE}^{\pm}$ is the ASE power in a bandwidth B_{ref}, propagating in the direction $\pm$.

One difference between this equation and equation 2.3 for the signal is the additional inhomogeneous source term in the differential equation. This source term includes a phonon occupancy factor, $\eta\left(T\right)$:

$$\eta_{ij}\left(T\right) = \left[\exp\left(\frac{h\Delta\nu)}{k_B T} - 1\right)\right]^{-1} \tag{2.35}$$

where *h* is the Planck constant, k_B is Boltzmann constant, *T* is the absolute temperature of the fiber in kelvins, and $\Delta\nu$ is the frequency separation between the pump and signal. The boundary conditions set that $P_{ASE}^{+}\left(z=0\right) = 0$ and $P_{ASE}^{-}\left(z=L\right) = 0$, however, initial values can be assumed when the pump is not purely monocromatic [11].

It has been demonstrated that the amount of accumulated ASE depends on the amplification scheme. Typically copropagated pumping schemes are less noisy because most of the Raman gain is concentrated in the fiber input; however the counterpropagated pumping is often employed in practice because of the transfer of the pump noise transfer This issues is discussed later.

The noise figure of an optical amplifier amounts the degradation of the optical signal to noise ratio when the signals are amplified. As said above, the most important source of noise in optical amplifiers is ASE, which, for Raman amplifiers is due to spontaneous scattering. Assuming that the signals are initially as noiseless as possible, and that their degradation is due to signals spontaneous beat noise produced by ASE [12], the noise figure, in linear units, is given by [2], [13], :

$$NF \approx \left(\frac{2P_{ASE}^{+}\left(z=L\right)}{h\nu_{ASE}B_{ref}} + 1\right)\frac{1}{G} \tag{2.36}$$

where *G* is the net gain. The first term corresponds to the noise from the signal spontaneous beating and the second one to shot noise.

Another quantity, named effective noise figure, accounts the noise figure that a discrete amplifier placed at the end of an unpumped fiber link would need to provide the same noise performance that a distributed Raman amplifier. In decibel units, the effective noise figure is computed using:

$$NF_{eff}^{dB} = NF^{dB} - \alpha L^{dB} \tag{2.37}$$

The spectra depicted in Figure 2.8 represent the net gain of effective noise figure of a distributed RFA composed by two bidirectional pumps at 1440 nm and 1500 nm with a total power of 1 W (500 mW each) and and 25×400 GHz data signals along a span of 50 km SSMF. The results were obtained by simulation using the collocation method.

The simulation had considered attenuation coefficients of 0.25 dB/km and 0.22 dB/km for pumps and data signals respectively. The step size is adaptative. On looking at

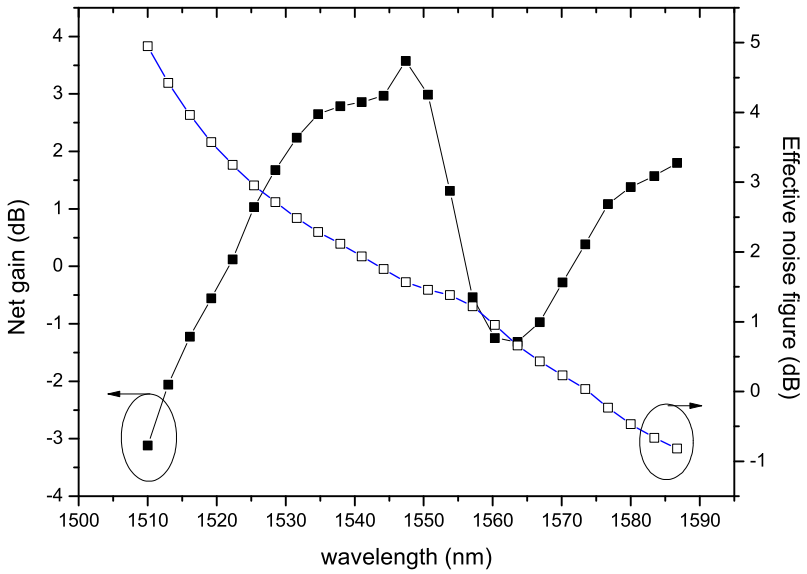

Figure 2.8: Net gain and effective noise figure spectra for a system with two bidirectional pumps and 25×400 GHz data signals along a span of 50 km SSMF.

the noise figure spectrum, it is noticeable that there is a decreasing tilt with frequency. This effect is due to the different amount of gain experiencied by the data signals from the pump. The longest wavelength pump signal provides more gain the longest wavelength data signals and is also amplified by the shorter wavelength pumps. As a result, the is gain is more evenly distributed along the fiber and the noise figure has a better performance. Additionally, as the frequency separation between pump and shorter wavelength data signals decreases, the amount of generated ASE is higher. This tilt is also dependent on temperature, as explained below.

The performance of Raman amplifiers in terms of low noise is determined by bandwidth, as demonstrated by Fludger *et al* [14], where a fundamental compromise must be founded. Thus, The quantum limit noise figure is not obtained at finite temperature at room temperature, showing variations at shorter wavelengths due to the increase in spontaneous wavelengths.

Using the undepleted pump approximation and considering that pump and data signals have the same attenuation, the net gain in linear unit is given by:

$$G = \exp\left(-\alpha L + L_{eff}\sum_i g_{Ri}P_{pi}\right) = \exp\left(-\alpha L\right)\prod_i g_i \tag{2.38}$$

where L is the fiber length and L_{eff} its effective length, α is the attenuation, g_{Ri} is the Raman gain efficiency for a data signal interacting the i^{th} pump signal. The amplifier spontaneous emission (ASE) at the fiber output is given by [15]:

$$P_{ASE}(L) = h\nu \left[\frac{\sum_i E_i \ln(g_i)}{\sum_i \ln(g_i)}\right] \left\{\left(1 + \frac{\alpha L_{eff} \exp(\alpha L)}{\sum_i \ln(g_i)}\right) G - \left(1 + \frac{\alpha L_{eff}}{\sum_i \ln(g_i)}\right)\right\} \quad (2.39)$$

where h is the Planck constant and E_i is is a Bose distribution that takes into account the thermal population of phonons in the ground state [16], [17], given by:

$$E_i = 1 + \eta(T) \quad (2.40)$$

The noise figure given by equation 2.36 can be approximated by the following expression:

$$NF \approx 2\frac{\sum_i E_i \ln(g_i)}{\sum_i \ln(g_i)} \quad (2.41)$$

Equations 2.38 and 2.41 were implemented for a broadband Raman amplifier with a spectral width of 120 nm. The data signals are amplified by means of five backward pump signals at 1402 nm, 1423 nm, 1443 nm, 1464 nm and 1495 nm, each of them with an input power of 125 mW in a span of 25 km of SSMF. The Raman gain efficiency values were obtained from Figure 2.3 and an attenuation of 0.22 dB/km was considered for pumps and data signals. The results of the noise figure for at absolute temperatures of 300 K, 200 K, 100 K and 0 K are displayed in Figure 2.9.

The results of the noise figure spectra exhibit a decaying on the ripple as the temperature approaches the 0 K. The noise figure of shorter wavelengths data signals is higher than the one observed at larger wavelengths because the spontaneous emission increases as the signal wavelengths approach the pump wavelengths. At lower temperatures, the phonon distribution is reduced and the occupancy factor tends to one, reducing the noise figure to 3 dB, the value defined by the theoretical quantum limit [18].

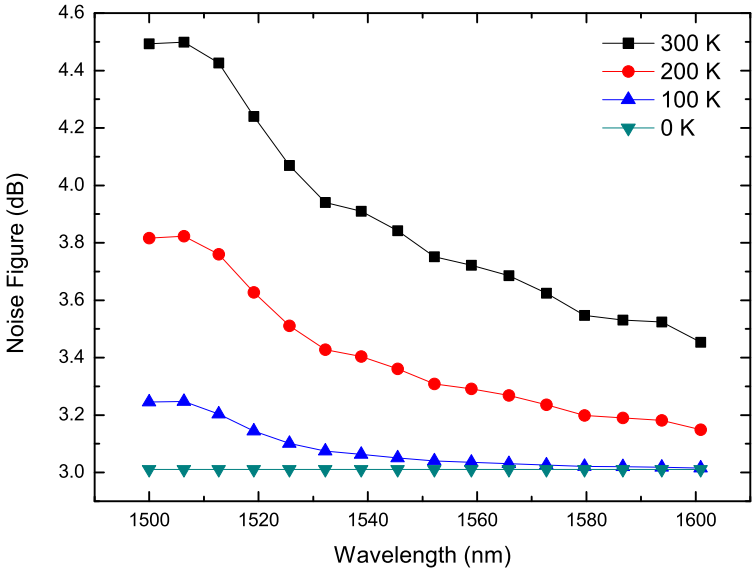

Figure 2.9: Noise Figure spectra for temperatures equal to 300 K, 200 K, 100 K and 0 K.

2.4.2 Multipath interference

The double Rayleigh backscattering, also known as MPI is a phenomenon that limits the performance of distributed Raman amplifiers. It consists of an elastic reflection of light in the sub-micron inhomogeneities in the fiber refractive index. When the signal is backscattered twice and experience significant gain it can create crosstalk in the copropagating direction [19], appearing as a noise source. Thus this fenomenon sets a fundamental limit on the maximum amount of distributed Raman gain that can be used before MPI dominates. The simulation of this effects can be implemented using the following equations [20]:

$$-\frac{dP_{SRB}}{dz} = -\alpha_s P_{SRB} + g_R P_p P_{SRB} + f_r \alpha_r P_s \tag{2.42}$$

$$\frac{dP_{DRB}}{dz} = -\alpha_s P_{DRB} + g_R P_p P_{DRB} + f_r \alpha_r P_{SRB} \tag{2.43}$$

where P_{SRB} and P_{DRB} represent average power levels of noise created by single and double Rayleigh backscattering, respectively, α_r is Rayleigh scattering loss and f_r the fraction that is recaptured by the fiber mode.

In the small signal approximation approach, the fraction of the input power coming up with the data signal, $f_{DRB} = P_{DRB}/P_s$, is given by the following equation

[21]:

$$f_{DRB} = (f_r \alpha_r)^2 \int_0^L G^{-2}(z)\, dz \int_z^L G^2(z')\, dz' \tag{2.44}$$

The crosstalk originated by multipath interference can lead to large power penalties, especially in long haul systems where this crosstalk accumulates over multiple amplifiers.

2.4.3 Pump noise transfer

Pump noise transfer is fundamentally due to fluctuations in the pump power. Since the Raman effect acts very fast (in a femtosecond time scale) those fluctuations of power are transferred to the signal as noise. In distributed Raman amplifiers, the gain is built as the waves travel in the fiber. This produces an averaging effect that limits the bandwidth over which pump noise is transferred to the signals. This phenomenon can be described in the frequency domain as a transfer of relative intensity noise (RIN) from a pump to a signal, using a frequency-dependent transfer function, $H(f)$, that depends on the pumping direction, the pump and signal wavelengths, and the amount of on-off Raman gain [22].

$$RIN_s(f) = H(f)\, RIN_p(f) \tag{2.45}$$

In a forward pumping scheme with low dispersion, signal and pump are traveling together and any power fluctuation of the pump is perceived by the signal in the same temporal window. However, for the case of backward pump the signal moves out of the temporal window of the pump and perceived an average gain. The same effects could be obtained in a forward pumping scheme if the fiber dispersion is sufficiently high to separate temporally the pump and signal waves.

The amount of Q-factor degradation for a given amplifier design can be estimated using [22]:

$$\Delta Q_{dB} = 10 \log_{10} \left(1 + Q_s \int_{f_1}^{f_2} RIN_s(f)\, df \right) \tag{2.46}$$

where $Q_s$is the reference Q-factor in linear units without RIN transfer, while f_1 and f_2 lower and upper frequency limits of the receiver.

2.5 Chapter summary

This chapter described the theory that suppors Raman fiber amplifiers. As said above, the thoroughness of the approached theory is the stricly necessary for the understanding of the work that was carried one in the subsequent chapters. Thus, spontaneous and stimulated Raman scattering are explained as inelastic

scatterings with the generation of Stokes and anti-Stokes radiation. We proceeded with the analysis of simpler cases, namely the small signal approximation where pump depletion is neglected in order to obtain analytical solutions. An analytical approach of pump depletion is also presented for a simple case of single forward pumping. Detrimental effects that impair the performance of Raman amplifiers are then presented and analyzed for broadband Raman amplifiers in order to understand the architectures that are currently used in modern communication systems.

References

[1] C. Headley and G. Agrawal, *Raman amplification in fiber optical communication systems*. Elsevier Academic Press, 2005.

[2] J. Bromage, "Raman amplification for fiber communications systems," *Journal of Lightwave Technology*, vol. 22, no. 1, p. 79, 2004.

[3] J. AuYeung and A. Yariv, "Spontaneous and stimulated Raman scattering in long low loss fibers," *IEEE Journal of Quantum Electronics*, vol. 14, no. 5, pp. 347–352, 1978.

[4] G. Agrawal, *Nonlinear Fiber Optics*. Elsevier Academic Press, 2007.

[5] C. Kittel *et al.*, *Introduction to solid state physics*. Wiley New York, 1996.

[6] A. Atieh, P. Myslinski, J. Chrostowski, and P. Galko, "Measuring the Raman Time Constant (T_R) for Soliton Pulses in Standard Single-Mode Fiber," *J. Lightwave Technol*, vol. 17, pp. 17–2, 1999.

[7] P. Andre, R. Correia, L. Borghesi, A. Teixeira, R. Nogueira, M. Lima, H. Kalinowski, F. Da Rocha, and J. Pinto, "Raman gain characterization in standard single mode optical fibres for optical simulation purposes," *Optica Applicata*, vol. 33, no. 4, pp. 559–574, 2003.

[8] A. Yariv, "Coupled-mode theory for guided-wave optics," *IEEE Journal of Quantum Electronics*, vol. 9, no. 9, pp. 919–933, 1973.

[9] D. Wang and C. Menyuk, "Calculation of Penalties Due to Polarization Effects in a Long-Haul WDM System Using a StokesParameter Model," *Journal of Lightwave Technology*, vol. 19, no. 4, p. 487, 2001.

[10] G. Foschini and C. Poole, "Statistical theory of polarization dispersion in single mode fibers," *Lightwave Technology, Journal of*, vol. 9, no. 11, pp. 1439–1456, 1991.

[11] A. Rocha, B. Neto, M. Facao, and P. Andre, "Study of raman amplification with low cost incoherent pumps," *Microwave and Optical Technology Letters*, vol. 50, no. 2, pp. 301–303, 2008.

[12] N. A. Olsson, "Lightwave systems with optical amplifiers," *Lightwave Technology, Journal of*, vol. 7, no. 7, pp. 1071–1082, 1989.

[13] D. Derickson, *Fiber Optic Test and Measurement*. Packard professional books, Prentice Hall PTR, Upper Saddle River, New Jersey, 1998.

[14] C. Fludger, V. Handerek, N. Jolley, and R. Mears, "Fundamental noise limits in broadband raman amplifiers," in *Optical Fiber Communication Conference*. Optical Society of America, 2001, p. MA5. [Online]. Available: http://www.opticsinfobase.org/abstract.cfm?URI=OFC-2001-MA5

[15] S. R. Chinn, "Analysis of counter-pumped small-signal fibre Raman amplifiers," *Electronics Letters*, vol. 33, no. 7, pp. 607–608, 1997.

[16] M. A. Farahani and T. Gogolla, "Spontaneous raman scattering in optical fibers with modulated probe light for distributed temperature raman remote sensing," *J. Lightwave Technol.*, vol. 17, no. 8, p. 1379, 1999. [Online]. Available: http://jlt.osa.org/abstract.cfm?URI=JLT-17-8-1379

[17] K. Rottwitt, M. Nissov, and F. Kerfoot, "Detailed analysis of Raman amplifiers for long haul transmission," in *Optical Fiber Communication Conference and Exhibit, 1998. OFC'98., Technical Digest*, 1998, pp. 30–31.

[18] E. Desurvire, *Erbium-doped fiber amplifiers: principles and applications*. Wiley New York, 1994.

[19] C. Kim, J. Bromage, and R. Jopson, "Reflection-induced penalty in Raman amplified systems," *IEEE Photonics Technology Letters*, vol. 14, no. 4, pp. 573–575, 2002.

[20] J. Bromage, P. Winzer, and R. Essiambre, "Multiple path interference and its impact on system design," *Raman Amplifiers for Telecommunications 2*, pp. 491–568, 2004.

[21] M. Nissov, K. Rottwitt, H. Kidorf, M. Ma, T. Ltd, and N. Eatintown, "Rayleigh crosstalk in long cascades of distributed unsaturated Raman amplifiers," *Electronics Letters*, vol. 35, no. 12, pp. 997–998, 1999.

[22] C. R. S. Fludger, V. Handerek, and R. J. Mears, "Pump to signal RIN transfer in Raman fiber amplifiers," *Lightwave Technology, Journal of*, vol. 19, pp. 1140–1148, 2001.

Chapter 3

Modeling Raman fiber amplifiers

3.1 Introduction

The most accurate and straightforward approach in designing a RFA is solving the Raman amplifier propagation equations. The practical application of this approach, however, is limited by its low efficiency because the set of ODEs is nonlinear. The lack of efficiency is also affected by the fact that RFAs being traditionally operated in the backward-pumping geometry to minimize the polarization dependent gain and the noise induced by the fluctuation of the pumps power [1], [2]. With this geometry, the coupled differential equations of RFAs become boundary value problems (BVPs), which are much more difficult to be solved than the initial value problem (IVP) involved in the forward-pumping situation.

The methodologies used to solve the set of Raman propagation equations rely essentially on numerical methods. Depending on the chosen method, the solutions are accurate although not necessarily efficient because their computational implementation is usually time consumming. However, some qualitative insigths about the solutions behaviour can be provided by means of stability analysis. Semi-analytical methods can improve significantly the efficiency of the solutions computation, such as APA.

This chapter is concerned with the simulation of Raman fiber Amplifiers and several methods will be discussed. These methods can be either numerical (shooting, collocation) or semi-analytical (APA) but no analytical solution is available due to the nonlinearity of the ordinary differential equations that describes the system. However, qualitative analysis can provide deeper insigths about the solutions behaviour in the vicinity of critical points. Thus, an analysis for Raman propagation equations near their critical points was carried out by linearization and also using Lyapunov second method. The only critical point with physical significance was identified as the origin of the phase plane and demonstrated to be asymptotically stable. Additionally some trajectories were also plotted in the phase plane.

3.2 Mathematical model

The model for power evolution in Raman amplifiers assuming, a multipump multisignal configuration is often based on an unified treatment of channels, pumps and spectral components of ASE. The major interactions can be reasonably drawn by considering the pump-to-pump, signal-to-signal and pump-to-signal power transfer, attenuation, Rayleigh backscattering, spontaneous Raman emission and its temperature dependence as well as the ASE. Other effects, such as noise generation due to spontaneous anti-Stokes scattering, polarization and nonlinear index are neglected. It must be noted that signal channels and Raman pumps are treated as fields at single frequencies, so ignoring the interactions due to the spectral shape of signals and pumps.

In a general approach, the power evolution of pumps, signals and ASE (in forward and backward directions), with time along the fiber distance is given by the following set of coupled differential equation [3]. For N_p pumps, N_s probe signals and N_{ASE} spectral components for ASE, the system is formed by $N_p + N_s + 2N_{ASE}$ equations.

$$\begin{aligned}\frac{\partial P_i^{\pm}(z,t)}{\partial z} \mp \frac{1}{V_i}\frac{\partial P_i^{\pm}(z,t)}{\partial t} &= \mp \alpha_i P_i^{\pm}(z,t) \pm \gamma_i P_i^{\pm}(z,t) \\ &\pm P_i^{\pm}(z,t)\sum_{j=1}^{i-1} g_{ji}\left[P_j^{+}(z,t) + P_j^{-}(z,t)\right] \\ &\mp P_i^{\pm}(z,t)\sum_{j=i+1}^{m}\frac{\nu_i}{\nu_j} g_{ij}\left[P_j^{+}(z,t) + P_j^{-}(z,t)\right] \\ &\mp 2h\nu_i\sum_{j=1}^{i-1} g_{ji}\left[P_j^{+}(z,t) + P_j^{-}(z,t)\right](1+\eta_{ji})\,\Delta\nu \\ &\mp 4h\nu_i P_i^{\pm}(z,t)\sum_{j=i+1}^{m} g_{ij}(1+\eta_{ij})\,\Delta\nu \end{aligned} \tag{3.1}$$

V_i is the frequency dependent group velocity. The $\pm$ signs stand for the forward or backward propagating waves, respectively, being α_i and γ_i the attenuation and Rayleigh coefficients of the i^{th} wave at frequency ν_i. The phonon occupancy factor is given by:

$$\eta_{ij} = \left[\exp\left(\frac{h(\nu_i - \nu_j)}{k_B T} - 1\right)\right]^{-1} \tag{3.2}$$

where h and k_B are the Planck and Boltzmann constants, respectively, and T is the fiber absolute temperature.

The frequencies ν_i are numbered by their decreasing value (the lower order corresponds to the higher frequency). By this way, the terms in the summation in

equation 3.1, from $j = 1$ to $j = i - 1$ cause amplification since the wave *i* is receiving power from the lower order waves (with higher frequency). For the same reason, the terms in the summation from $j = i + 1$ to $j = m$ originate attenuation. For mathematical convenience the gain spectrum was divided into spectral slices of width $\Delta\nu$, spanning the range over which ASE spectral components are significant.

The terms that contain a product of powers describe the coupling via stimulated Raman Scattering, being its strength determined by the Raman gain efficiency of the fiber, g_{ij} obtained by:

$$g_{ij} = \frac{\gamma_R \left(\nu_i - \nu_j\right)}{\Gamma A_{eff}} \tag{3.3}$$

where A_{eff} is the effective area of the fiber and the factor Γ is a dimensionless quantity comprised between 1 and 2 that takes into account the polarization random effects. The achieved gain, as well as the slope of the gain spectrum, depends on the transmission fiber [4], [5] as depicted in Figure 2.3.

To obtain a steady-state power distribution, the time derivative in 3.1 is settled equal to zero, and the set of equation takes the form of.

$$\begin{aligned}
\frac{dP_i^{\pm}(z)}{dz} = & \mp \alpha_i P_i^{\pm}(z) \pm \gamma_i P_i^{\pm}(z) \\
& \pm P_i^{\pm}(z) \sum_{j=1}^{i-1} g_{ji} \left[P_j^{+}(z) + P_j^{-}(z)\right] \\
& \mp P_i^{\pm}(z) \sum_{j=i+1}^{m} \frac{\nu_i}{\nu_j} g_{ij} \left[P_j^{+}(z) + P_j^{-}(z)\right] \\
& \mp 2h\nu_i \sum_{j=1}^{i-1} g_{ji} \left[P_j^{+}(z) + P_j^{-}(z)\right] (1 + \eta_{ji}) \Delta\nu \\
& \mp 4h\nu_i P_i^{\pm}(z) \sum_{j=i+1}^{m} g_{ij} (1 + \eta_{ij}) \Delta\nu
\end{aligned} \tag{3.4}$$

If the purpose of the simulation is to obtain only a gain profile [6], spontaneous Raman scattering and Rayleigh backscattering can be ignored in 3.4, and the system of equations become:

$$\begin{aligned}\frac{dP_i^{\pm}(z)}{dz} &= \mp \alpha_i P_i^{\pm}(z) \\ &\pm P_i^{\pm}(z) \sum_{j=1}^{i-1} g_{ji} \left[P_j^{+}(z) + P_j^{-}(z)\right] \\ &\mp P_i^{\pm}(z) \sum_{j=i+1}^{m} \frac{\nu_i}{\nu_j} g_{ij} \left[P_j^{+}(z) + P_j^{-}(z)\right]\end{aligned} \tag{3.5}$$

3.3 Numerical approaches

Basically, there are two distinct classes of numerical methods for solving BVP: shooting methods and relaxation methods [7]. The set of ODEs, which cannot be solved analytically have also to be implemented numerically through well known methods such as Runge-Kutta (RK), Adams-Bashforth (AB), Adams-Bashforth-Moulton (ABM), among others. However, for the specific application of Raman propagation equations, novel approaches have been devoloped, in order to provide fast and reliable solutions [8]. These techniques which are based on the above referred methods are able to support BVP solvers, such as shooting, by increasing their accuracy and efficiency. Since a complete revision of those numerical methods is beyond the scope of this thesis, only some example are provided, namely shooting method with enahnced Runge-Kutta developed by Xueming Liu [9]. Additonally, collocation method is presented and its application to Raman amplifiers through the Matlab solver *bvp4c* described extensively.

3.3.1 Shooting Method

In direct shooting methods, we choose values for all the dependent variables at one boundary, solve the system of ODEs as an IVP and verify if the obtained values on the other boundary are consistent with the stipulated values (boundary conditions) [7], [10], [11]. The IVP integration can be carried out by the fourth order Runge-Kutta methods with adaptative step-size, taking into account that its absolute stability region is (-2.785, 0) where Wilf criterion is fulfilled [12]. Then, the parameters are repeatedly changed using some correction scheme until this goal is attained. The selection of the correction scheme is crucial for stability and efficiency of the resulting algorithm [7]. The basic difficulty to shooting is that a perfectly nice BVP can require the integration of IVP that are unstable. The solution of a BVP can be insensitive to changes in boundary values, yet the solution of the IVP of shooting are sensitive to changes in

initial values.

The work developed by Liu and Lee [9] use direct shooting to solve backward or bidirectional pumping Raman amplifiers but the converted IVP is solved by an enhanced fourth-order Runge-Kutta method. This method was developed to promote faster convergence avoiding the solutions to blow up before reaching the end of the fiber. The method is described bellow.

Considering that an initial value problem can be written as:

$$\frac{d\mathbf{x}}{dt} = \mathbf{f}\left(t, \mathbf{x}\right) \tag{3.6}$$

where $\mathbf{x}$ is a vector given by $\mathbf{x} = \left[x_1\left(t\right), x_2\left(t\right), x_3\left(t\right), \ldots\right]$ with the following initial conditions:

$$\mathbf{x}\left(t = 0\right) = \mathbf{x}_0 \tag{3.7}$$

Numerical solutions based on Runge-Kutta (RK) are based on the iterative implementation of 3.8 and 3.9:

$$\mathbf{x}_{n+1} = \mathbf{x}_n + \sum_{i=1}^{m} w_i \mathbf{k}_i \tag{3.8}$$

$$\mathbf{k}_i = h\mathbf{f}\left(t_n + c_i, \mathbf{x}_n + \sum_{j=1}^{m} d_{ij}\mathbf{k}_j\right) \tag{3.9}$$

where $\{w_i, c_i, d_{ij}\}$ denote all the parameters and h the spatial step.

By introducing $\mathbf{y} = \ln \mathbf{x}$ and $\mathbf{g}\left(t, \mathbf{x}\right) = f\left(t, \mathbf{x}\right)/\mathbf{x}$, equation 3.6 becomes:

$$\frac{d\mathbf{y}}{dt} = \mathbf{g}\left(t, \exp\left(\mathbf{y}\right)\right) \tag{3.10}$$

According to the operational process of 3.8 and 3.9, the system of ODE can be solved as:

$$\mathbf{y}_{n+1} = \mathbf{y}_n + \sum_{i=1}^{m} w_i \mathbf{q}_i \tag{3.11}$$

$$\mathbf{q}_i = h\mathbf{g}\left(t_n + c_i, \exp\left(\mathbf{y}_n\right)\left(1 + \sum_{j=1}^{m} d_{ij}\mathbf{q}_j\right)\right) \tag{3.12}$$

Returning to the variable $\mathbf{x}$ and using the fourth-order Runge-Kutta method, the numerical implementation is given by 3.13 to 3.18:

$$\mathbf{x}_{n+1} = \mathbf{x}_n \exp\left[\left(\mathbf{q}_1 + 2\mathbf{q}_2 + 2\mathbf{q}_3 + \mathbf{q}_4\right)h/6\right] \tag{3.13}$$

$$\mathbf{q}_1 = \mathbf{g}\left(t_n, \mathbf{x}_n\right) \tag{3.14}$$

$$\mathbf{q}_2 = \mathbf{g}\left(t_n + h/2, \mathbf{x}_n + \mathbf{x}_n \mathbf{q}_1 h/2\right) \tag{3.15}$$

$$\mathbf{q}_3 = \mathbf{g}\left(t_n + h/2, \mathbf{x}_n + \mathbf{x}_n \mathbf{q}_2 h/2\right) \tag{3.16}$$

$$\mathbf{q}_4 = \mathbf{g}\left(t_n + h, \mathbf{x}_n + \mathbf{x}_n \mathbf{q}_3 h\right) \tag{3.17}$$

$$\mathbf{g}\left(t_n\right) = \mathbf{f}\left(t_n\right) / \mathbf{x}_n \tag{3.18}$$

The exponential change of variable $x = \exp(y)$ is advantageous in amplifier simulations because light amplification or attenuation resembles the exponential pattern with propagation distance. Thus, such a change of variable may lead to faster convergence than some linear or polynomial approximation.

The implementaion of the direct shooting using this enhanced Runge-Kutta formula, allows the solutions to reach the fiber end without crashing.

To demonstrate those results, a Raman amplifier with one 1550 nm probe signal with 1 mW of initial power and one 1450 nm backward pump signal with 0.5 W of initial power was implemented using direct shooting method with both fourth order Runge-Kutta (RK4) methods. The Raman efficiency was obtained from the SSMF values plotted in Figure 2.3. The solution that uses simple RK4 crashed at a maximum fiber length equal to 38 km, but the solution misleading behaviour was already assessible, as depicted in Figure 3.1 where the pump power solutions obatined through both methods along the fiber are plotted.

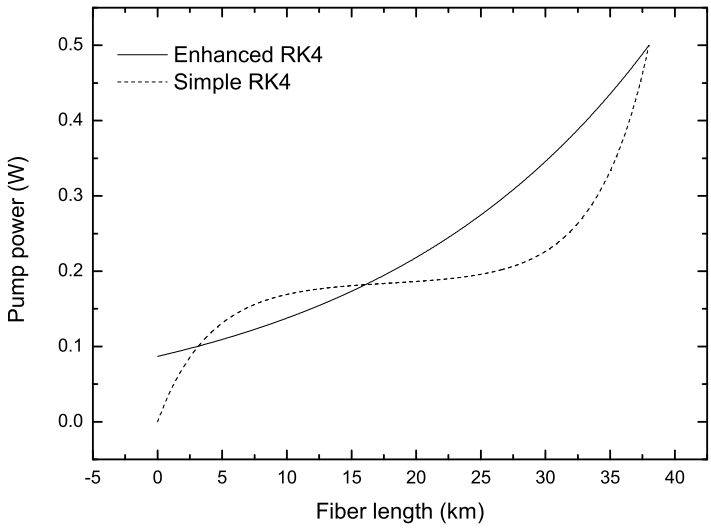

Figure 3.1: Pump power solutions obtained through direct shooting along the fiber length. (solid line) - Enhanced RK4, (dashed line) - Simple RK4.

Recently, some shooting algorithms with different correction schemes for the design of Raman fiber amplifiers have been proposed in order to improve convergence of the solutions even for larger fiber lengths [8]. This scheme is obtained by modifying the numerical method used to perform the IVP integration (fourth order Runge-Kutta, Runge-Kutta-Felhberg, etc [11]). In other variant of the shooting method, we can guess boundary values at both ends of the domain, integrate the equation to a common midpoint and repeatedly adjust the guessed boundary values so that the solution tends to the same value at the middle point. This adjustment task is usually performed by the Newton-Raphson method. Other approaches propose a shooting method to a fitting point using a correction scheme based on a modified Newton approach [13]. Therefore, by introducing the Broydens rank-one method [14] into the modified Newton method, the algorithm becomes more efficient and stable. This happens because the intensive numerical calculations of the Jacobi matrix are substituted by simpler algebraic calculations [13].

3.3.2 Collocation Method

An alternative to shooting methods can rely on expansion methods, namely collocation. Unlike shooting, collocation method approximate the solution over the whole interval of integration on a mesh of collocation points, z_i. The solution of the differential equations are then approximated by a polynomial in each sub-intervals $[z_i, z_{i+1}]$ where the boundary conditions in the midpoints and extremities must be

satisfied. The BVP becomes a system of algebraic non-linear equations that can be solved iteratively. It is important to remark that the resulting polynomials must be continuous functions in each sub-intervals and therefore the residuals are forced to become optimally zero or to reach an acceptable minimum [15], [16], [17].

The collocation method can be implemented by a MATLAB, *bvp4c*, which implements the collocation method for BVP in the interval $[z = 0, z = L]$. The function *bvp4c* is composed by three parts: the function *odes* to describe the ODEs, the function *bcs* to calculate the residuals and the function *bvpinit* to implement the mesh of points. An initial hint for the solution *guess* is also provided to start the iterations [18].

The needed computation time to implement *bvp4c* will depend mostly on the number of points on the mesh. The solver will provide a number of 10 points by default, however depending on the problem under study, other mesh configuration could be more benefitial. Another important issue rely on the fact that the algorithm can provide more than one solution compliant with the boundary conditions. So it is important to supply the solver with an initial hypothesis that can evolve to the desired solution. This guessed solution, given by *guess*, needs to take into account the behaviour of the system. Establishing this initial solution requires a particular knowledge of the problem and is definitely the most difficult task on using this method. To implement the solution of Raman propagation equations, the file *odes* is used to describe the sustem of ODEs, while the hint for the pumps was provided considering the small signal approximation situation and thus it includes only the effect of attenuation. For the transmission channels, the hint is a constant function equal to the initial power.

$$P_b^+(z_i) = \left(P_b^+\right)_0 \exp\left(-\alpha z_i\right) \tag{3.19}$$

$$P_b^-(z_i) = \left(P_b^-\right)_0 \exp\left(-\alpha\left(L - z_i\right)\right) \tag{3.20}$$

$$P_t(z_i) = \left(P_t\right)_0 \tag{3.21}$$

The solver *bvp4c* also controls the residuals in each iterations. The solution is found when the latter are uniform in all the points on the mesh and below 1×10^{-100}.

3.4 Stability analysis

An alternative to traditional numerical methods can rely on analytical approaches. Unlike numerical methods, a stability analysis can provide additional insights about the behaviour of the solutions in terms of trajectories in phase plane and in the vivinity of critical points. This knowledge is potentially very helful when a general understanding of the solutions is required.

The stability analysis of nonlinear systems is a mathematical formalism that allows the acquisition of qualitative information about the solution rather than the solutions itself. The methods employed are essentially geometrical making use of the representation of the solutions trajectories in the phase plane. These trajectories provide important information about the solutions behaviour, namely in asymptotic conditions and in the vicinity of the critical points, the ones where the derivatives are set equal to zero.

Consider a general autonomous system with the form $d\mathbf{x}/dt = \mathbf{A}\vec{x}$, where $\mathbf{A}$ is a 2×2 constant matrix and $\mathbf{x}$ is a 2×1 vector. The solution of such system has the form $\mathbf{x} = \xi e^{rt}$, which by direct substituion origins:

$$(\mathbf{A} - r\mathbf{I})\,\xi = 0 \tag{3.22}$$

Thus, r is an eigenvalue and ξ the corresponding eigenvector of the coefficient matrix $\mathbf{A}$. The eigenvalues are the roots of the following polynomial equation:

$$det\,(\mathbf{A} - r\mathbf{I}) = 0 \tag{3.23}$$

The critical points of the system are obtained making $\mathbf{Ax} = 0$ being the corresponding solutions constant on those points. According to the eigenvalues some assumptions about the stability of the critical point can be inferred, as summarized in Table 3.1. If the matrix $\mathbf{A}$ is singular, its determinant will not vanish and the only critical point is $\mathbf{x} = 0$.

Table 3.1: Stability properties of linear systems.

Eigenvalues	Type of critical point	Stability
$r_1 > r_2 > 0$	Node	Unstable
$r_1 < r_2 < 0$	Node	Asymptotically stable
$r_1 = r_2 > 0$	Saddle point	Unstable
$r_1 = r_2 < 0$	Proper or improper node	Unstable
$r_1, r_2 = \lambda + i\mu$	Proper or improper node	Asymptotically stable
$\lambda > 0$	Spiral point	Unstable
$\mu < 0$	Spiral point	Asymptotically stable
$r_1 = i\mu, r_2 = -i\mu$	Center	Stable

A general solution of equation 3.23 can be viewed as a parametric representation of a curve in the x_1x_2 plane, the so called phase plane. The shape of the curve in the vicinity of the critical point depends on the eigenvalues of the matrix and gives qualitative information about the systems stability [19], [20].

For the situation of nonlinear differential equations, qualitative information around the system critical points can still be inferred by linearizing the system. The

center manifold theorem is a powerful tool to analyze the dynamics of nonlinear systems near equilibrium points and states that associated with an equilibrium point there exists an invariant manifold containing that point. The manifold is unique for stable and unstable equilibrium points [21]. Therefore, it is possible to determine the eigenvalues in order to classify the system stability and also obtain analytical solutions that are valid in the vicinity of the critical point.

By looking at equations 3.5 , we notice that the origin $(P_i = 0)$ is an equilibrium point of system independently of the number of waves m. The stability of the equilibrium point can be determined by the stability of the following equivalent linearized system [22]:

$$\pm \frac{dP_i}{dz} = J_{ij} P_j \tag{3.24}$$

where *J* is the Jacobi matrix.

Concerning the study of Raman equations, our study will be previously focused on the simplest case, the one signal, one forward pump situation, for a matter of simplicity. Thus, the system is given by the set of equations 2.3 and 2.4. By setting the derivatives equal to zero, we obtain the following critical points:

$$\left(P_s^c, P_p^c\right) = (0, 0) \tag{3.25}$$

$$\left(P_s^c, P_p^c\right) = \left(-\frac{\alpha_s \nu_s}{g_R \nu_p}, \frac{\alpha_p}{g_R}\right) \tag{3.26}$$

Since the second critical point has a negative abscissa and both probe and pump signals powers must be positive values, the only point physically relevant is the origin of the phase plane.

To examine the local behavior of the solution near the critical point, we can neglect the nonlinear terms in equations 2.3 and 2.4 to obtain the corresponding linear system:

$$\frac{d}{dz}\begin{pmatrix} P_s \\ P_p \end{pmatrix} = \begin{pmatrix} -\alpha_s & 0 \\ 0 & -\alpha_p \end{pmatrix}\begin{pmatrix} P_s \\ P_p \end{pmatrix} \tag{3.27}$$

The eigenvalues and eigenvectors of 3.27 are respectively:

$$r_1 = -\alpha_s, \;\; \xi^{(1)} = \begin{pmatrix} 1 \\ 0 \end{pmatrix} \tag{3.28}$$

$$r_2 = -\alpha_p, \;\; \xi^{(2)} = \begin{pmatrix} 0 \\ 1 \end{pmatrix} \tag{3.29}$$

The solution is then given by the following equation:

$$\begin{pmatrix} P_s \\ P_p \end{pmatrix} = C_1 \begin{pmatrix} 1 \\ 0 \end{pmatrix} \exp\left(-\alpha_s z\right) + C_2 \begin{pmatrix} 0 \\ 1 \end{pmatrix} \exp\left(-\alpha_p z\right) \tag{3.30}$$

where the constants C_1 and C_2 are computed with the initial conditions.

The eigenvalues are both real and negative, so, by looking at Table 3.1 we conclude that the origin of the phase plane is a node asymptotically stable. It follows from equation 3.30 that when $z \to \infty$, $(P_s, P_p) \to 0$ regardless of the value of C_1 or C_2. In other words, all solutions approach the critical point as $z \to \infty$. If the solution starts on the line $\xi^{(1)}$ then $C_2 = 0$. Consequently the solution remains in the line $\xi^{(1)}$ for all z and approaches the origin as $z \to \infty$.

Returning to the nonlinear system 2.3 and 2.4, by dividing equation 2.4 by equation 2.3, we obtain the following:

$$\frac{dP_p}{dP_s} = \frac{-\left(\alpha_p + \frac{\nu_p}{\nu_s} g_R\right) P_p}{\left(-\alpha_s + g_R\right) P_s} \tag{3.31}$$

Equation 3.31 is separable and can be written in the following way:

$$\frac{-\alpha_s + g_R P_p}{P_p} dP_p = \frac{-\alpha_p + \frac{\nu_p}{\nu_s} g_R P_s}{P_s} dP_s \tag{3.32}$$

By integrating implicitly, we obtain the equation bellow:

$$\frac{\nu_p}{\nu_s} g_R P_s + \alpha_p \ln P_s - \alpha_s \ln P_p = C \tag{3.33}$$

where C is a constant of integration.

The representation of the curves assigned by equation 3.33 in the phase plane is designated by phase portrait of the system. For pump and signal wavelengths at 1445 nm and 1562 nm, the phase portrait is depicted in Figure 3.2. We plot only the first quadrant because only this part of the phase portrait is physically meaningful.

3.4.1 Lyapunov second method

The concept of Lyapunov stability is a broader method that requires no knowledge of the solution of the system of 3.24. The conclusions about the stability are obtained by constructing a suitable auxiliary function [23]. The technique is very powerful and provides a more global type of information being valid for equations that are definitely nonlinear.

Basically, Lyapunov second method is a generalization of two physical principles for conservative systems, (i) a rest position is stable if the potential energy is a local

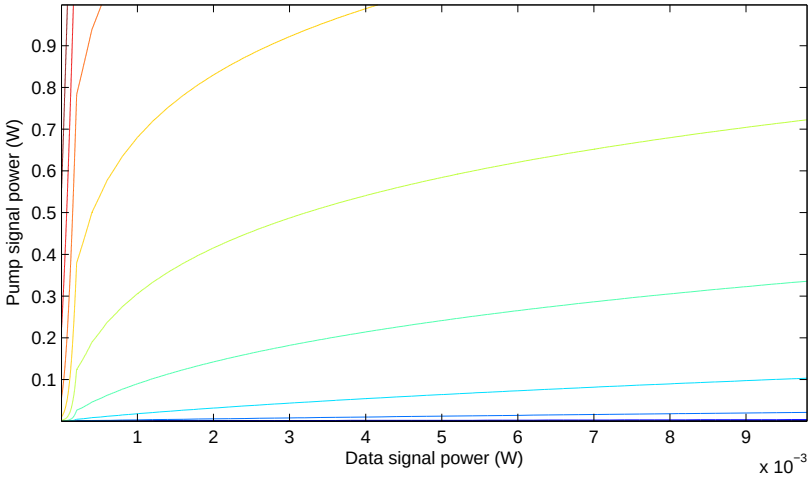

Figure 3.2: Phase portrait.

minimum, otherwise it is unstable, and (ii) the total energy is constant during any motion. Hence, to use Lyapunov second method to analyze the stability of the origin, a positive definite auxiliary function V that contains the critical point has to be constructed. This function has to be continuous, with continuous partial derivatives. If the derivative of that function is negative definite, then the origin is a asymptotically stable point.

For our problem, in the one forward pump one signal situation, V was defined as [22]:

$$V\left(P_p, P_s\right) = aP_p^2 + bP_pP_s + cP_s^2 \tag{3.34}$$

where $a > 0$ and $4ac > b^2$, with $P_p, P_s > 0$.

Since the partial derivatives in respect to P_1 and P_2 are continuous and V is positive definite for the domain of interest, we only need to study the signal of its spatial derivative. Thus:

$$\frac{dV}{dz} = \left(2aP_p + bP_s\right)\left(-\alpha_pP_p + g_RP_pP_s\right) + \left(2cP_s + bP_p\right)\left(-\alpha_sP_s - \frac{\nu_p}{\nu_s}g_RP_pP_s\right) \tag{3.35}$$

The derivative of V is negative definite if $c > a\nu_s/\nu_p$.

3.4.2 Second equilibrium point

For a general Raman amplifier with m waves, to obtain the second equilibrium point, it is necessary to solve the equation below:

$$-\alpha_i + A_{ij}P_j = 0 \tag{3.36}$$

where A_{ij} is given by:

$$A_{ij} = \left\{ \begin{array}{c} 0 \Longleftarrow i = j \\ -\frac{\nu_i}{\nu_j} g_{ij} \Longleftarrow i < j \\ g_{ij} \Longleftarrow i > j \end{array} \right\} \tag{3.37}$$

For waves with equally spaced frequencies Δ and simplifying g by a linear function of $\Delta\nu$ from 0 to 13 THz and zero elsewhere, matrix **A** is given by:

$$A_{ij} = \left\{ \begin{array}{c} 0 \Longleftarrow i = j \\ -\left(1 - \frac{\nu_i}{\Delta}\right)(j-i)\frac{g_{max}}{\Delta\nu_{max}} \Longleftarrow i < j \\ (j-i)\frac{g_{max}}{\Delta\nu_{max}} \Longleftarrow i > j \end{array} \right\} \tag{3.38}$$

For a generic number of equations m, it is not possible to find an expression for the inverse matrix A^{-1}, so the inverse must be computed for each situation using Gauss Jordan elimination or LU decomposition among other methods [24].

3.5 Average Power Analysis

The Raman propagation equations are also solvable through semi-analytical methods, using the average power analysis (APA) presented by Min *et al* [25]. This technique that proved to be successful in the simulation of multi-signal EDFAs [26] consists on the implementation of an analytical solution of the system over an infinitesimal length in which there is no powers dependency with position. Thus, the amplifier is splited into n small segments, in order to avoid the position dependency of the powers of equations 3.4, 3.5 which are then solved analytically in each segment, considering as input conditions the outputs provided by the solution on the previous segment. Equations 3.39 to 3.43 show how the powers are iteratively computed. The output pump/signal power at each section end is given by:

$$P_{out}^{\pm} = P_{in}^{\pm} G(z, \nu) \tag{3.39}$$

being $G(z, \nu)$ the section gain, as stated below.

$$G(z, \nu) = \exp\left[\left(-\alpha_\nu + A_\nu - B_\nu\right)\Delta z\right] \tag{3.40}$$

The constants, A_ν and B_ν are obtained through:

$$A_\nu = \sum_{j=1}^{i-1} g_{ij} \bar{P}_j \tag{3.41}$$

$$B_\nu = \sum_{j=i+1}^{m} g_{ij} \bar{P}_j \tag{3.42}$$

The optical power term in each section can be substituted by its length averaged values given by:

$$\bar{P} = P_{in}^{\pm} \frac{G_\nu - 1}{\ln G_\nu} \tag{3.43}$$

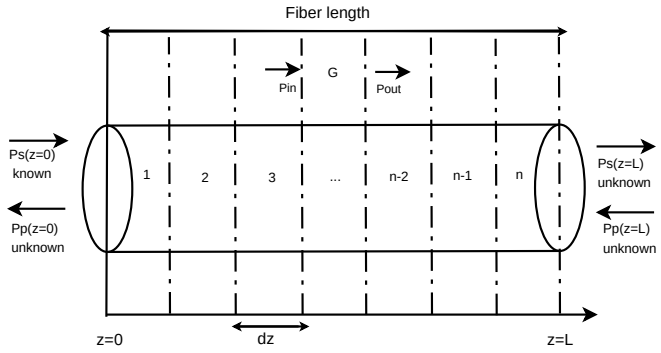

Figure 3.3: Sheme of the implemented method for one data signal and one backward pump.

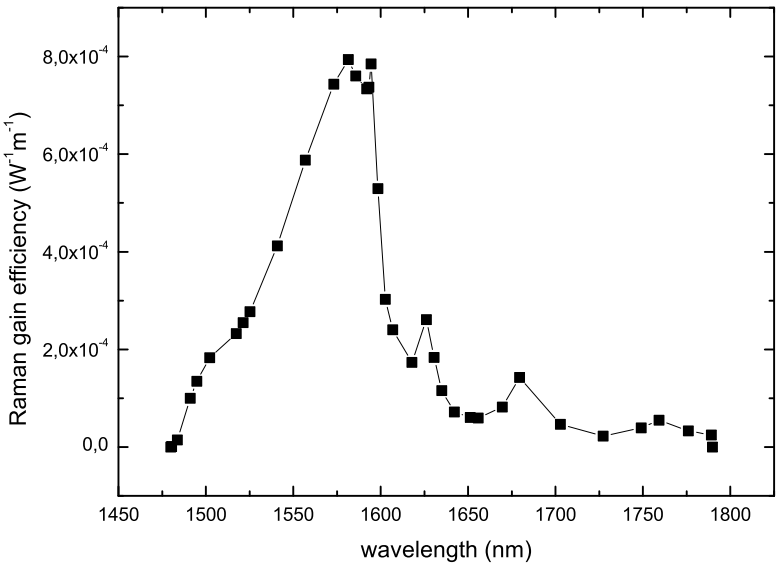

Figure 3.4: Raman gain efficiency spectrum. The points were obtained experimentally according to [27].

The numerical issues due to the backward pumping can be surpassed by assuming that the pump inputs are located at the same fiber end that the signal inputs. Therefore, the pump equations are integrated reversely as if they were backward by multiplying them by (-1). A guessed initial input is necessary to perform the integration, but the algorithm is able to adjust it using an optimization routine that

adjust the initial input until the output at the fiber end reaches the real backward pump input. A scheme of the procedure for the simpler situation of one data signal and one backward pump is depecited in Figure 3.3.

To demonstrate the numerical resolution of the steady-state Raman propagation equations, we assume the scheme in Figure 2.4, where three bidirectional pumps (two backward and one forward) and four probe signals are considered. The counter propagated pumps have power levels set equal to 0.1 W, working at 1450 nm and 1460 nm, respectively. The co propagated pump is working at 1470 nm with an output power also equal to 0.1 W. The forward pumping signal are then injected into 40 km of SSMF fiber and combined with 4×1000 GHz spaced C band probe signals with an initial optical power equal to 1 μW. The simulation has considered attenuation coefficients of 0.22 dB/km and 0.25 dB/km for data signals and pumps, respectively. The Raman gain efficiencies are the ones depicted in Figure 3.4 where an effective are of $80\ \mu m^2$) was considered. The convergence of solutions using a spatial step of 500 m was assessed previously and thus used in the APA implementation. The spatial evolution of pumps and probe signals are displayed in Figures 3.5 and 3.6.

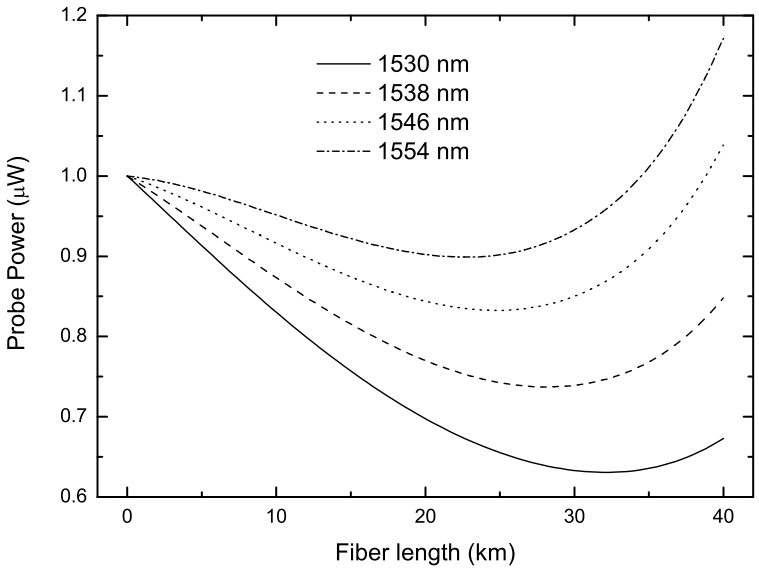

Figure 3.5: Spatial evolution of 2 counter propagated pumps, 1 co propagate pump and 4 probe signal along a 40 km SSMF fiber span amplifier. Probe signals evolution.

Although the backward or bidirectional pumping schemes require the use optimization routines to determine the conditions at $z = 0$ that could potentially increase the computational effort of the implementation, it remains efficient because a semi-analytical method is used to implement Raman equations. Indeed, the use of the APA approach has shown a reduction of two orders of magnitude in the computation

time, being the obtained results in agreement with the ones resulting from traditional numerical methods. In chapter 4, where optimization issues are studied, it will be demonstrated that APA is a very reliable method to accomplish a Raman amplifier simulator.

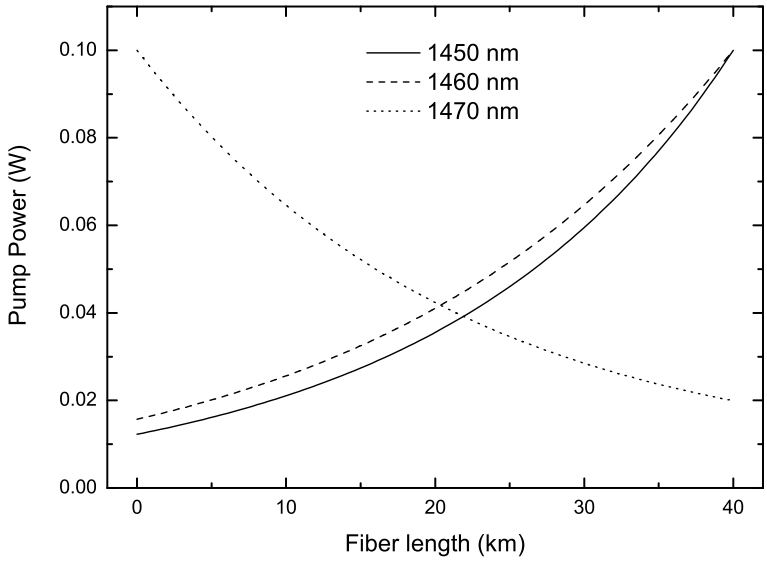

Figure 3.6: Spatial evolution of 2 counter propagated pumps, 1 co propagate pump and 4 probe signal along a 40 km SSMF fiber span amplifier. Pump signals evolution.

3.6 Experimental validation

To validate the results obtained from the numerical methods, namely collocation and APA, the experiments described in [28], [29] were carried .

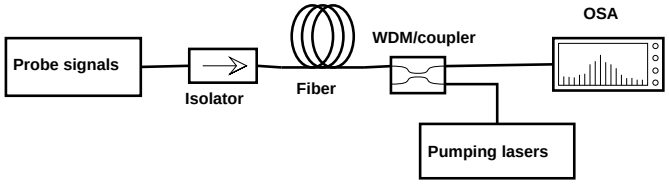

Figure 3.7: Scheme of the experimental setup.

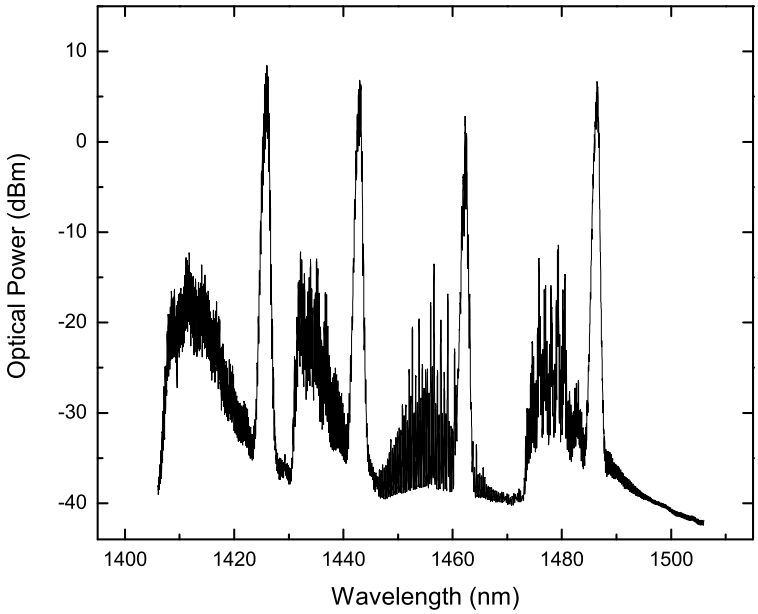

Figure 3.8: Measured optical spectrum for the 4-pump Raman module at 20 percent of the total power (A 3 dB attenuator was considered in this measurement).

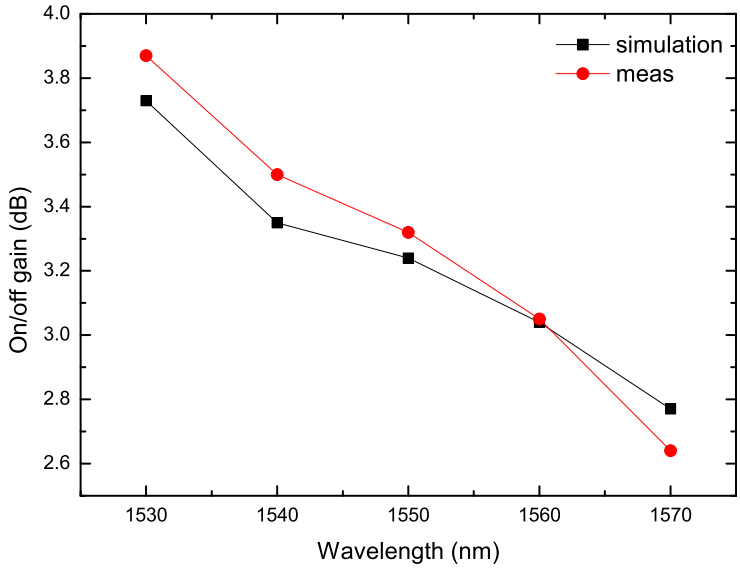

Figure 3.9: Measured and simulated on/off gain.

The setup is composed by a tuneable laser to generate the probe signals (1530, 1540, 1550, 1560 and 1570 nm) and a backward pumping module (Amonics ARA-

CL-4B-R) with 4 diode lasers at 1426, 1444, 1462 and 1487 nm. The propagating medium is 40 km of SSMF. A passive coupler is used to assemble the probe and pumps signals and an isolator was used before the fiber to protect the signal source, according to the scheme depicted in Figure 3.7. The used fiber Raman gain coefficient was based in previously published results [27]. We set the signal initial power equal to 3 dBm and measured the fiber input and output powers at each wavelength with a power meter. The signal power was firstly assessed with the pumping module off and then with the module at 20 percent of the total power. Afterward, the on/off gain was computed. Figure 3.8 depicts the spectrum of the 4-pump Raman module at 20 percent of total power (corresponding to the 78.14 mW, 55.76 mW, 15.80 mW and 59.20 mW for the pump signals), measured with an Optical Spectrum Analyser (Advantest), with a resolution of 0.1 nm. This configuration for the pumps optical powers produces the gain spectrum depicted in Figure 3.9. The reduced chi-square between the experimental and simulation data attained a value of 0.0655 which demonstrates that the experimental and simulation results are in good agreement. Further indirect experimental validations of the simulation were carried on, namely to study the enlargement and optimization of gain excamined in chapter 4.

3.7 Chapter summary

This chapter described the work that was carried out concerning the modeling of Raman Fiber amplifiers. It starts with an introduction that sets the main mathematical challenges on the implementation of Raman propagation equations, namely the intrinsic difficulties of nonlinear ordinary differential equations defined by boundary value problems. A mathematical model for multi-pump and multi-signal RFA is then introduced, given by the time and space evolution of pumps and signals, being a steady state model presented afterwards. The practical issues related to the numerical implementation of the steady state model are discussed and some methods are introduced such as shooting and collocation. Improvements to the traditional shooting are then discussed in terms of accuracy and efficiency, namely an enhanced Runge-Kutta method proposed by Xueming Liu. The numerical analysis proceeds with the explaination of collocation method and its practical implementation using the Matlab solver, *bvp4c* is also explained and discussed. After the survey on numerical methods, some analytical approaches are presented. Important insigths are provided by stability analysis and Lyapunov second method. In the scope of Raman propagation equations, we conclude that the only critical point with physical significance is the origin and that it is a node, asymptotically stable. The trajectories of the solutions in the phase plane demonstrate this conclusion. After that, efficient methods based on semi-analytical integration, such as APA are presented and their accuracy compared with pure numerical methods, as collocation.

References

[1] A. A. Tio and P. Shum, "Gain properties of multi-wavelength time division multiplexed raman amplifier," *Opt. Express*, vol. 14, no. 12, pp. 5061–5066, 2006. [Online]. Available: http://www.opticsexpress.org/abstract.cfm?URI=oe-14-12-5061

[2] M. Tang, P. Shum, and Y. Gong, "Design of double-pass discrete raman amplifier and the impairments induced by rayleigh backscattering," *Opt. Express*, vol. 11, no. 16, pp. 1887–1893, 2003. [Online]. Available: http://www.opticsexpress.org/abstract.cfm?URI=oe-11-16-1887

[3] I. Model, "Time-domain simulation of power transients in Raman fibre amplifiers," *Int. J. Numer. Model*, vol. 17, pp. 165–176, 2004.

[4] P. Andre, R. Correia, L. Borghesi, A. Teixeira, R. Nogueira, M. Lima, H. Kalinowski, F. Da Rocha, and J. Pinto, "Raman gain characterization in standard single mode optical fibres for optical simulation purposes," *Optica Applicata*, vol. 33, no. 4, pp. 559–574, 2003.

[5] J. Bromage, "Raman amplification for fiber communications systems," *Journal of Lightwave Technology*, vol. 22, no. 1, p. 79, 2004.

[6] V. Perlin and H. Winful, "Optimal design of flat-gain wide-band fiber Raman amplifiers," *Journal of lightwave technology*, vol. 20, no. 2, p. 250, 2002.

[7] W. Press, S. Teukolsky, W. Vetterling, and B. Flannery, *Numerical recipes in FORTRAN: the art of scientific computing*. Cambridge Univ Pr, 1992.

[8] X. Liu, "Fast and accurate algorithms for solving model equations of fibre amplifiers," *Journal of Optics A: Pure and Applied Optics*, vol. 6, p. 961, 2004.

[9] X. Liu and B. Lee, "Effective shooting algorithm and its application to fiber amplifiers," *Opt. Express*, vol. 11, no. 12, pp. 1452–1461, 2003. [Online]. Available: http://www.opticsexpress.org/abstract.cfm?URI=oe-11-12-1452

[10] U. Ascher, R. Mattheij, and R. Russell, *Numerical solution of boundary value problems for ordinary differential equations*. Society for Industrial Mathematics, 1995.

[11] L. Shampine, *Numerical solution of ordinary differential equations*. Chapman & Hall/CRC, 1994.

[12] A. Karim and I. Abbas, "The stability of the fourth order Runge-Kutta method for the solution of systems of differential equations," *Communications of the ACM*, vol. 9, no. 2, pp. 113–116, 1966.

[13] Q. Han, J. Ning, H. Zhang, and Z. Chen, "Novel shooting algorithm for highly efficient analysis of fiber raman amplifiers," *Lightwave Technology, Journal of*, vol. 24, no. 4, pp. 1946 – 1952, april 2006.

[14] J. Stoer and R. Bulirsch, *Introduction to numerical analysis*. Springer Verlag, 2002.

[15] G. Hall and J. Watt, *Modern numerical methods for ordinary differential equations*. Oxford University Press, USA, 1976.

[16] J. Kierzenka and L. Shampine, "A BVP solver based on residual control and the Maltab PSE," *ACM Transactions on Mathematical Software (TOMS)*, vol. 27, no. 3, p. 316, 2001.

[17] L. Shampine, J. Kierzenka, and M. Reichelt, "Solving boundary value problems for ordinary differential equations in Matlab with bvp4c," *Manuscript, available at ftp://ftp. mathworks. com/pub/doc/papers/bvp*, 2000.

[18] L. Shampine, I. Gladwell, and S. Thompson, *Solving odes with matlab*. Cambridge Univ Pr, 2003.

[19] W. Boyce and R. DiPrima, *Elementary differential equations and boundary value problems*. Wiley New York, 2001.

[20] M. Gockenbach, *Partial differential equations: analytical and numerical methods*. Society for Industrial Mathematics, 2002.

[21] E. Chauvet, J. Paullet, J. Previte, and Z. Walls, "A Lotka-Volterra three-species food chain," *Mathematics magazine*, vol. 75, no. 4, pp. 243–255, 2002.

[22] B. Neto, M. Rodrigues, E. Rocha, and P. Andre, "Stability analysis of raman propagation equations," in *Transparent Optical Networks, 2009. ICTON '09. 11th International Conference on*, june 2009, pp. 1 –4.

[23] J. La Salle and S. Lefschetz, *Stability by Liapunov's direct method: with applications*. Academic Press New York, 1961.

[24] S. Lipschutz and M. Lipson, *Schaum's outlines: linear algebra*. Schaum's Outline Series, 2008.

[25] B. Min, W. J. Lee, and N. Park, "Efficient formulation of raman amplifier propagation equations with average power analysis," *Photonics Technology Letters, IEEE*, vol. 12, no. 11, pp. 1486 – 1488, nov 2000.

[26] T. Hodgkinson, "Improved average power analysis technique for erbium-doped fiberamplifiers," *IEEE Photonics Technology Letters*, vol. 4, no. 11, pp. 1273–1275, 1992.

[27] M. Fugihara and A. Pinto, "Low-cost Raman amplifier for CWDM systems," *Microwave and Optical Technology Letters*, vol. 50, no. 2, pp. 297–301, 2008.

[28] B. Neto, C. Reis, A. Teixeira, P. Andre, and N. Wada, "Gain equalization technique for raman amplification systems based on the hybrid optimization algorithm," in *Microwave and Optoelectronics Conference (IMOC), 2009 SBMO/IEEE MTT-S International*, 3-6 2009, pp. 687 –689.

[29] D. Sperti, P. André, B. Neto, A. Rocha, A. Bononi, F. da Rocha, and M. Facão, "Experimental assessment of some Raman fiber amplifiers solutions for coarse wavelength division multiplexing applications," *Photonic Network Communications*, vol. 16, no. 3, pp. 195–202, 2008.

Chapter 4

Gain optimization of Raman amplifiers

4.1 Introduction

One of the most impressive features of Raman fiber amplifiers is assuredly the possibility to achieve gain at any wavelength, by selecting the appropriate pump wavelengths. By this way, it is possible to operate in spectral regions outside the Erbium doped fiber amplifiers bands over a wide bandwidth (encompassing the S, C and the L spectral transmission bands).The feasibility of this feature is assured by assembling several pumps through WDM couplers into a single fiber to realize a composite Raman gain. The composite Raman gain created by different pump wavelengths can therefore be taylored in order to be arbitrarily broad and equalized. The practical implementation of WDM-pumping requires that the pump lasers ought to have narrow and stable lasing spectra. Typically, laser diodes with output powers in the 100-200 mW range and operating in the 14XX nm region can be used in a multipump scheme. Until the mid-nineties of the twentieth century, the costs related to the deployment of those pumping lasers have been a barrier for the wide implementation of multipump Raman amplification. However, numerous efforts and the evolution of technology have allowed this field to evolve and nowadays high power pumps are commercially available. Theoretically, the higher the number of pumps, the better the gain equalization. Nevertheless there are economic and safety issues that prohibit the use of an arbitrary number of pumps. Thus, a balance between the system performance and the cost of amplification must be settled. The practical implementaion of Coarse WDM based systems had also open the way for the development of low cost Raman solutions because the latter are not demanding in terms of wavelength stability [1]. Thus, alternative pumping techniques, such as incoherent single pumping [2], [3], [4] [5], an array of low power pumps [6] or hiher order Raman pumping are valuable [7], [8].

Raman amplification using incoherent single pumping is a technique that proved to be sucessful on the purpose of providing flat gain at low cost. This pumping method approximates the pump spectrum by a high number of pumps with narrow spectral width, which in practise works as an array of pumps. In contrast to the conventional coherent pumping source, the pumping power of incoherent source spreads over a wide wavelength range from several nanometers to tens of nanometers,

being the phase and polarization completely random. Thus, the Four-wave mixing generation by the interaction of pump-pump, pump-ASE noise and pump-signal is significantly reduced. Another advantage of using incoherent pumping is that the polarization multiplexer for pumping sources can be eliminated due to the random polarization of pumping sources. In terms of gain equalization, the benefits of this technique are similar to multi-pumping, but there are competitive advantages in terms of power budget because expensive multiplexers with high insertion losses are no longer needed. A better noise performance is also obtained at lower cost. For Raman amplification using conventional coherent pumping, a bi-directional scheme is needed to obtain simultaneously equalized gain and noise figure, as well as OSNR, however, incoherent pump sources can improve the latter because the ASE peak can be shifted outside of the transmission window [9].

The techniques that makes use of an array of low power WDM pumps for Raman amplification has also demonstrated to be efficient, but the number of pumps to achieve Raman gain threshold must be high and the additional insertion losses resulting from multiplex them also need to be accounted for. However, this technique has the merit of using affordable lasers that lasers that in practise produce better performance in terms of gain enlargement then single pump. Published studies have suggested the feasibility of this technique for the amplification of L-band transmission channels using as pumps C-band lasers [6], among others assessments.

The multiple order Raman pumping is another interesting technique for gain enlargement and equalization that makes use of a single pump. As incoherent pumping, this technique needs no multiplexers, so the asociated insertion losses are no longer a problem. The performance improvement provided by higher-order cascaded counter-propagating Raman amplifiers arises from the fact that the final pump is developd within the transmission span itself and, as a result, the incoming signals are amplified earlier i.e. further from the receiver terminal. As shown in [10], the optical signal-to-noise ratio increases as the order of the Raman pumping is increased, at least for second- and third-order pumping. Bouteiller *et al* have shown the feasibility of a dual order Raman pump for telecommunications using a single laser cavity. By using this pumping technique, the performance in terms of noise figure is enhanced, allowing flexibility for gain flattening [7]. Six order cascaded Raman pumping using signgle Yb laser operating at 1091 nm was also demonstrated to be helpul in the purpose of gain flattening and an improvement of 10 dB in the power budget was presented [8].

The implementation of multipump Raman amplifiers presented several challenging features, namely the strong Raman interaction between the pumps (pump depletion). Since the higher frequency pump is responsible for the amplification of the lower frequency signals, more pumping power is needed, as some will also be transferred to the lower frequency pumps. This interaction between pumps also

affects the noise properties of the amplifier. However, some novel pumping schemes have been recently proposed in order to avoid those unwanted effects: time dependent Raman pumping, higher order pumping and broad-band pumping. Besides that, multipump architecture requires that the pump operating parameters (powers and wavelengths) must be properly settled in order to provide a defined level of gain. This technique, so-called pump allocation, is usually based on powerful algorithms that use time consuming heuristics.

The work presented in this chapter is mainly based on the implementaion of an optimization tool in a way that is pretented to be simultaneously accurate and efficient, followed by its subsequent experimental validation. A inovative heuristics based on hybrid genetic algorithm (GA) is presented and the performance results compared with simple GA. The results have demonstrated the feasibility of this metodology in a pratical context because the needed simulation efforts are compatible with the network reconfiguration times.

4.2 Multi-pump allocation

As said above the technique of multi-pump allocation consists on the determination of initial powers and emitting wavelengths of the lasers pumps that results on a flat gain around a pre-defined value. In such a metodology, the gain enlargement is an imediate consequence of the addition of more pumps. The principle beyond this technique is illustrated in Figure 4.1.

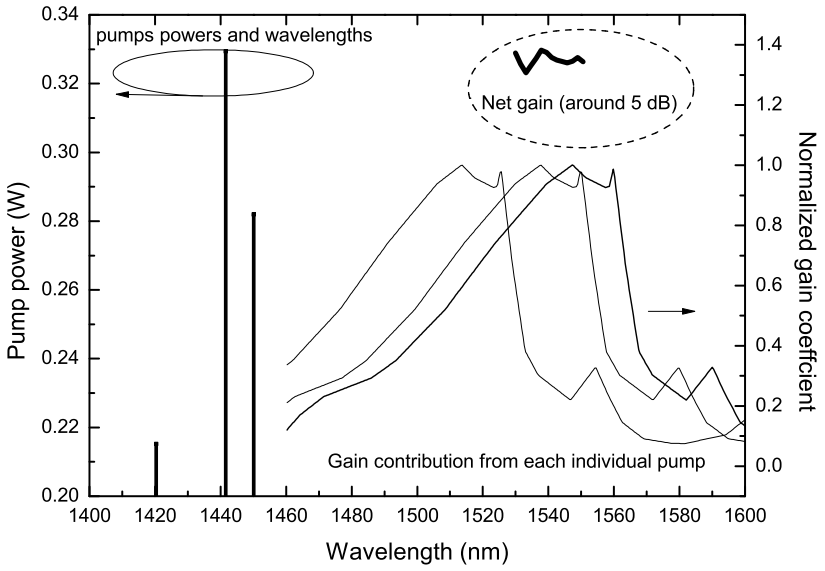

Figure 4.1: Gain enlargement and equalization using multi-pump allocation.

It is noticeable that the asymmetry of the Raman gain efficiency spectrum denotes that gain at the longest wavelengths is determined essentially by the location of the longest wavelength pumps signals. On the other hand, the shorter wavelengths receive gain contributions more uniformly from several pumps.

The gain equalization of channels in a small bandwidth by using a large number of pumps is an easy tasks that a priori does not require the use or sophisticated optimizations methods. On the other way, achieving a flat gain on a large bandwidth (80-100 nm) using a small number of pumps (typically bellow 12) is a very cumbersome task which requires the use of metaheuristics [11], [12].

The use of those methods for optimization for the gain spectrum has been widely performed, namely neural networks [13], simulated annealing [14] and genetic algorithm (GA) [15]. This optimization problem has multi-variables (the pumping parameters, usually twice the number of pumps) and can also be multi-objective if additional conditions are settled. During the search process, the pump powers and frequencies are directly substituted into the system of propagation equations to calculate de gain profile. Hence, the optimization involve the resolution of a highly nonlinear problem. Depending on the speed of the numerical method used to integrate the system of equations, the amount of numerical computations involved can be considerably large and the optimization inevitably time consuming. Those solutions are not suitable for practical applications where the real optimal solution must be provided in a short time.

4.3 Metaheuristics

In computer science, a heuristic is a technique designed to solve a problem that ignores whether the solution can be proven to be correct, but which usually produces a good solution or solves a simpler problem that contains or intersects with the solution of the more complex problem [16]. An heuristic can be designated by metaheuristic if the solving is based on the combination of back-box procedures, which are usually heuristics too. Depending on the type of problem which needs to be solved, the option for a metaheuristic should be cautious because the latter can be wasteful if used indiscriminately and straitforward methods such as gradient based are much more efficient.

The problem of gain optimization is typically suitable for metaheuristics because it is multi-variable, highly nonlinear and presents constraints.

Genetic algorithms belong to the vaste body of evolutionary algorithms which mimics the evolution of species [17]. In the context of the evolutionary algorithms, the individuals that are subjected to evolution are the solutions, more or less efficient, for a given problem. These solutions belong to the search space of the optimization problem. If the problem is minimization one the best outcome is zero and the

proximity to that value is designated by fitness. The set of the individuals treated simultaneously by the evolutionary algorithm constitutes a population. It evolves during a succession of iterations called generations until a termination criterion, which takes into account a priori the quality of the solutions obtained, is satisfied. During each generation, a succession of operators is applied to the individuals of a population to generate the new population for the next generation. When one or more individuals are used by an operator, they are called the parents. The individuals originating from the application of the operator are their offspring. Thus, when two operators are applied successively, the offspring generated by one can become parents for the other.

The selection is the way to choose from the individuals of a population of possible solutions the ones who will create offsprings for the next generations, and how many offsprings each of them will create. The purpose of selection is to distinguish between the fitter individuals in the population in hope that their offsprings will in turn have even better fitness [17] [18].

The variation operators allow the algorithm to find better solutions than those represented in the current population. The variation operators are able to transform a given solution that was previously produced recurring to the selection operator. They are classified into two categories:

1. mutation operators produce random change in an element of a string within the given population;

2. crossover operators exchange the string fragments between two selected. members of the population.

There are many ways of implementing the crossover, for example having a single crossover point or multiple points which are randomly selected. A priori, it is not possible to identify the most adequate crossover because its success and failure depends on the particular fitness function, on the encoding and on other details [19]. The selection combined with the crossover gives the GA the bulk of its processing power. The mutation is a random change in an element of a string within the given population. As a matter of fact the mutation operator plays a secondary role in the GA, being considered as a secondary mechanism of its adaptation. The working principle of those operators, namely single point crossover and uniform mutation are summarized in Figure 4.2. In single point crossover, the string is broken in two and the two, being the resulting fragments recombined. In mutation a bit in the string can randomly change its value.

In each generation, a generic evolutionary algorithm implements the loop iteration summarized in Figure 4.3 that incorporates the application of the above mentioned operators on the population:

1. for the reproduction, selection of the parents among a population of n individuals to generate m offspring;

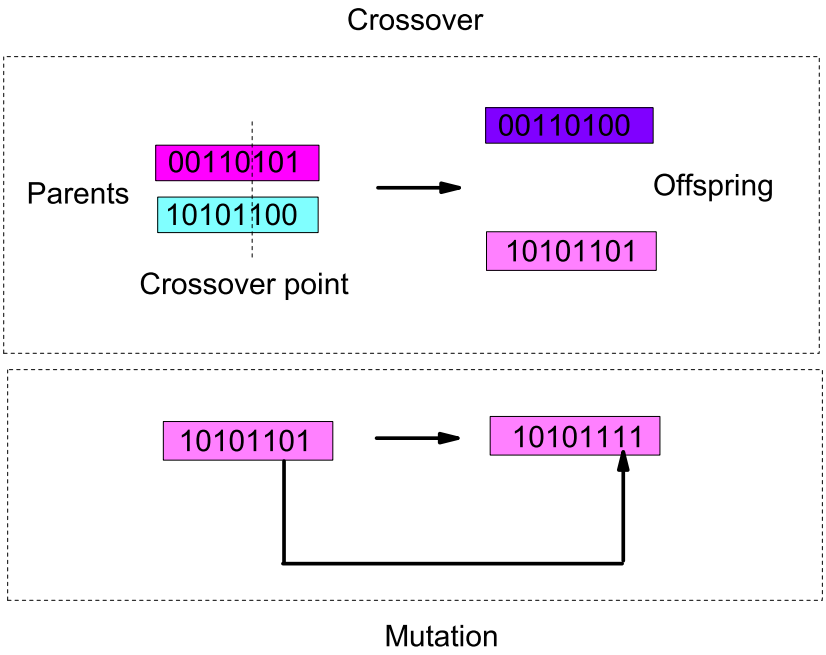

Figure 4.2: Crossover and mutation operation scheme.

2. crossover and mutation of the m selected individuals to generate m offspring;
3. fitness evaluation for the offspring;
4. selection for the survival of n individuals among the m offspring and n parents, or only among the m offspring, according to the choice made by the user, in order to build the population for the next generation.

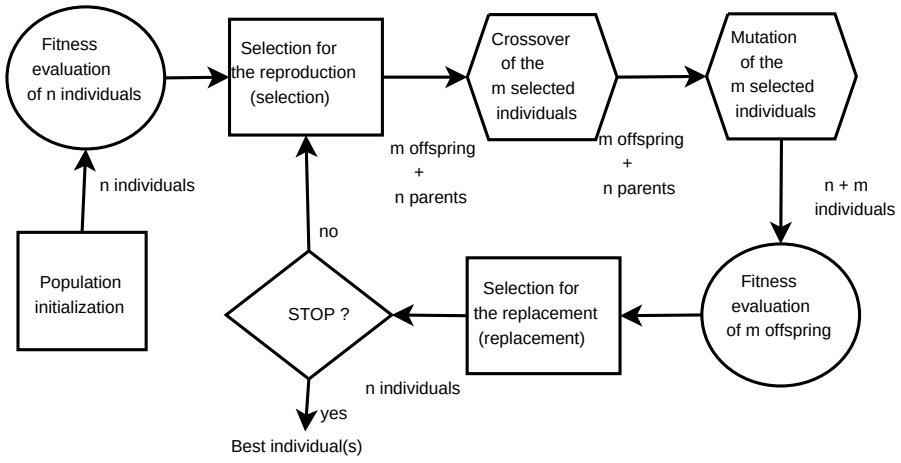

Figure 4.3: The generic evolutionay algorithm.

Although an intensive comprehention of evolutionary computation is beyond the scope of this thesis, it is important to understand how the algorithm was implemented

to surpass the issues related to selective pressure. Indeed, there is a large amount of work.

The performance of a genetic algorithm, like any global optimization algorithm, depends on the mechanism for balancing the two conflicting objectives: exploiting the best solutions and their ability to reproduce and at the same time exploring the search space for promising solutions. In theory, the GA can combine both exploration and exploitation at the same time if the following conditions are verified [20]:

1. the population is infinite;

2. the fitness function accuratey reflects the utility of a solution;

3. the genes in a chromossome do not interact significantly.

In practice, the population size is finite, which influences the sampling ability of a genetic algorithm and as a result affects its performance. Due to its limited population size, a genetic algorithm may also sample bad representatives of good search regions and good representatives of bad regions. Thus, two important issues must be accounted when dimensioning the selection operator: the maintenance of diversity within the population and the selective pressure. These concepts can be understand as the pression that individuals fitness exert on the overall evolution. The individuals having the best fitnesses are reproduced more often than the others and replace the worst ones. If the variation operators are inhibited, the best individual should reproduce more quickly than the others, until its copies completely take over the population. Thus the selective pressure will decide whether the algorithm produces premature convergence or not. The stochastic nature of the selection operator also introduce errors designated by genetic drift [21], [22].

There are several schemes for the selection process probability methods, scaling techniques, tournament, elitist models and ranking models [17]. Probability methods, such as roulette wheel, assign a probability of selection, P_j to each individual *j* based on its fitness value. Thus, a serie of N random numbers of individuals is generated and compared against the cumulative probability of the population, $C_i = \sum_{j=1}^{i} P_j$. In the particular case of roulette wheel the propability of selection is given by:

$$P_i = \frac{F_i}{\sum_{j=1}^{PopSize} F_j} \tag{4.1}$$

Ranking methods assign P_i based on the rank of a solution *i* when all solutions are sorted. In the case of normalized ranking, the probability of selection is given by [23]:

$$P_i = q' \left(1 - q\right)^{r-1} \tag{4.2}$$

where q is the probability of selection the best individual, r, the rank of the individuals considering that 1 is the best and q' is:

$$q' = \frac{q}{1-(1-q)^{PopSize}} \tag{4.3}$$

Tournament selects j individuals randomly, with replacement from the population and inserts the best of the j into the new population, repeating the process until N individuals are selected.

In stochastic universal selection, we considers a straight line segment partitioned in as many zones as there are individuals in the population, each zone having its size proportional to the fitness. However, the selected individuals are designated by a set of equidistant points, their number being equal to the number of offsprings. This method is different from the proportional methods as here only one random drawing is required to place the origin of the series of equidistant points and thus to generate all the offspring in the population. As a results, the variance of the process being weaker than in the roulette wheel method, the genetic drift is smaller. The issue of genetic drift was considered as the dominant one in the optimization of Raman gain spectrum.

A more deterministic selection option is Remainder, which performs two steps. In the first step, the function selects parents deterministically according to the integer part of the scaled value for each individual. For example, if an individual's scaled value is 2.3, the function selects that individual twice as a parent. In the second step, the selection function selects additional parents using the fractional parts of the scaled values, as in stochastic uniform selection. The function lays out a line in sections, whose lengths are proportional to the fractional part of the scaled value of the individuals, and moves along the line in equal steps to select the parents. Note that if the fractional parts of the scaled values all equal 0, as can occur using Top scaling, the selection is entirely deterministic [24] .

Incorporating a local search method within a genetic algorithm can help to overcome most of the obstacles that arise as a result of finite population sizes. Although genetic algorithms can rapidly locate the region in which the global optimum exists, they take a relatively long time to locate the exact local optimum in the region of convergence [25]. A combination of a genetic algorithm and a local search method can speed up the search to locate the exact global optimum. In such a hybrid methodology, applying a local search to the solutions that are guided by a genetic algorithm to the most promising region can accelerate convergence to the global optimum. The time needed to reach the global optimum can be further reduced if local search methods and local knowledge are used to accelerate locating the most promising search region in addition to locating the global optimum starting within its basin of attraction.

To enhance the efficiency of the GA, without any expense of accuracy, some hybrid approaches have been proposed. A combination of GA and simulated annealing is employed in [26] to optimize the power levels of 20 equally spaced pumps. GA is implemented and a simulated annealing step is inserted after mutation to renew the population of solutions and avoid premature convergence. Despite the flattening of the spectral gain was achieved over a 100 nm bandwidth, the obtained ripple remains relatively high (0.74 dB). Hybrid GA based upon clustering, sharing, crowding and adaptative probability is used in [27]. This methodology explores the possibility of finding multiple optima instead of only one by forcing the GA to maintain a diverse population throughout its search. Therefore, several pumps schemes were tested (with 2, 3, 4, 5, 6 and seven pumps) having been demonstrated that the improvements in flattening the gain decrease the signal bandwidth.

4.4 Hybrid Genetic Algorithm

Considering the above reffered issues, the use of a hybrid GA (GA combined with local search method) was the preferred methodology used in this thesis for the gain optimization of broadband Raman amplifiers. Our approach is based on performing GA until it reaches the optimal region instead of the optimal solution itself. The remaining search can be done with the local search method. The question is to decide the right moment to switch from one method to the other so that the algorithm improves its optimization efficiency without lack of accuracy.

The Nelder-Mead method attempts to minimize a scalar-valued nonlinear function of N real variables using only function values, without any derivative information (explicit or implicit). The Nelder-Mead method thus falls in the general class of direct search methods [28].

The method uses the concept of a simplex, which is a special polytope of $N + 1$ vertices in N dimensions. Examples of simplices include a line segment on a line, a triangle on a plane, a tetrahedron in three-dimensional space and so on.

In the Matlab environment the Nelder-Mead is implemented in the optimization toolbox using the function *fminsearch*. The algorithm first makes a simplex around the initial guess x_0 by adding 5 percent of each component $x_0(i)$ to x_0, and using these N vectors as elements of the simplex in addition to x_0. Then, the algorithm modifies the simplex repeatedly according to the following procedure.

1. Let $x(i)$ denote the list of points in the current simplex, $i = 1, ..., N + 1$.

2. Order the points in the simplex from lowest function value $f(x(1))$ to highest $f(x(N + 1))$. At each step in the iteration, the algorithm discards the current worst point $x(N+1)$, and accepts another point into the simplex. [Or, in the case of step 7 below, it changes all N points with values above $f(x(1))$].

3. Generate the reflected point:

$$r = 2m - x(N+1)$$

where

$$m = \sum \frac{x(i)}{N}, i = 1, ..., N$$

and calculate $f(r)$

4. If $f(x(1)) \leq f(r) < f(x(n))$, accept *r* and terminate this iteration. **Reflect**

5. If $f(r) < f(x(1))$, calculate the expansion point *s*

$$s = m + 2\left[m - x(N+1)\right]$$

and calculate $f(s)$.

- If $f(s) < f(r)$, accept s and terminate the iteration. **Expand**
- Otherwise, accept *r* and terminate the iteration. **Reflect**

6. If $f(r) \leq x(N)$, perform a contraction between *m* and the better of $x(N+1)$ and *r*:

- If $f(r) < f(x(N+1))$ (i.e., *r* is better than $x(N+1)$), calculate

$$c = m + \frac{(rm)}{2}$$

and calculate If $f(c) < f(r)$, accept *c* and terminate the iteration. **Contract outside**.
Otherwise, continue with Step 7 (Shrink).

- If $f(r) \geq f(x(N+1)$,

$$cc = m + \frac{(x(n+1)m)}{2}$$

and calculate $f(cc)$. If $f(cc) < f(x(n+1))$, accept cc and terminate the iteration. **Contract inside**. Otherwise, continue with Step 7 (Shrink).

7. Calculate the N points:

$$v(i) = x(1) + \frac{(x(i)x(1))}{2}$$

and calculate $f(v(i)), i = 2, ..., N+1$.
The simplex at the next iteration is $x(1), v(2), ..., v(N+1)$ **Shrink**

The scheme depicted in Figure 4.4 shows the points that *fminsearch* might calculate in the procedure, along with each possible new simplex. The original simplex has a bold outline. The iterations proceed until they meet a stopping criterion.

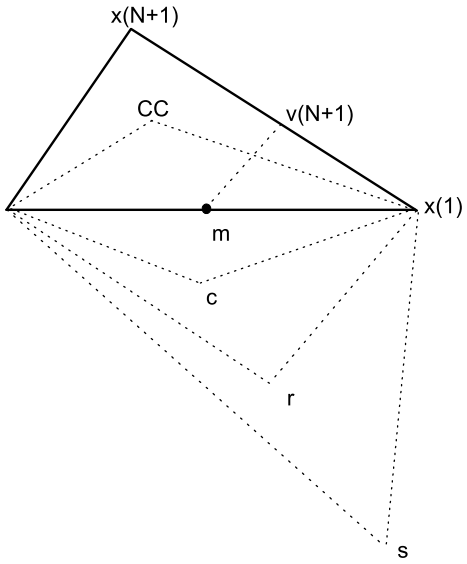

Figure 4.4: Scheme of the Nelder-Mead algorithm.

4.5 Simulation implementation

To enlighten the conclusions presented in the above section, we present the pratical situation depicted in Figure 4.5. It is composed by 5 backward pumps injected into the fiber by a multiplexer coupler and 16×400 GHz (from 1529.55 nm to 1577.86 nm) with an initial power of 1 mW. Pumps and probe signals are then combined and injected into 25 km of SSMF fiber. The signals were analyzed recurring to an optical spectrum analyser (OSA) [29].

The simulation was carried out in a Matlab environment using the APA code described in chapter 3 and the genetic algorithm toolbox [30] [23]. The toolbox enables the implementation of different standardized operators for selection, crossover and mutation. The fitness function was settled as the norm of the vector given by the difference between each signal net gain and a target value. Additionally, a penalty function was introduce to avoid the exploration of unwanted regions in the search space, namely, negative valued powers and wavelengths.

The gain optimization simulation with this hybrid GA algorithm provided a mean ripple below 0.17 dB. The optimized values for the pumps powers and wavelengths are listed on Table 4.1.

4.5.1 Dimensioning of operators

Although the hybrid GA is always able to perform the gain optimization with a ripple below 0.5 dB, some steps can be taken to improve the optimization in order

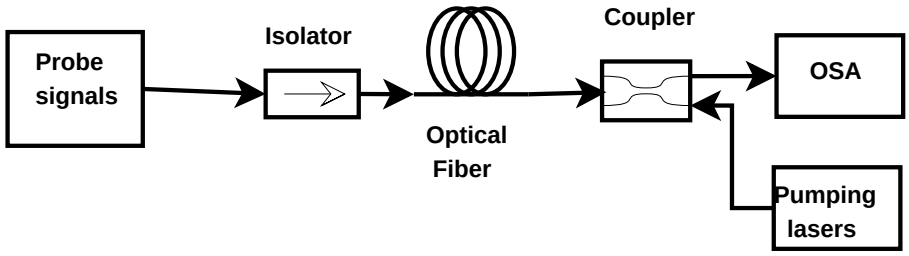

Figure 4.5: Scheme of the implemented setup for the 5 pumps scenario.

Table 4.1: Optimized pumps wavelengths and powers.

Pumps	Wavelengths (nm)	Powers (mW)
1	1424.42	142.23
2	1433.28	89.58
3	1441.44	117.29
4	1464.71	187.54
5	1481.19	124.03

to reduce the number of function evaluations. The initial population where the GA is achieved, as well as the GA operators, can be properly dimensioned so that the algorithm is brought nearer the optimum in a faster way. Another important feature is the number of generations needed to perform the GA before switching to the direct search method. It is expectable that the increase in the number of generations provides more chances to produce good fitted individuals enhancing in this way the process of finding the minima. But the use of the hybrid configuration, i. e, the use of the GA followed by a direct search method can avoid this necessity whenever the minima reached by the GA are small enough.

The initial population range is the limit established for pump powers and wavelengths at one end of the fiber. In the backward pumping scheme, the input power values are not the real ones because the equation is integrated reversely. So, it is advisable to try previously some values and to look to the output power values at the other end of the fiber. Since the higher frequency pumps transfer more power to the other waves it is expectable that at the end of the fiber length their powers are lower. Therefore, it is advisable to try lower power values for the higher frequency pumps and then increase them for the lower frequency pumps. Regarding the pumps wavelengths, theoretical assumptions about Raman gain spectrum state that in order to obtain a maximum gain, the signal beam is downshifted from the pump frequency by 13.2 THz (about 100 nm in the 1500 nm region) [31] [32] [33]. So, it is advisable to divide our spectral range into the number of pumps and then downshift those values by 13.2 THz.

A good choice for the initial population range, i.e., a population range that

allows an exhaustive search from the algorithm is very important, because the next generations are framed upon the best fitted members of the previous generation. Based on the above mentioned statements and taking our five backward pumps problem, the initial population for the powers are comprised between 1 mW and 10 mW for the first three higher frequency pumps. The powers for the other pumps are settled between 10 mW and 100 mW. The initial population for the wavelengths are [1430; 1440] nm, [1440; 1450] nm, [1450; 1460] nm; [1460; 1470] nm and [1470; 1480] nm, respectively.

In general it can be stated that the higher the number of individuals, the better the fitness. Therefore, a better minimum will be found at the end of the run of the GA. The inconvenient is that the running time can be too long because the simulation time is proportional to the population size. In our scenario, we decided to perform the GA 10 times (since the random nature of GA will produce a different result at each run) and to record the optimized gain ripples at the end of the first generation. Populations with 25, 50, 75 and 100 individuals were tested. For each population, the mean of the optimized ripples and the standard deviation were listed in Table 4.2. Although the listed values suggest that higher sized populations present better minima, the improvement is not worthwhile due to the increase in the simulation time. It should be noted that exceptions to that rule sometimes occur on account of the above mentioned random nature of this algorithm.

Table 4.2: Optimized ripples (means and standard deviations) obtained in 10 trials at the end of the first generation for population sized with 25, 50, 75 and 100 individuals.

Population size	Mean value (dB)	Standard deviation (dB)
25	4.176	0.596
50	3.871	0.464
75	3.607	0.449
100	3.591	0.587

The considered GA selection methods are: stochastic uniform, roulette wheel, tournament and remainder, which were explained section 4.3. For crossover we can try different functions as heuristic, single point, two points, intermediate, and scattered, which designates the way in which the individuals string is fragmented and reconfigured. Heuristic crossover produces a linear extrapolation of the two individuals taking into account their fitness values. The mutation can be performed in two ways: uniform or gaussian. The uniform mutation selects one individual and adds a random variable. A disadvantage of this mutation method is that it does not prevent the solution of being trapped in a local minimum. Gaussian mutation adds to an individual a Gaussian random variable $N(0, \sigma)$, of zero average and standard

deviation σ, which has a probability density of:

$$f(y) = \frac{1}{2\pi\sigma} \exp\left(-\frac{1}{2}\left(\frac{y}{\sigma}\right)^2\right) \tag{4.4}$$

Several computational experiments for the five backward pumps problem were performed taking different kinds of selection methods: stochastic uniform, roulette wheel, tournament and remainder. For each selection method, ten simulations were carried out and the optimized ripples at the end of the GA were registered. Those values are shown in Table 4.3. From the listed results (mean and standard deviation) it is possible to conclude that the stochastic uniform method is the most appropriate selection method for our purposes, being the tournament method the one that presents the worse results.

Table 4.3: Optimized ripples (means and standard deviations) obtained in 10 trials for different types of selection methods at the end of 10 generations.

Selection	Mean value (dB)	Standard deviation (dB)
Stochastic Uniform	2.139	0.435
Roulette wheel	2.323	0.635
Tournament	2.768	0.637
Remainder	2.477	0.653

In order to find the best crossover function for our purposes, a GA with a population size of 25 individuals was run along with 10 generations for the five backward pumps problem. Among the available crossover functions, we concluded that best one is the scattered crossover and the worse one is the intermediate crossover, as displayed in Table 4.4 where the mean values of the optimized ripples for ten trials are displayed as well as their standard deviation.

Table 4.4: Optimized ripples (means and standard deviations) obtained in 10 trials for different types of crossover methods at the end of 10 generations.

Crossover	Mean value (dB)	Standard deviation (dB)
Scattered	2.139	0.435
Two points	2.541	0.561
Intermediate	2.809	0.501
Single point	2.267	0.618
Heuristic	2.566	0.775

Lastly, the same procedure was implemented for the mutation operator, being the optimized ripples (mean and standard deviation) listed in Table 4.5. The best mutation operator is uniform.

Table 4.5: Optimized ripples (means and standard deviations) obtained in 10 trials for different types of mutation methods at the end of 10 generations.

Mutation	Mean value (dB)	Standard deviation (dB)
$Uniform$	2.139	0.435
$Gaussian$	2.446	0.725

In conclusion the best GA operators are stochastic uniform for selection, scattered for crossover and uniform for mutation.

4.5.2 Dimensioning hybrid GA

After checking the most adequate GA operators for the defined 5 backward pumps problem, it is time to implement the hybrid algorithm (the GA followed by the Nelder-Mead method). We said previously that this methodology was efficient and accurate. To prove that the hybrid GA is more accurate then the simple GA, we have implemented it and registered the optimized ripples of the simple GA and hybrid GA with the number of generations. A population of 50 individuals was considered and the adequate operators found in the section above were used. The Nelder-Mead algorithm runs until the average change of the objective function, defined here as the best attained gain ripple, is less than 1×10^{-6}.

In Figure 4.6, the GA and the hybrid GA minima are plotted for different number of generations. It is clear that even when the algorithm is switched at a higher minimum (the 5 generations situation) the Nelder-Mead method is able to reach a desirable minimum. Hence, the hybrid method is assuredly more accurate then the simple GA. It is also noticeable that the GA minima present exponential decay behaviour ($r^2 = 0.99549$) with the number of generations and consequently present an asymptotic behaviour as the number of generations increase unlimitedly. Thus, we can conclude that it is not worthwhile the unlimited increase the number of generations in the hope of improving the method accuracy. To improve the efficiency of the hybrid GA, we have to identify which situation is the fastest or, alternatively, to identify the right moment to switch from one method to another. By examining Figure 4.6, we realize that the ripple variation performed by the Nelder-Mead method is higher for GA with smaller number of generations (bellow 15), so it is expectable that more function evaluations are needed and consequently more computational time.

Considering the 5 generations situation as a reference, we decided to plot the relative computational time and the ripple variation attained by the Nelder-Mead method against the number of generations and display the results in Figure 4.7. Since both results decay when the number of generations is increased, the Nelder Mead time is primarily dependent of the ripple value where it starts the search.

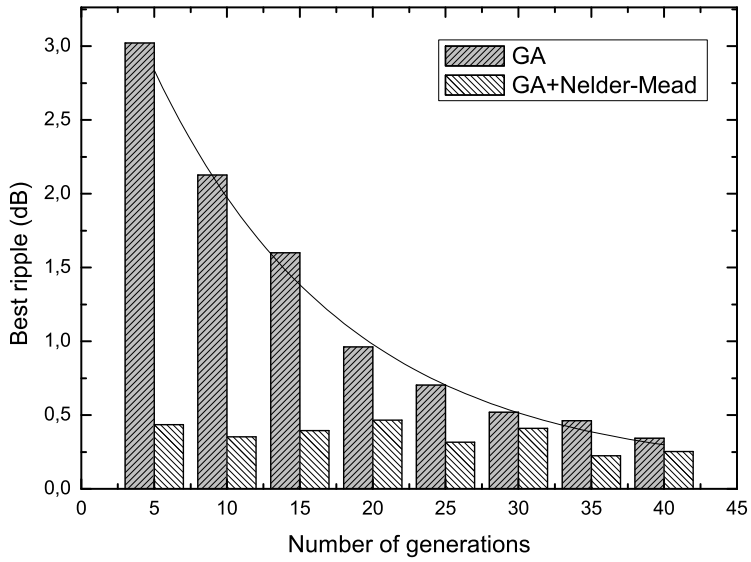

Figure 4.6: Optimized ripples at the end of the GA and the hybrid GA for different number of generations for a population size of 50 individuals. The line is the exponential interpolation.

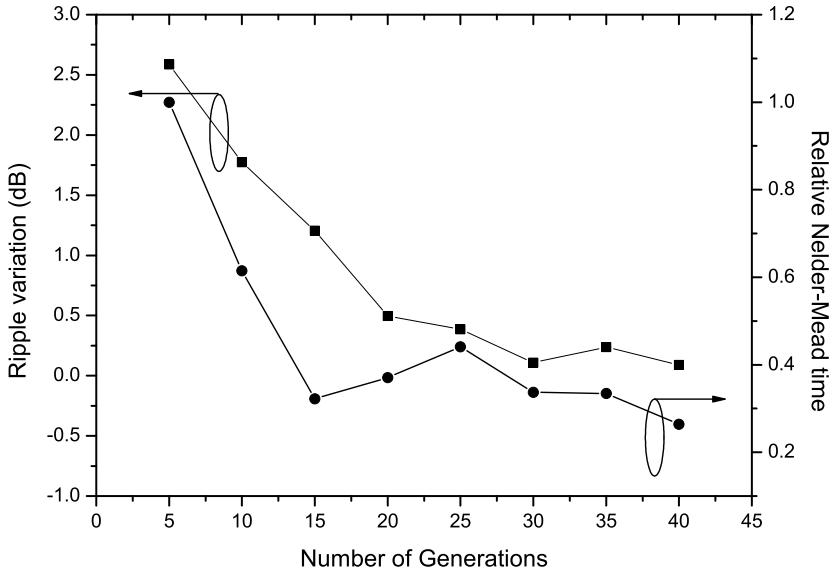

Figure 4.7: Relative Nelder-Mead time and the corresponding ripple variation. The lines are visual guides.

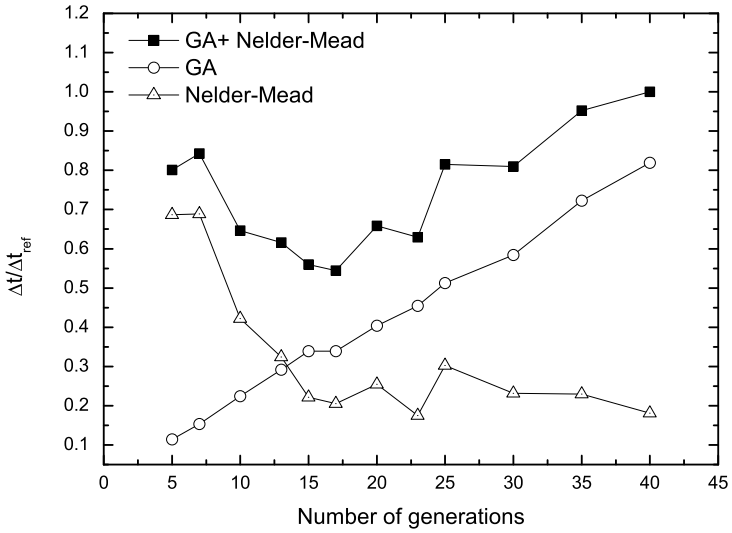

Figure 4.8: The GA, the Nelder-Mead and the total simulation times for a hybrid GA against the number of generations for a population size of 50 individuals. The lines are visual guides.

In Figure 4.8, we plotted the GA, the Nelder-Mead and the GA + Nelder-Mead relative simulation times against the number of generations. The reference is the time necessary to accomplish an optimization using 40 generations in the GA and continued by the Nelder-Mead. Here, we took the 40 generations situation as a reference. We noticed that the computation time of the simple GA increases linearly with the number of generations and that the tendency of the Nelder-Mead simulation time is to decay. An optimal situation is attained when both the GA and the Nelder-Mead achieve their computation taking a similar amount of time; thus, we realize that this situation is verified when 17 generations are used in the GA.

4.6 Experimental validation

The work reported in this section describes the experimental assessment of the use of multipump architecture instead of single pump and also validates the optimization algorithm described above. The work was carried out in the optical communications laboratory of the Instituto de Telecomunicações (IT) cited in Aveiro and in the facilities of the National Institute of Communications and Information Technology cited in Tokyo - Japan, in colaboaration with the Photonic Network group.

An important feature to properly design an amplification scheme is the evaluation of the information channels bandwidth that is needed and the channel spacing. In CWDM, both bandwidth and channel spacing are large, therefore, we have to chose the best pumping scheme that produces a flat spectrum gain as large as possible.

To demonstrate a proper pumping scheme (one, two or three pumps), some experiments were carried out [1]. A MUX with a set of three CW lasers was used as a pumping unit, being either one, two or three lasers used in each experiment. The copropagating pumps are centred at 1470 nm, 1490 nm and 1509 nm, each with an output power of 22 dBm. A span of 40 km of SSMF with $\alpha = 0.22$ dB/km and $A_{eff} = 80\ \mu m^2$ is the propagation medium. The experiments were carried out with the measurement of the system performance (on/off gain and noise figure) for each scheme using a forward pumping configuration. The scheme depicted in Figure 4.9 reproduces the implemented experimental setup.

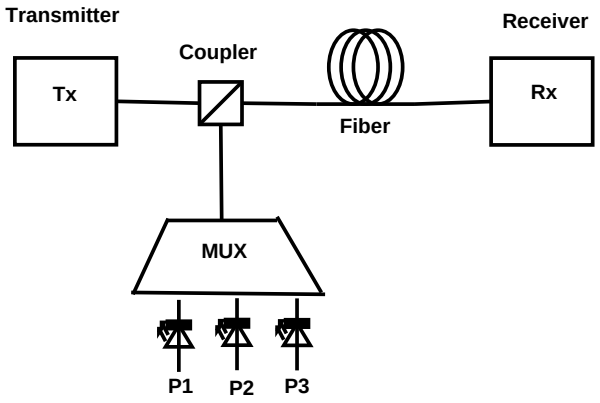

Figure 4.9: Scheme of the used experimental setup.

A comb of 12 wavelengths is used, but only three are turned on in each measurement. The three active channels are equally spaced by 20 nm (the CWDM channel spacing), starting with the triplet (1530, 1550, 1570 nm), then rigidly shifting the three wavelength by 10 nm. Usually, this kind of measurements is taken with only one active channel but measurements using three active channels simultaneously instead of only one provide a more accurate assessment of the system performance. For a single pump scheme, both simulation and experimental gain results are displayed in Figure 4.10.

We observe that the results comply with the theoretical statement that the gain peak is obtained for a wavelength upshifted from the pump by 100 nm [32]. This peak decays rapidly with the wavelength, decreasing 1 dB for a small wavelength variation. A 1 dB decay is equivalent to a declining of 20 percent of the maximum gain, in linear units, and used to define the effective gain bandwidth. Therefore, the effective average gain bandwidth is equal to 39 nm, allowing the use of only two active channels for CWDM purposes. It must be noted that all three pumps present the same behavior.

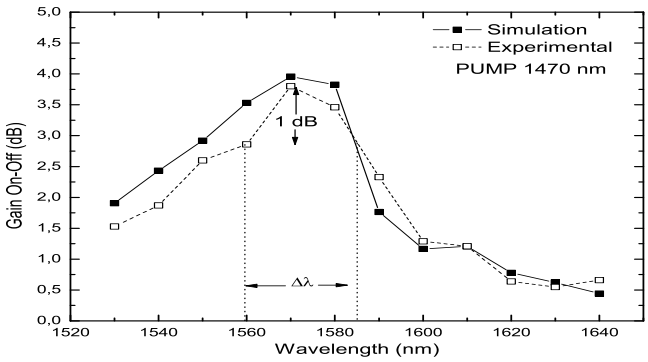

(a) 1470 nm pump

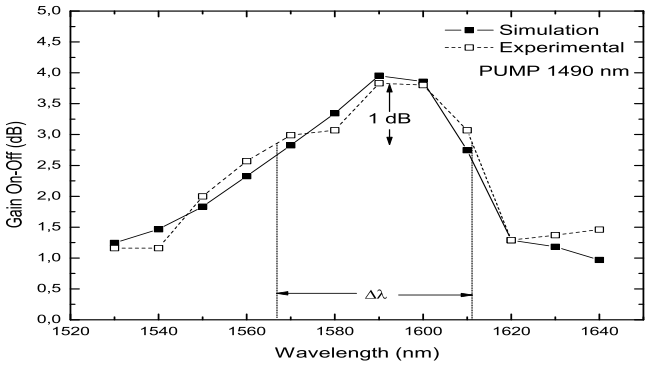

(b) 1490 nm pump.

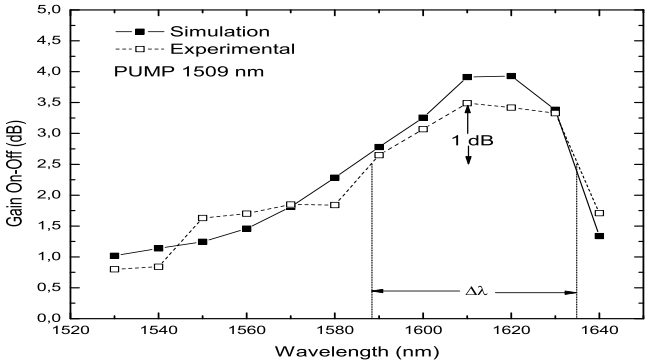

(c) 1509 nm pump.

Figure 4.10: Gain spectrum for the single pump scheme. Only the experimental bandwidth is assigned in the graphs.

After assessing the system performance using a single pump, we perform the evaluation for multipump schemes, using the three pumps simultaneously. The

obtained gain spectrum is plotted in Figure 4.11. As opposed to the single pump case, the deployed gain is higher and broader; being the effective bandwidth equal to 48 nm. An 78 nm bandwidth was measured at 3 dB. Since the channel spacing in CWDM is 20 nm, this pumping configuration allows the allocation of three active channels.

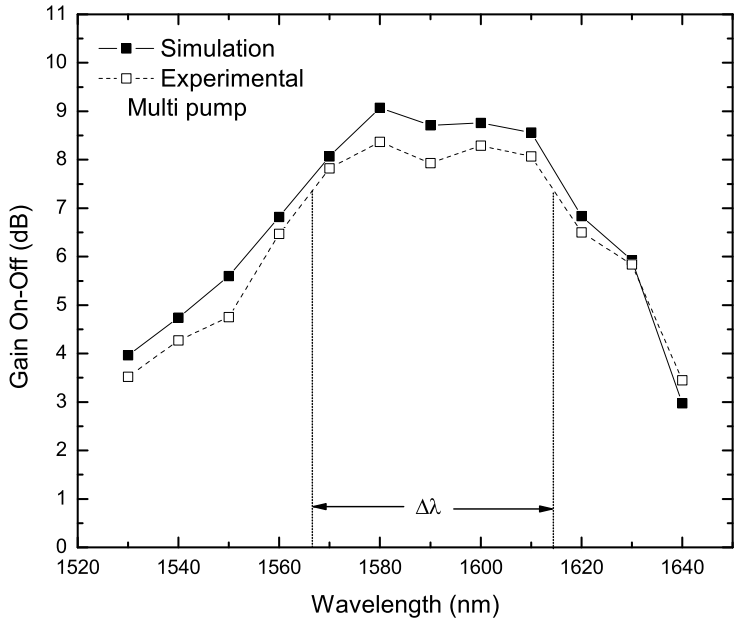

Figure 4.11: Gain spectrum for multipump scheme. Only the experimental bandwidth is assigned in the graphs.

Concerning optimization, two different experiment are described, one for C band optimization [34] and another focused on broadband amplification. Although the second experiment requires an intensive simulational work, boths tasks were succeded using the hybrid GA.

This experiment was used to verify gain equalization for transmission channels in the C-band. The experimental setup follows the scheme depicted in Figure 4.5 and is composed by tuneable lasers to generate the test signals (1530, 1540, 1550, 1560 and 1570 nm) and a backward pumping module (Amonics ARA-CL-4B-R), with 4 diode lasers at 1426, 1444, 1462 and 1487 nm with a total pumping power around 1 W. The measured spectrum of the module is available in Figure 3.8, where the powers were set at at 20 percent of the total power and a 3 dB attenuator was used to protect the OSA.The propagating medium is 40 km of SSMF with an average attenuation of 0.22 dB/km. A passive coupler is used to assemble the test and pumps signals, being used an isolator before the fiber to protect the signal source. The used fiber Raman

gain coefficient was based in previously published results [35].

The test signals had an initial optical power of 3 dBm. The fiber output test signals power was firstly assessed with the pumps off and then with the pumps at a given percentage of their maximum power. Afterward, the on/off gain was computed from these values. The optical power of each pump was optimized, through the hybrid algorithm using the methodology described in the section above. Thus, we employ a population of 50 individuals with following GA operators: stochastic uniform for selection, scattered for crossover and uniform for mutation. The GA was evolved over 17 generations and switched to the Nelder-Mead method. The objective function was settled as the gain ripple around a target on/off gain of 4 dB. The obtained experimental and simulation on/off gain are displayed in Figure 4.12. The reduced chi-square between the experimental and simulation optimized data attained a value of 0.054.

Analyzing the experimental and simulation results, we notice that they are in good agreement (reduced chi-square value of 0.054). For the optimized situation, the obtained experimental gain ripple was equal to 0.24 dB. This demonstrates that the hybrid GA algorithm is suitable to perform optimization for the Raman gain in reconfigurable optical networks.

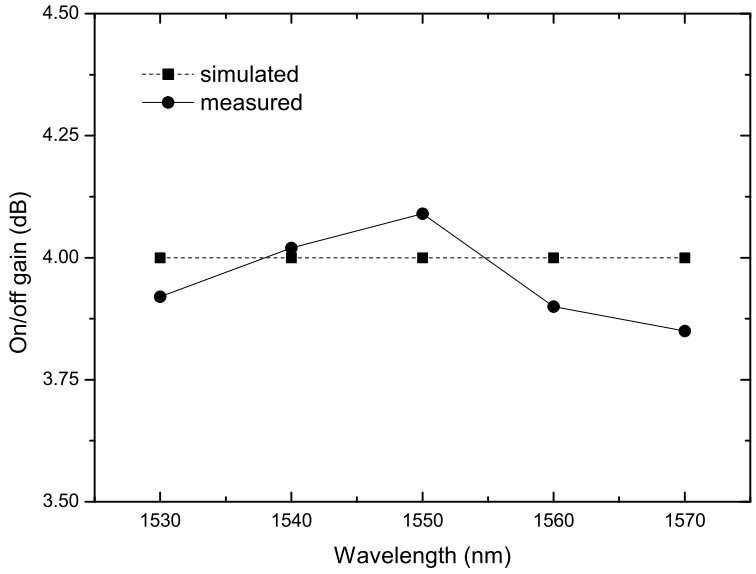

Figure 4.12: Measured and simulated on/off gain for optimized pumping power.

As done with the C-band equalization, an experiment to equalize the gain of channels in a wide bandwidth (around 80 nm) was carried out. Thus, a Raman amplified system with 20 km of SMF fiber, 20 probe signals and 7 backward pumps privided by the Raman module (Fitel HPU-CL12W14D-00077) was implemented.

Since the pump wavelengths are already settled, only the optimization of the power levels is needed. The simulation used the hybrid GA explained above being the GA operators chosen to make to algorithm more efficient. Hence, the stochastic uniform method was used for selection, being the scattered uniform methods used for crossover and mutation. A population of 50 individuals was randomly created within an predifined interval and a number of generations equal to 35 were considered. The spatial evolution of the pumps signals optimized values are displayed in Figure 4.13 jointly with the pump signals experimental values. In Figure 4.14, the optimized and experimental on/off gain spectra are presented.

This is a good agreement between the optimization modeling and the experiment. The maximum ripple attained by the optimization is 0.41 dB being the experimental maximum ripple equal to 0.23 dB. The mean square error between simulation and experimental results is equal to 0.0036. Indeed, a flat gain over a wide bandwidth (aroung 80 nm) was attained, using seven pumps with a total input power equal to 453 mW.

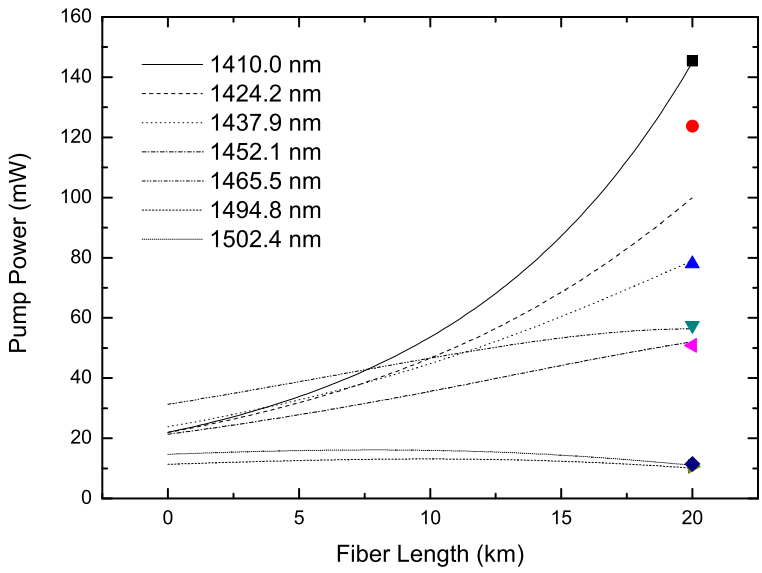

Figure 4.13: Power evolution of optimized pumps along 20 km of SMF (lines). The geometric shapes stand for the used experimental values.

Depite the arguments against, such as the cost of pump multiplexers and the detrimental pump depletion effect and nonlinear effects as Four-wave mixing (FWM), the multipump allocation is still a good solution for the purpose of gain enlargement and equalization mainly due to the flexibility on setting the pumps architecture. Even incoherent pumping, that is a very affordable solution does not allow a simultaneous gain enlargement and equalization as efficient as multipumping because

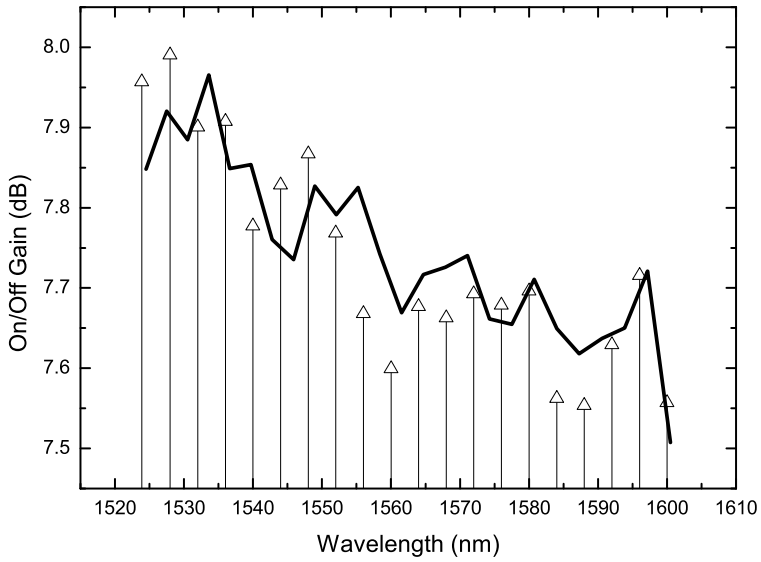

Figure 4.14: Experimental (arrows) and simulation (line) on/off spectral gain for the 20 probe signals and 7 counter propagated pumps, over 20 km of SMF fiber.

the operational pump frequencies are simetrically placed around a central frequency. Thus, when as the gain is enlarged, it becomes less equalized.

As demonstrated in this chapter, the problem of finding the pump parameters, traditionally very time consuming, has been surpassed. Efficient and accurate numerical solutions are able to provide the proper pump parameters for a particular situation enabling the pratical implementation of the simulated solutions. Thus, the option for this methododoly among others is still vantageous.

4.7 Chapter summary

This chapter described the work that was carried out within the topic of Raman gain equalization, namely the gain enlargement and equalization by multi-pump allocation. The chapter starts with an introduction presenting the state of the art of this research topic and some important published methodologies to achieve Raman gain equalization, such as incoherent pumping, pumping by an array of low power lasers and multiple order Raman pumping are reffered. The approach developed in this thesis is then presented and theoretically framed. Since the work requires intensive computational effort and the use of robust optimization, the option for metaheuristics is justified and the genetic algorithm principle of operation is explained. Practical aspects concerning its implementation are also discussed and contextualized in the problem of Raman gain equalization, being introduced, for that purpose, a practical

simulation situation. In order to improve the efficiency of the method, a hybrid approach that combines Genetic Algorithm with a local search method is presented and compared with simple GA. The results demonstrate that the computation time can be reduced by a factor of two. To enligthen the results obtained in simulation, two experiments were carried out. The first one assesses the possibility of obtaining gain enlargement for CWDM applications, the last two achieve gain equalization for (i) C band signals, using a backward 4-pump Raman module and (ii) over a wide bandwidth (80 nm) using 7 backward pumps. The practical implementation has shown that the simulation times are compatible with the network reconfiguration.

References

[1] D. Sperti, P. André, B. Neto, A. Rocha, A. Bononi, F. da Rocha, and M. Facão, "Experimental assessment of some Raman fiber amplifiers solutions for coarse wavelength division multiplexing applications," *Photonic Network Communications*, vol. 16, no. 3, pp. 195–202, 2008.

[2] B. Han, X. Zhang, G. Zhang, Z. Lu, and G. Yang, "Composite broad-band fiber raman amplifiers using incoherent pumping," *Opt. Express*, vol. 13, no. 16, pp. 6023–6032, 2005. [Online]. Available: http://www.opticsexpress.org/abstract.cfm?URI=oe-13-16-6023

[3] P. Andre, A. Pinto, A. Teixeira, B. Neto, S. Junior, D. Spertti, F. da Rocha, M. Bernardo, M. Fujiwara, A. Rocha, and M. Facao, "Raman amplification using incoherent pump sources," in *Transparent Optical Networks, 2007. ICTON '07. 9th International Conference on*, vol. 1, July 2007, pp. 136–139.

[4] T. Zhang, X. Zhang, and G. Zhang, "Distributed fiber raman amplifiers with incoherent pumping," *Photonics Technology Letters, IEEE*, vol. 17, no. 6, pp. 1175–1177, June 2005.

[5] A. Rocha, B. Neto, M. Facao, and P. Andre, "Study of raman amplification with low cost incoherent pumps," *Microwave and Optical Technology Letters*, vol. 50, no. 2, pp. 301–303, 2008.

[6] A. Teixeira, P. Andre, S. Stevan, T. Silveira, A. Tzanakaki, and I. Tomkos, "Raman amplification based on multiple low-power lasers," in *Telecommunications, 2006. AICT-ICIW '06. International Conference on Internet and Web Applications and Services/Advanced International Conference on*, Feb. 2006, pp. 85–85.

[7] J.-C. Bouteiller, K. Brar, J. Bromage, S. Radic, and C. Headley, "Dual-order raman pump," *Photonics Technology Letters, IEEE*, vol. 15, no. 2, pp. 212–214, Feb. 2003.

[8] S. Papernyi, V. Ivanov, Y. Koyano, and H. Yamamoto, "Sixth-order cascaded Raman amplification," in *Optical Fiber Commun. Conf.(OFC), Anaheim, CA*, 2005.

[9] D. Vakhshoori, M. Azimi, P. Chen, B. Han, M. Jiang, K. Knopp, C. Lu, Y. Shen, G. Rodes, S. Vote *et al.*, "Raman amplification using high-power incoherent semiconductor pump sources," in *Optical Fiber Communication Conference*, 2003.

[10] S. Papernyi, V. Karpov, and W. Clements, "Third-order cascaded raman amplification," in *Optical Fiber Communication Conference and Exhibit, 2002. OFC 2002*, Mar 2002, pp. FB4–1–FB4–3.

[11] J. Dréo, *Metaheuristics for hard optimization: methods and case studies*. Springer Verlag, 2006.

[12] P. Siarry and Z. Michalewicz, *Advances in metaheuristics for hard optimization*. Springer-Verlag New York Inc, 2008.

[13] P. Xiao, Q. Zeng, J. Huang, and J. Liu, "A new optimal algorithm for multipump sources of distributed fiber raman amplifier," *Photonics Technology Letters, IEEE*, vol. 15, no. 2, pp. 206–208, Feb. 2003.

[14] M. Yan, J. Chen, W. Jiang, J. Li, J. Chen, and X. Li, "Automatic design scheme for optical-fiber raman amplifiers backward-pumped with multiple laser diode pumps," *Photonics Technology Letters, IEEE*, vol. 13, no. 9, pp. 948–950, Sep 2001.

[15] X. Zhou, C. Lu, P. Shum, and T. Cheng, "A simplified model and optimal design of a multiwavelength backward-pumped fiber raman amplifier," *Photonics Technology Letters, IEEE*, vol. 13, no. 9, pp. 945–947, Sep 2001.

[16] E. Talbi, *Metaheuristics: from design to implementation*. Wiley-Blackwell, 2009.

[17] D. Goldberg, *Genetic Algorithms in Search and Optimization*. Addison-wesley, 1989.

[18] M. Mitchell, *An introduction to genetic algorithms*. The MIT press, 1998.

[19] J. Dréo, P. Siarry, A. Pétrowski, and E. Taillard, *Metaheuristics for hard optimization: methods and case studies*. Springer Verlag, 2006.

[20] J. Holland, *Adaptation in natural and artificial systems*. MIT press Cambridge, MA, 1992.

[21] A. Rogers and A. Prugel-Bennett, "Genetic drift in genetic algorithm selection schemes," *IEEE Transactions on Evolutionary Computation*, vol. 3, no. 4, pp. 298–303, 1999.

[22] D. Beasley, R. Martin, and D. Bull, "An overview of genetic algorithms: Part 1. Fundamentals," *University computing*, vol. 15, pp. 58–58, 1993.

[23] C. Houck, J. Joines, and M. Kay, "A genetic algorithm for function optimization: A Matlab implementation," *NCSU-IE TR*, vol. 95, no. 09, 1995.

[24] A. Chipperfield and P. Fleming, "The matlab genetic algorithm toolbox," in *COLLOQUIUM DIGEST-IEE*. Citeseer, 1995, pp. 10–10.

[25] T. El-Mihoub, A. Hopgood, L. Nolle, and A. Battersby, "ï£¡Hybrid genetic algorithms: A review," *Engineering Letters*, vol. 3, no. 2, pp. 124–137, 2006.

[26] J. Zhou, J. Chen, and X. Li, "A novel method to optimize optical-fiber Raman amplifiers using equally spaced low-power laser diode pumps," *Microwave and Optical Technology Letters*, vol. 40, no. 2, pp. 124–127, 2004.

[27] X. Lee, "Optimal design for ultra-broad-band amplifier," *J. Lightwave Technol*, vol. 21, pp. 21–12, 2003.

[28] J. Lagarias, J. Reeds, M. Wright, and P. Wright, "Convergence properties of the Nelder-Mead simplex method in low dimensions," *SIAM Journal on Optimization*, vol. 9, no. 1, pp. 112–147, 1999.

[29] B. Neto, A. Teixeira, N. Wada, and P. André, "Efficient use of hybrid genetic algorithms in the gain optimization of distributed raman amplifiers," *Optics Express*, vol. 15, no. 26, pp. 17 520–17 528, 2007.

[30] A. Chipperfield, P. Fleming, and C. Fonseca, "Genetic algorithm tools for control systems engineering," in *Proc. Adaptive Computing in Engineering Design and Control*, 1994, pp. 128–133.

[31] H. Kidorf, K. Rottwitt, M. Nissov, M. Ma, and E. Rabarijaona, "Pump interactions in a 100-nm bandwidth raman amplifier," *Photonics Technology Letters, IEEE*, vol. 11, no. 5, pp. 530–532, May 1999.

[32] J. Bromage, "Raman amplification for fiber communications systems," *Journal of Lightwave Technology*, vol. 22, no. 1, p. 79, 2004.

[33] C. Headley and G. Agrawal, *Raman amplification in fiber optical communication systems*. Elsevier Academic Press, 2005.

[34] B. Neto, C. Reis, A. Teixeira, P. Andre, and N. Wada, "Gain equalization technique for raman amplification systems based on the hybrid optimization algorithm," in *Microwave and Optoelectronics Conference (IMOC), 2009 SBMO/IEEE MTT-S International*, 3-6 2009, pp. 687 –689.

[35] M. Fugihara and A. Pinto, "Low-cost Raman amplifier for CWDM systems," *Microwave and Optical Technology Letters*, vol. 50, no. 2, pp. 297–301, 2008.

Chapter 5

Optical amplifiers in access networks

5.1 Introduction

The fiber-to-the-home/premise (FTTH/P) access solutions are of high technological and economical interest since they can implement a structure in the field with reduced Capital expenditures (CapEx) and operational expenditures (OpEx) dealing with increasing network data traffic. Access networks operate in a local scale being connected to the metropolitan and then to the core networks.

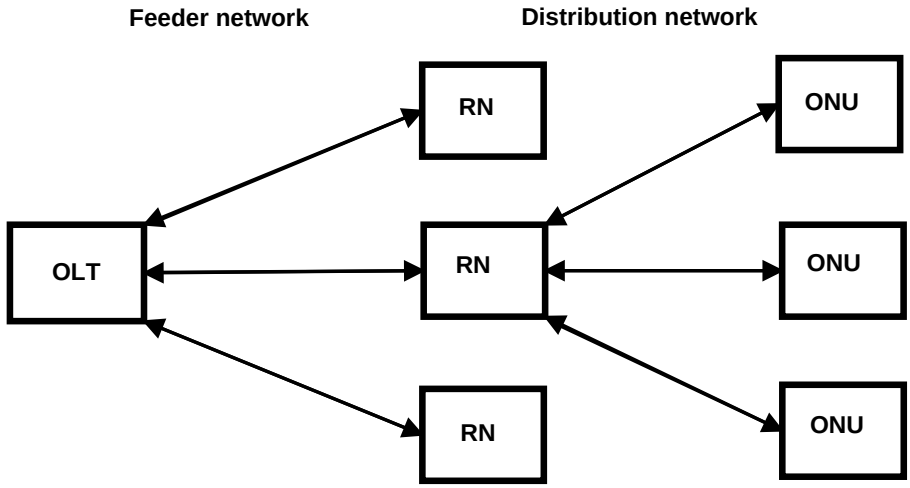

Figure 5.1: General scheme of a PON and its subnetworks: feeder and distribution.

These so-called passive optical networks (PONs) consist of three fundamental elements: the optical line terminal (OLT) at the service provider's central office (CO), the remote node (RN) and the optical network units (ONUs) in the end users. The OLT is the equipment that enables the user services and controls the quality-of-service (QoS) among other tasks. The OLT also carries out the multiplexing of users in the optical fiber. The ONU converts the optical signal ariving from the OLT into an adequate format to the end user, such as asynchronous transfer mode (ATM), Ethernet, internet protocol (IP), etc. Inside the access network, two sub-networks can be defined, the feeder and the distribution networks. The first one tranports the traffic between the OLT and the RNs, and the second from the RNs to the ONUs. By definition, no active elements can be included inside the distribution network. A general scheme of a PON

and its elements is displayed in Figure 5.1. In the access network, two traffic directions are allowed, one coming from the service provider to the end user, the down-stream (DS), and another flowing in the opposite direction, the up-stream (US). The latter can be assigned with equal of different wavelengths. If the same wavelength is used for both DS and US, a pair of fiber is needed [1], otherwise, they can be multiplexed into a single fiber, but their wavelengths must be chosen on order to prevent impairments. The optical splitter/combiner in the RN distributes the DS information from the OLT among the ONUs and combines the US coming from the distribution network. Thus, all the elements are interconned using a low cost structure.

The deployment of broadband solutions , boosted by the proliferation of new web applications, going from traditional search to social networks and video streaming, had undergone a huge development thanks to WDM technology. However, due to the limitation of access networks, the backhaul traffic can suffer a bottleneck in the access structure pressing out the necessity of standartizing networks that provide broadband services: broadband PONs (BPONs) [2], ethernet PON (BPON) [3] and gigabit PON (GPON) [4]). The latter are currently based on time division multiplexing techniques (time division multiplexing - passive optical network (TDM-PON)) and have significant advantages in terms of instalation and OpEx. For TDM-PON, a passive power splitter is used as the remote terminal, neing the signals multiplexed in the time domain.

A counter part technology is wavelength division multiplexing where each ONU is served by a single wavelength. This technology allows to increase the network capacity and simplify the management as all the connections are point-to-point. Besides that they exhibit a range of inherent advantages such as protocol transparency and QoS. In Figure 5.2 are presented the two different approaches to provide FTTH/P: TDM-PON and wavelength division multiplexing - passive optical network (WDM-PON).

Until recently, the deployment of WDM-PON was limited by the costs because the latter require additional transceivers operating on new enhancement bands and filters to separate the wavelengths in the system [6] [7]. However, enabling technologies are expected to upgrade the current TDM-PON to WDM-PON enabling a smooth migration from one technology to the other. In [8], a migration strategy is suggested using centralized ligth sources and novel scheduling algorithms to share tunable components. In alternative, hybrid architectures such as wavelength division multiplexing/time division multiplexing - passive optical network (WDM/TDM-PON) [9], [10]or CWDM/TDM-PON [11]are valuable but still experimental. However, these approaches are being pointed out as a possible solution for the deployment for next generation access (NGA) networks and in FTTH/P segment.

The maximum reach and split of a PON are determined by both the PON protocol

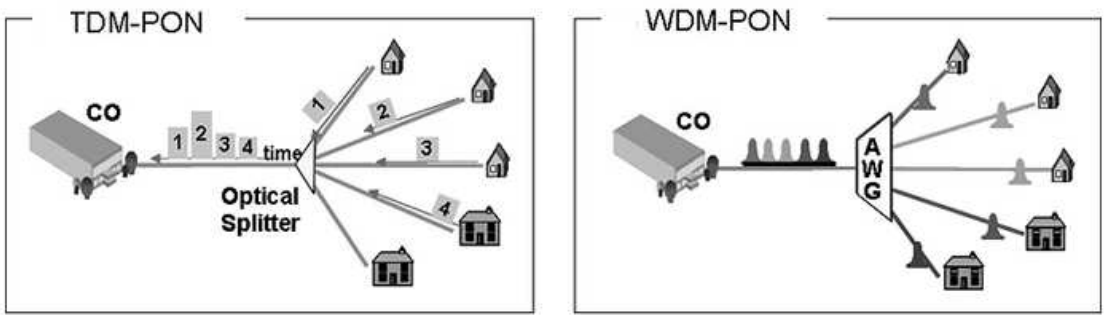

Figure 5.2: Two different PON architectures: (left) TDM-PON; (rigth) WDM-PON [5].

and the physical layer optical reach. Extending the reach of a PON allows the consolidation of the access and metro networks, reducing the number of switching nodes which results in cost savings. The concept of increasing the reach and splitting of a PON by means of optical amplifiers, had become a topic of research interest and reach extenders have been standartized recently by the ITU-T (G.984.6). Solutions based on the deployment in the field of optical amplifiers are valuable because, unlike electronic equipments, they allow transparency to traffic format, bit rate and simple network management. However, reach extenders may not be cost effective because they require the use of electrically powered units in the field containing optical amplifiers denying in this way the intrinsic benefits of PON [12]. Thus, the most attractive solution for network operators rely on achieving extended reach while maintaining the passiveness outside plant of the PON structure.

Typically, due to the 28 dB loss budget for Class B^+ [12], the GPON deployments are 1:32 split with a reach up to 20 km. Similarly, GE-PON offers loss budget of 20 and 24 dB, and achieves a maximum distance of 10-20 km. However, extended reach have been achieved by adding in line amplifiers to existent infrastruture, with the above mentioned drawback that this extenders need supply points along the feeder line. However, Raman amplification solutions have intrinsic benefits because the transmission medium is also the amplification medium so no power supply is needed along the line, being the pumps located at the CO. As a consequence, Raman approaches vary essentially in the type of pumping architecture. In [13] extended reach access is attained with single fiber, bidirectional backhaul link and distributed Raman amplification, achieving 80 km long reach PON link with symmetric up and downstream data rate of 10 Gb/s. Alternatively, dual pumping at 1239 nm and 1427 nm can be used at the CO to extend the reach of GPON be means of Raman amplification in AllWave fiber at 2.5 Gb/s, enabling a system reach of 60 km and

a 1:64 split ratio total in an entirely passive outside plant [14]. Lee *et al* have used a similar approach in a rural scenario GPON, attaining 60 km extended reach and 1:32 plit ratio on a symmetric 2.5 Gb/s bidirectional transmission [15]. Raman amplification can also be used on WDM-PON using backward and bidirectional pumping schemes. Additonally, pump recycling techniques can be valuable. In [16] the re-use of non-negligible residual Raman pump power as a pump for an Erbium fiber-based upstream broadband ASE source allows for fully-centralized control of light sources at optical network units (ONUs), while distributed Raman amplification over a transmission link enables us to obtain lossless low power signal transmission.

In WDM/TDM-PON architecture, the combined use of Raman amplification and EDFA or remotely pumped EDF in a hybrid amplification scheme can have significant merits because it allows the C+L bandwidth enlargement and introduce simplicity by achieving with one 1480 nm laser the simultaneous pumping of EDFA and Raman. However,this architecture brings additional issues coming from the transients.

Power transients can be caused by a sudden channel addition or removal in the WDM environment caused by either unintentional failures, or by deliberate network reconfigurations [17]. Thus, changes in the number of WDM channels will affect the power of the surviving channels in a timescale proportional to the number of amplifiers in the network [18]. During the transience, if the signal power increases, the enhanced nonlinearities may distort the signal, while decreased signal power may lead to OSNR impairment; and both effects will degrade the system performance [19]. Additionally, burst mode traffic can also originate transients. The main operational concern with is effect is its duration and the amount of gain excursion.

It has been demonstrated that the effect of transients are more detrimental when EDFA are used, because they are related with the population dynamics of the dopant ions, and can be much faster than the ions relaxation time, depending on the signals saturating power. Transients are also observed in RFA due to the dynamic pump-to-pump and signal-to-signal interactions in the above described network invironment. However, the transient duration and power surges is more noticeable in forward multipump architectures. Surprisingly, transients have also been experimentally observed even in counter-pumped single-channel saturated Raman amplifiers [20], [21], [22]. The reason is that the strong power of the signal leading edge depletes the injected pump, and thus the main body of the signal pulse does not enjoy the same high gain as the signal front.

The work reported in this chapter addresses the use of optical amplifiers in PON, namely RFA and EDFA (or remotely pumped EDF). The specific architecture of SARDANA which is a hybrid WDM/TDM-PON is analyzed more thoroughly concerning important operational issues such as the transients due to the addition/dropping of channels and the ones owing to bursty/packeted traffic. Concerning the EDFA or remotely pumped EDFA transients, mitigations

strategies based on optical gain clamping were proposed and implememented in a laboratorial context. Besides that, challenges concerning the bandwidth enlargement covering C+L bands and the gain equalization were also projected recurring to hybrid amplification schemes. Hence, an optimization strategy was developed by introducing and enhanced order to add/drop channels and optimized EDF lengths.

5.2 Transients in Raman amplifiers

As said in the introduction section, the use of optical amplifiers, namely RFA for burst-mode transmission, can originate transients. Although they are expected to be more detrimental in saturated amplifiers such as EDFA, their occurence in RFA was also demonstrated.

In RFA, the phenomenon of stimulated Raman scattering occur in a timescale compliant with Raman time constant, T_R, which assumes values in the fentoseconds order for Silica based fibers. As approached in chapter 2, Raman scattering can physically be interpreted by considering a short high power temporal optical pulse incident on a Silica molecule. As a consequence, the molecule electrical polarization vibrates with a very short period. Because this vibration period is very small when compared with the duration of the pulse, molecular vibrations are induced. The second term of the third-order nonlinear susceptibility, $\chi^{(3)}$, is used to account the molecular vibration and to model Raman effects [23], [24]. Thus, besides Raman gain coefficient, γ_R, which is given by equation 2.1 the Raman time constant, T_R, is related to the slope of the Raman gain by [25]:

$$T_R = \frac{2\pi}{nn_2}\left[\frac{d\left(Im\left(\chi^{(3)}\right)\right)}{d\left(\Delta\omega\right)}\right]_{\Delta\omega=0} \tag{5.1}$$

Unlike EDFA which exhibit relaxation times in the order of the tens of milisecons, the Silica medium responds almost instantaneously by stimulated Raman scattering. However, when a suden variation in the total power that propagates inside an optical fiber is observed, a time delay due to the propagation of data and pump signals through the kilometers long gain medium fiber will cause a relatively slow response on the amplifier. This effect is usually designated by Raman transient. The response will depend deeply in the degree of gain saturation of the amplifier. If the amplifier is operated at a linear gain regime the transient change in the gain will not be so large. The observation of transients is commonly observed in WDM systems due to the temporal variation of cross gain modulation when data signals are added/dropped [26], [27]. In that situation the so-called surviving channel(s) will experience temporarily more (or less) available pump power over a time interval defined by the propagation of the perturbation along the fiber. Typically, the effect is more penalizing in backwardly pumped systems [28]. Transience can be observed

for single data signal transmission backwardly amplified in a saturated amplification regime [22]. The reason is that the strong power of the signal leading edge depletes the opposite traversing pump, and thus the main body of the signal pulse does not enjoy the same high gain as the signal front.

The computation of Raman transients are possible numerically by solving the system of equations 3.1. The procedure starts by solving the system in steady state conditions, using the methods described in chapter 3 and perform time evolution of pumps, signals, and ASE waves. It must be noted that the time interval, Δt, and the space interval, Δz, are connected by the group velocity, V_i, the perturbations will propagate along the optical fiber. For backwardly pumped amplifiers, the perturbation follows a retardated time frame $t_i = t - z/V_i$. An analytical computation of the gain excursion and transient time constant is also possible and accurate for backwardy pumped Raman amplifiers. [22]. This approach is based on the derivation of a relative integrated pump variation, measured in the signals retarded time frame.

For burst/packeted switching mode signal propagation, a perturbation of the standing wave operated by an incoming packet at the frequency ν_i creates a notch in the pump power that propagates backwards to the input. The reaction time of the standing wave is at least the propagation time inside the amplifier. Hence, by the time the standing wave reacts to the signal power variation, the notch has propagated to the input, and thus we have an undampened power excursion across the signal output pulse. This outcome is only possible for saturated Raman amplifiers.

To assess the impact of the use of burst traffic under Raman amplification, an experiment was carried out. The underlying idea was to use different traffic features, burst lengths and idle times, analyze the system performance and compare it with EDFA.

The implemented experimental setup consists of an external cavity laser peaking at 1550 nm, followed by a polarization controller and a Mach-Zehnder external modulator driven at 10 Gbit/s. After passing through an optical isolator the optical signal is injected into 45 km of SSMF. As a receiver, a NEL photonic packet, an Agilent digital oscilloscope and an Anritsu BER tester were used.

To achieve Raman counterpropagation amplification we use a Fitel HPU-CL12W pump set, containing 14 pump lasers, at the following wavelengths: 1410.0, 1410.2, 1416.9, 1417.3, 1424.2, 1429.8, 1437.9, 1444.3, 1452.1, 1458.1, 1465.5, 1472.6, 1494.8, and 1502.4 nm. The latter were driven with 500 mA, representing an aggregate optical power of 1029 mW. The EDFA amplification scheme was implemented with one device from IPG. In both cases, the optical power at the receiver was 0 dBm.

The tests were performed at 10 Gbit/s with $2^{23} - 1$ PRBS packet signals. For these tests a composite signal was constructed, with packet sizes equal to 5000, 10,000, 15,000, and 20,000 bits, having all an off time equivalent to the previous burst size. Table 5.1 displays the digital bit test sequence with a total length of 10 μs.

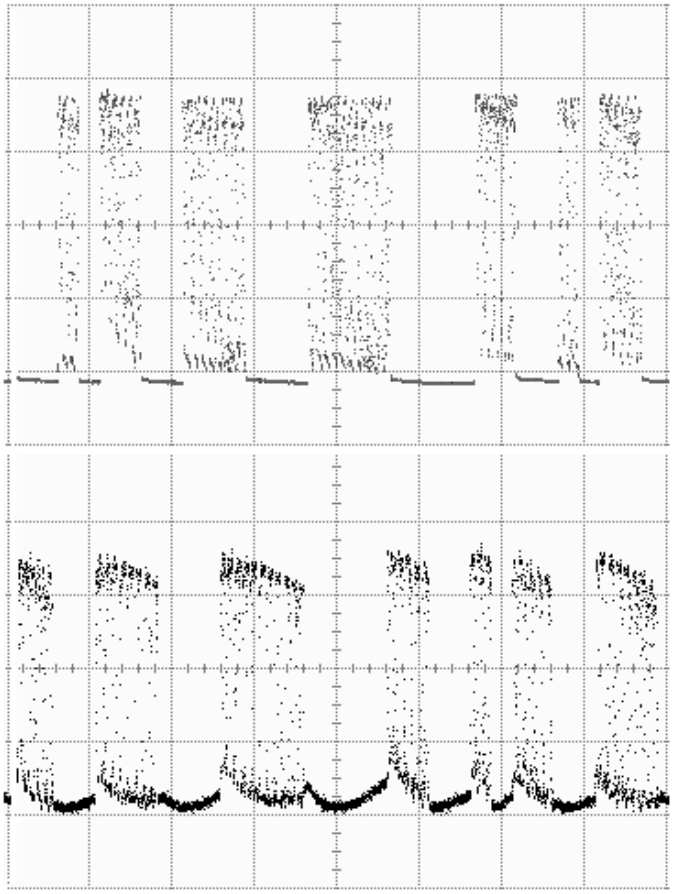

Figure 5.3: Bit sequence at the receiver: top - Raman amplification, bottom- EDFA amplification. The vertical scale is arbitrary and the horizontal scale is 500 ns/div.

Table 5.1: Tested bit sequence.

5000 PRBS	5000 zeros	10000 PRBS	10000 zeros	15000 PRBS	15000 zeros	20000 PRBS	20000 zeros

The transient effect could be clearly noticed on the time domain, by observing the bit sequence on the oscilloscope, for each amplification scheme, as shown in Figure 5.3.

Concerning the system performance, BER measurements were performed for the two previously described amplification schemes, Raman and EDFAs, as well as the back to back situation. The results are displayed in Figure 5.4. The difference between the two configuration power penalties is 1.1 dB (for a BER at 10^{-11}), being more penalizing for the EDFAs amplification scheme. This could be mainly due to the ASE noise and to transient effect associated with the EDFAs.

To access the network performance in the presence of packet traffic, we have analyzed the Q factor at the receiver, as function of the inter-packet spacing in

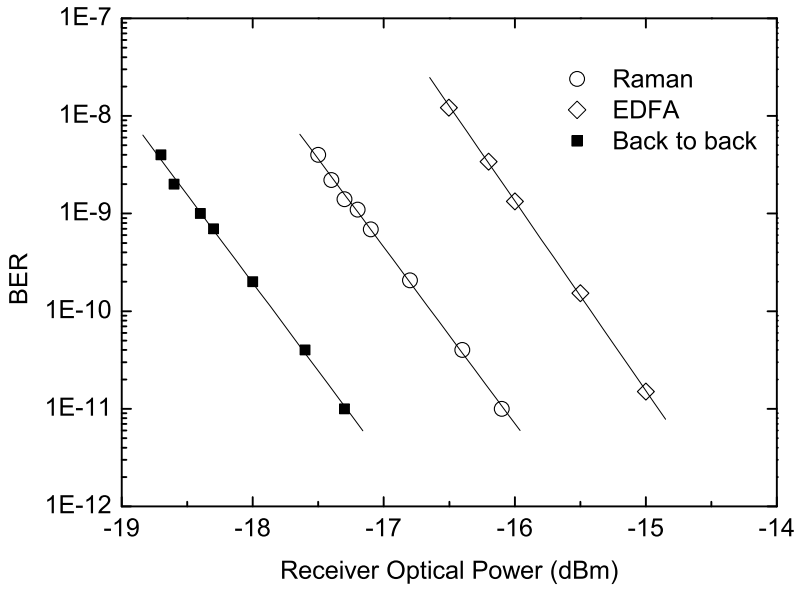

Figure 5.4: Experimental BER for the Raman and EDFA amplification, and the back to back situation. The lines are visual guides.

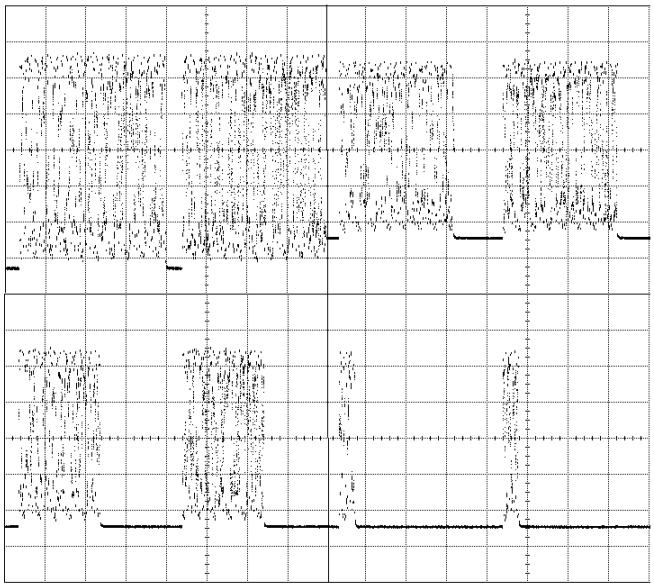

Figure 5.5: Packet signals bit sequences, the time between burst is 2 μs. Packet occupancy densities: from left to right and from top to bottom: 90, 70, 50, and 20 percent. The vertical scale is arbitrary and the horizontal scale is 500 ns/div.

the presence of Raman amplification with counterpropagation pumping. Figure 5.5 displays the test bit sequence for four distinct packets sizes, considering, in all cases, time spacing between packets equivalent to 20000 bit. The packets size varies from

2000 to 18000 bits.

To understand the Raman amplification impact on the signal QoS, we compared the Q factor in the back-to-back and in the transmission conditions. The results are shown in Figure 5.6. On the same graph we display the difference between the two curves, in order to analyze the packet occupancy density.

As predicted by the time constant of the Raman phenomenon, there is negligible degradation on the Q as function of the packet density when the optical signal is subject to Raman amplification scheme.

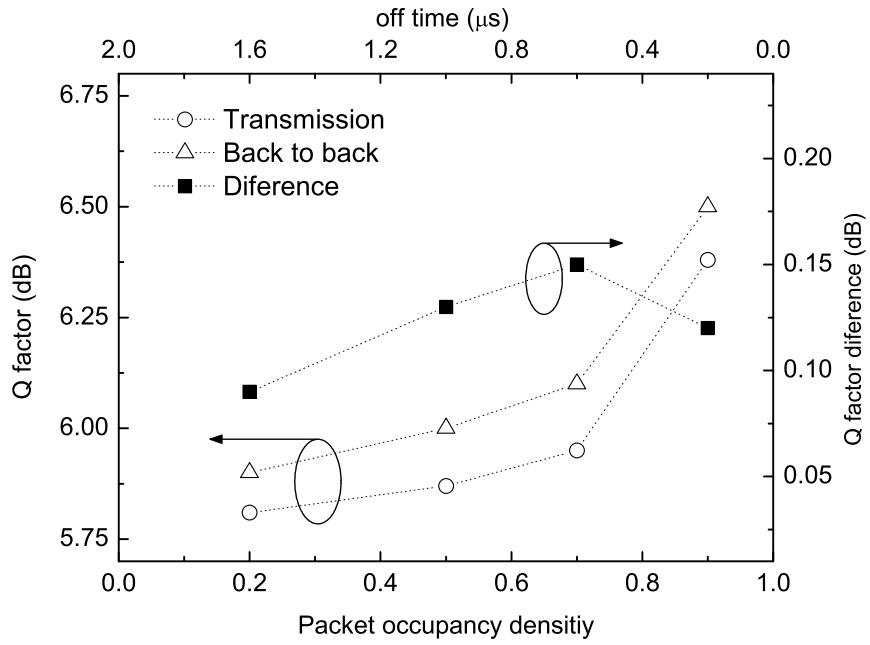

Figure 5.6: Q factor as function of the packet occupancy density. The lines are visual guides..

5.3 Raman amplification in hybrid WDM/TDM-PON

As said above, the use of combined multiplexing schemes, wavelength division multiplexing/time division multiplexing (WDM/TDM) is pointed out as a possible solution for the deployment for next generation access (NGA) networks. As an example of NGA networks, the recently proposed scalable advanced ring-based passive dense access network architecture (SARDANA) seeks to establish an optical passive transparent infrastructure over a dense extended-range area, capable of supporting future broadband services [1]. This kind of network transparently merges TDM-tree sections connected to a metro WDM double-fibre ring, by means of passive Remote Nodes (RNs), as depicted in Figure 5.7. This architecture finds a compromise between WDM-PONs and TDM-PONs in terms of capacity and cost while offering

centralized management and bandwidth allocation from the OLT, simplifying the TDM upstream protocol [9]. This is possible by using wavelength routing based on two stages of matched arrayed-waveguide gratings (AWGs) that create a virtual point-to-point connection between the OLT and the ONU. This network also provides extended reach due to optical amplification, such as RFA and remotely pumped EDF. The latter can be placed placed at the RNs or in line with the fiber and are pumped from the CO while the optical fiber of the links provides Raman gain.

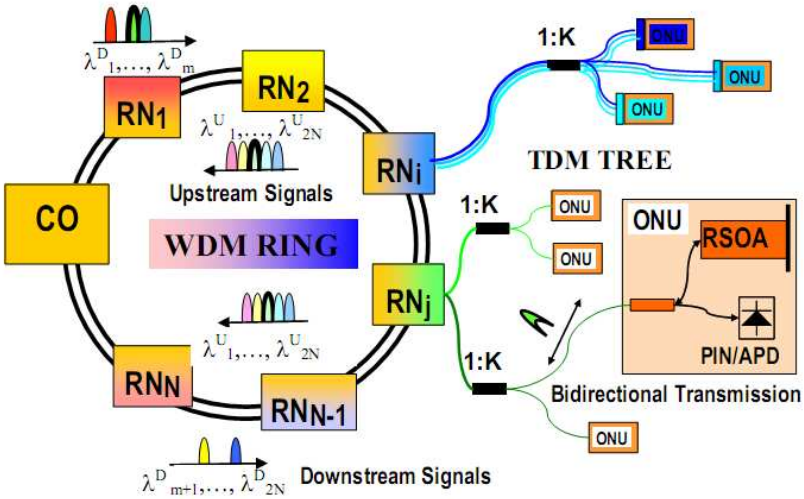

Figure 5.7: SARDANA architecture scheme.

Due to the use of a ring architecture, the network is able to provide traffic balance through the shorter path and resiliency in case of fiber, splice, connector or component failure, being the signals redirected for the other path. DS and US are wavelength multiplexed, so each RN drops 2 DS signals and insert 2 US signals from/to the ring. The number of RNs is a key parameter in terms of network performance because it determines the number of wavelengths of the network and the total network capacity.

In terms of ring architecture and RNs, two scenarios are primarilly defined: rural and urban. The rural scenario is conceived to operate over larger distances with a smaller number of users. Typically, a maximal distance of 100 km can be achieved, using 16 transmission channels, hence, a number of 256 ONUs can be reached. For urban applications, the distances can be reduced but the number of users is significantly increased. Thus the number of transmission channels duplicates, the splitting ratio reduces to a half and the number of ONUs is then 1024. A list of operational features for rural and urban scanerios is displayed in Table 5.2.

The principal aims of SARDANA network are primarily focused on deploying C-band, mainly due to the availability of lower cost and mature devices in this

Table 5.2: Summary of possible scenarios of deployment of SARDANA network.

Scenario	Ring (km)	channels	Splitter	ONUs
Rural	80	16	1:16	256
Urban	17	32	1:32	1024

spectral Band. Nevertheless, the extension of back-bone networks into the L-band is driving a new development of active and passive devices adapted to operation in this wavelength band. Those new devices are nowadays more expensive than their related C-band devices, but they could be sold at competitive prices in a medium term. Thus a bandwidth enlargement encompassing the C+L transmission band is potentially very valuable due to the increase of the network capacity. Since the latter is intended to have extended reach, the feasibility of amplification solutions in C+L bands must be accounted for. Concerning the latter, this thesis was focused mainly on the implementation in rural scenarios as summarized in Table 5.2, in both operation modes. The simulation work presented bellow concerns the possibility of obtaing enlarged gain in the WDM ring of the SARDANA network using solely Raman amplification. This approach is analyzed in a normal and resilient operation modes with a fixed pre-defined channel dropping order [29]. The OSNR is computed and used as a performance indicator.

The first scenario (situation A) uses a bidirectional laser emitting at 1480 nm with total power of 2 W (1 W in each direction for normal scenario) to pump 16 channels spaced by 100 GHz (8 C band + 8 L band) comprised between 189.3 THz to 190.8 THz in order to avoid the current GPON DS Video overlay (1550-1570 nm) as described in Table 5.3. The channels leave the central office with an optical power of 0 dBm. The transmission has accounted for that the bypass losses are 0.53 dB for channels and 1.01 dB for the pump. The simulated fiber is a SSMF with attenuations of 0.20 dB/km and 0.25 dB/km for data and pump signals respectively.

Consider the general scheme depicted in Figure 5.7 with 8 RN. The normal scenario is defined to be bidirectional, thus the data and pump signals are split in both directions according to the following paths [RN1, RN2, RN3, RN4] and [RN8. RN7, RN6, RN5].

The second analyzed scenario (situation B) also uses a bidirectional laser emitting at 1480 nm from the CO to pump 16 channels, but unlike Situation A the total pumping power was reduced to 1 W (500 mW for each side). In this situation, the channels frequencies (8 C band + 8 L band) are also changed because the spacing was now increased to 400 GHz comprised between 192.5 THz to 186.3 THz (see Table 5.4) and the current GPON DS Video overlay was not avoided.

The results concerning situation A were only assessed using Raman amplification. Thus, a previous simulation using the VPI simulator with all nonlinearities was

Table 5.3: Channel dropping order along the ring (2 channels per node) for Situation A.

RN number	f_1 (THz)	f_2 (THz)
1	190.8	190.7
2	190.6	191.5
3	190.4	190.3
4	190.2	190.1
5	189.4	189.3
6	189.6	189.5
7	189.8	189.7
8	190.0	189.9

Table 5.4: Channel dropping order along the ring (2 channels per node) for Situation B.

RN number	f_1 (THz)	f_2 (THz)
1	190.1	190.5
2	190.9	191.3
3	191.7	192.1
4	192.5	192.9
5	189.3	189.7
6	188.5	188.9
7	187.7	188.1
8	186.9	187.3

carried out, enabling the assumption that Raman scattering is the nonlinear dominant effect and that spontaneous emission was the dominant source of noise. Thus, the APA was implemented numerically to obtain the power of channels along the ring, as well as the noise [30], [31]and [32]. These results are depicted in Figure 5.8.

In the resilient scenario, we consider that all the pump power and the 16 channels travel in the same direction which can be counterclock wise [RN1, RN2, RN3, RN4, RN5, RN6, RN7, RN8] or clock wise [RN8, RN7, RN6, RN5, RN4, RN3, RN2, RN1]. In both paths the channels dropping order is the one given by Table 5.3. The results concerning the net gain after dropping and OSNR are depicted in Figure 5.9 and Figure 5.10.

On looking at the results, we notice that the L band channels are more amplified than the C band which is expectable due to the maximal Raman gain coefficient by pumping at 1480 nm. Thus a gain ripple of 3.2 dB is achieved in normal operation scenario. We also observe that the OSNR is kept at very high value due to the dominance of stimulated Raman scattering and that it decreases as the channels travel over the ring. It must be noted that the pump depletion is enhanced in the propagation in the first links where the channels are more amplified, as displayed in Figure 5.11 where the pump power at each node are displayed for the studied scenarios. On

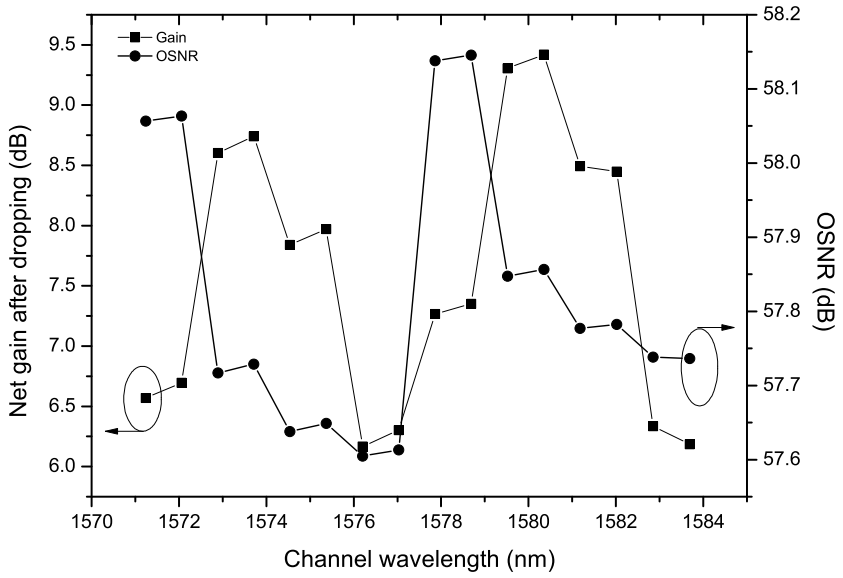

Figure 5.8: Net gain and OSNR spectra after dropping for normal scenario. Lines are guides for the eyes.

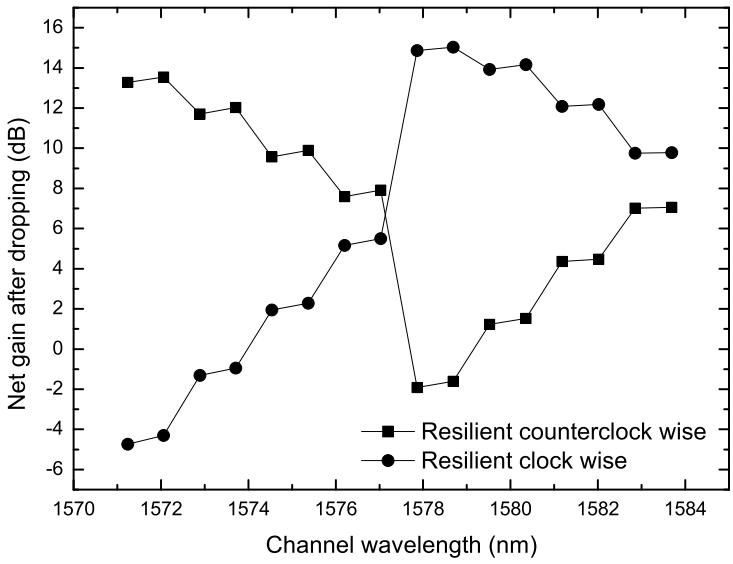

Figure 5.9: Net gain spectrum after dropping for resilient scenario. Lines are guides for the eyes.

looking the results regarding the resilient scenario, we observe that the gain varies in a wider range and the nonlinear effects are expected to by very penalizing. So,

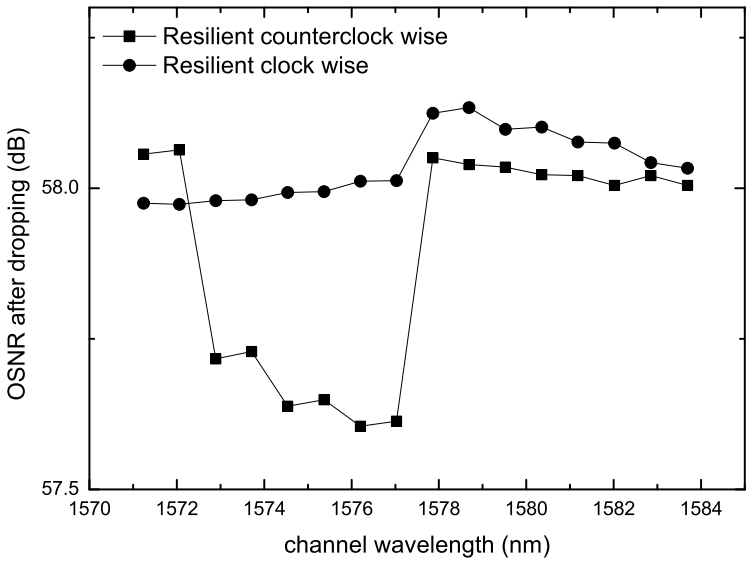

Figure 5.10: OSNR spectrum after dropping for the resilient scenarios. Lines are guides for the eyes.

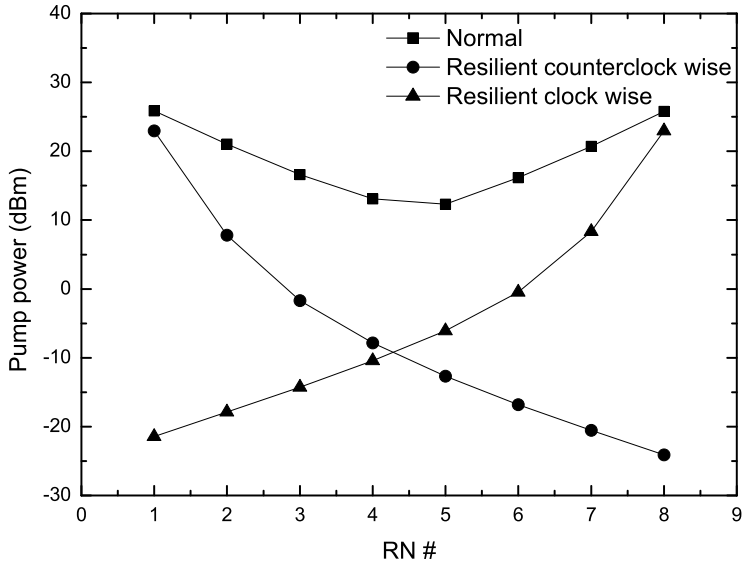

Figure 5.11: Pump power value in each node.

we can conclude that simple Raman amplification using a single 1480 nm pump is not a solution for C+L transimission band in the context of WDM/TDM-PON, such as SARDANA. An alternative solution could rely on hybrid amplifiers using an

association of distributed Raman amplification with in line remotely pumped EDFA. The following section describes the potentialities of such amplifiers. An optimization based on the dropping order and EDF span lengths was also accomplished in order to enhance the obtaining of equalized gain.

5.4 Hybrid amplification schemes

The association of different kinds of amplifiers inside an optical fiber network provides hybrid optimized solutions that make the most of each of their benefits, namely wider optical bandwidth and and flat gain, using only a single 1480 nm pump [33]. In metro-access network, such as SARDANA, the use of combinations of hybrid amplifiers in the WDM ring can enhance the gain bandwidth enabling possible solutions in the C+L spectral bands. In this thesis, we report some simulation approaches that were carried out to enlarge the gain of SARDANA, but also to optimize the gain of channels. However, the combined amplification scheme can exhibit transmission issues in the WDM ring, such as power transients, due the to add/drop. If EDFA are used in the RN, additional transients derived from the bursty nature of upstream traffic can also occur and be very detrimental. Thus, the following work is also addressed to those topics.

First, a sub-section introduces a brief theory about EDFAs, their numerical implementation and an analytical modeling of their dynamic effects. We proceed with experimental work that were carried on, namely the characterization of the transients under different traffic features in terms of gain excursion and decay times. Two mitigation schemes based on optical clamping are proposed and implemented experimentally, being their feasibility for access networks analyzed. For transmission at 10 Gb/s, the impact of hybrid amplifiers power transients on the system performance was assessed experimentally. The possibility of extending the transission band to C+L using hybrid amplifiers is also examined in a simulation environment for 10 Gb/s transmission. An optimization strategy to equalize the gain in the WDM ring is also proposed.

5.4.1 EDFA modeling

A charge distribution, such as Er^{3+}, in a glass host originates a permanent electric field. As a consequence, the Stark effect is induced, resulting into a splitting in the energy levels [34]. Each of the energy levels has a total orbital momentum *J* that splits into a manifold of energy sublevels $g = J + 1/2$. An energy diagram representing the Stark effect in a three level laser is depicted in Figure 5.12. This splitting occurs with uneven internal sub-population.

However, this system can be simplified into the three level energy system

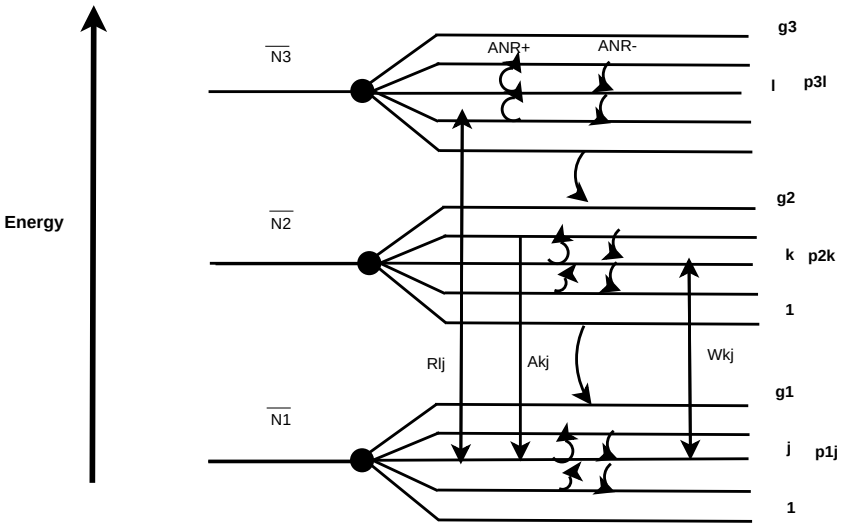

Figure 5.12: Energy level diagram corresponding to a Stark split three level laser system. The symbols $A^{\pm}_{NR}$ indicate the thermalization between adjacent Stark sub-levels, while W and A denote stimulated and spontaneous emission or absorption rates, respectively and R pump rate.

displayed in Figure 5.13, because the population distribution within the manifold is maintained constant due to thermalization (Boltzmann distribution), enabling the assumption of considering them as a single energy level [35].

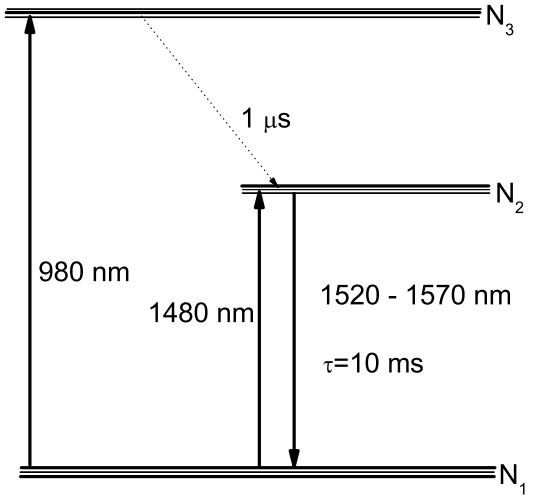

Figure 5.13: Erbium ion energy-level scheme.

Due to uneven distribution within the manifolds, it is possible by pumping Er^{3+} glass to obtain an inversion of population between levels 1 and 2 and simplify this system into a quasi-two-level system. This allows pumping at a wavelength near

1480 nm to provide gain in the 1525-1560-nm range [36]. This simplification will be kept along this chapter.

When a signal ligth of intensity I_s at wavelength λ_s traverses a slice of EDF of infinitesimal thickness dz and atomic densities N_1 and N_2 for the lower and upper energy levels respectively, the energy change dI_s is given by:

$$dI_s = \{\sigma_{21}(\lambda_s) N_2 - \sigma_{12}(\lambda_s) N_1\} I_s dz \tag{5.2}$$

where $\sigma_{12}(\lambda_s)$ and $\sigma_{21}(\lambda_s)$ are the absortion and emission cross sections of the laser transition at λ_s, respectively. The absorption and emission cross sections spectra for alumino germanosilicate Er^{3+} glass fiber are displayed in the Figure 5.14. The data were obtained from the VPI transmission maker librairies.

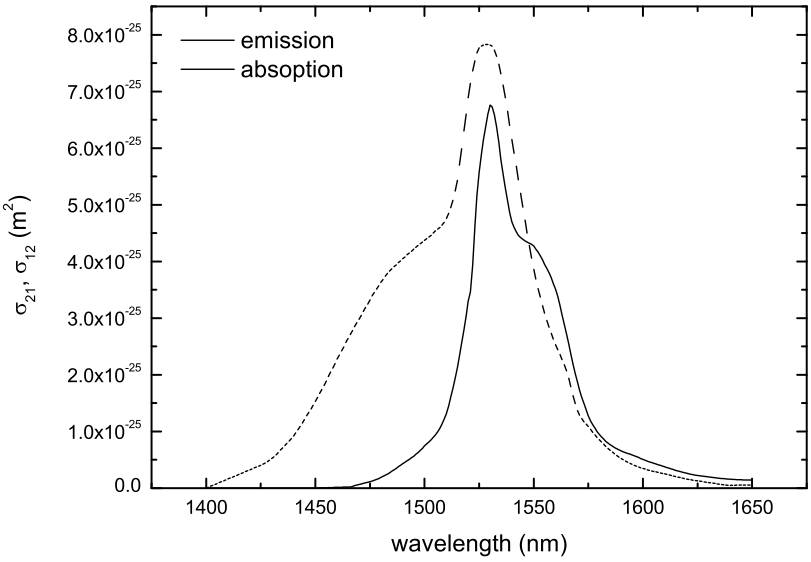

Figure 5.14: Emission and absoption cross sections spectra for alumino germanosilicate Er^{3+} glass fibers.

Equation 5.2 can also be rewritten as $dI_s/dz = gI_s$, where g is defined as the gain coefficient. Considering a total population density N_t, the relative inversion of population is given by $D = (N_2 - N_1)/N_t$. Thus, g can be expressed as:

$$g = \frac{N_t}{2} \{\sigma_{21}(\lambda_s)(1 + D) - \sigma_{12}(\lambda_s)(1 - D)\} \tag{5.3}$$

When $D = 1$, all the ions are in the excited state N_2 which means that a full inversion of population is achieved. On the contrary, if all the ions remain in the ground state, $D = -1$. Thus, D assumes values comprised between -1 and 1 which

corresponds to negative and positive values for the gain coefficient g. Figure 5.15 represents the gain coefficient spectra for differents values of D calculated using the absorption and emission cross sections displayed in Figure 5.14 for Alumino-germanosilicate Er^{3+} glass fibers. We noticed that $D = -1$ denotes that the medium is absorving at all wavelengths because the gain coefficient is negative. However, as the relative inversion increases, a positive gain coefficient is obtained for the longer wavelengths.

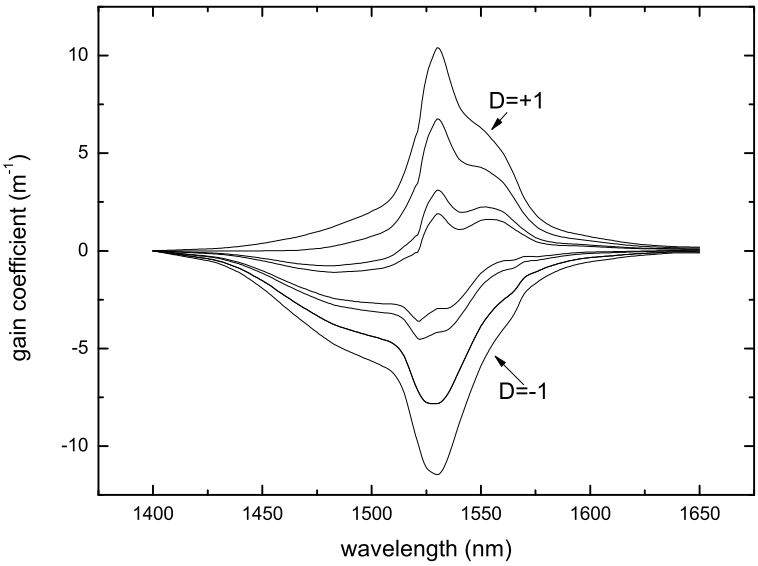

Figure 5.15: Gain coefficient spectra for different relative inversion of population for an alumino-germanosilicate Er fiber. $D = -1$ indicates that all the ions are in the gound state, while $D = +1$ denotes a fully inversion of population.

Considering that stimulated emission combined with spontaneous emission will introduce changes in the upper level population, the model needs to account for the variation of N_2. Therefore, the spatial power evolution along the longitudinal axis for an arbitrary number of *k* waves includes this effect. The following expression was also corrected, accounting for the forward (+1) and backward (-1) propagating terms in u_k and the overlap factor Γ_k. This formulation was presented by Saleh *et al* [37] and is from now on referred as the Saleh model. The equations 5.4 and 5.5 represent the rate equation for the fractional population of the upper state $N_2(z,t)$ and the change of power in the k^{th} beam, respectively.

$$\frac{\partial N_2(z,t)}{\partial t} = -\frac{N_2(z,t)}{\tau} - \frac{1}{N_t S}\sum_{1}^{N} u_j \frac{\partial P_j(z,t)}{\partial z} \tag{5.4}$$

where S stands for the active area and τ the spontaneous lifetime of the upper level.

$$\frac{\partial P_k(z,t)}{\partial z} = N_t u_k \Gamma_k \left[\left(\sigma_k^{21} + \sigma_k^{12}\right) N_2(z,t) - \sigma_k^{12}\right] P_k(z,t) \tag{5.5}$$

Under steady state conditions, the implementation of the above equations can follow the traditional numerical apporaches for ODE or alternatively use the average power analysis method (APA) presented in chapter 3. We recall that this method assumes that the powers are constant over an elemental section of fiber dz and consequentely, an analytical solution is obtainable within it.

For EDFA modelling, the APA allows a recursive computation of the power at the output of dz according to the following equations [38]:

$$P_k^{out} = P_k^{in} G_k(z) \tag{5.6}$$

$$G_k(z) = \exp\left(\left[\left(\sigma_{12}^k + \sigma_{21}^k\right) N_2 - \sigma_{12}^k N_t\right] \Gamma_k dz\right) \tag{5.7}$$

Averaging 5.6 along the length of the elemental section, after having substituted 5.7, it is easily shown that for each section the average power associated with the k^{th} wavelength is:

$$\langle P_k \rangle = P_k^{in} \frac{(G_k - 1)}{\ln(G_k)} \tag{5.8}$$

The calculation of N_2 in equation 5.7 is given by:

$$N_2 = \frac{N_t \sum_{k=1}^{N} \left(\frac{\langle P_k \rangle}{P_k^{IS}}\right)}{1 + \sum_{k=1}^{N} \frac{\langle P_k \rangle}{P_k^{IS}} \left(\frac{\sigma_{21}^k}{\sigma_{12}^k} + 1\right)} \tag{5.9}$$

where the intrinsic saturation power , P_k^{IS}; is equal to:

$$P_k^{IS}(\lambda_k) = \frac{h\nu S}{\left(\sigma_k^a + \sigma_k^e\right) \Gamma_k \tau} \tag{5.10}$$

A simulation using the method described above was implemented to obtain the net gain of 25 data signals comprised between 1520 nm and 1570 nm at the output of an EDFA. The latter is forwardly pumped at 1480 nm with a power of 100 mW, being the span of EDF 2.5 m, 5.0 m and 7.5 m. The simulation used an Erbium density of $7 \times 10^{24}\ m^{-3}$, a overlap factor of 0.43 and a fluorescence lifetime equal to 10 ms. The emission and absorption cross sections are the ones depicted in Figure 5.14, being the spatial step , Δz, equal to 2.5 cm. The gain results for the three lengths of EDF are are plotted in Figure 5.16.

On looking at the results, we verify that longer EDF provide more gain in the longer wavelength side. The results displayed in Figure 5.15 for the gain spetrum

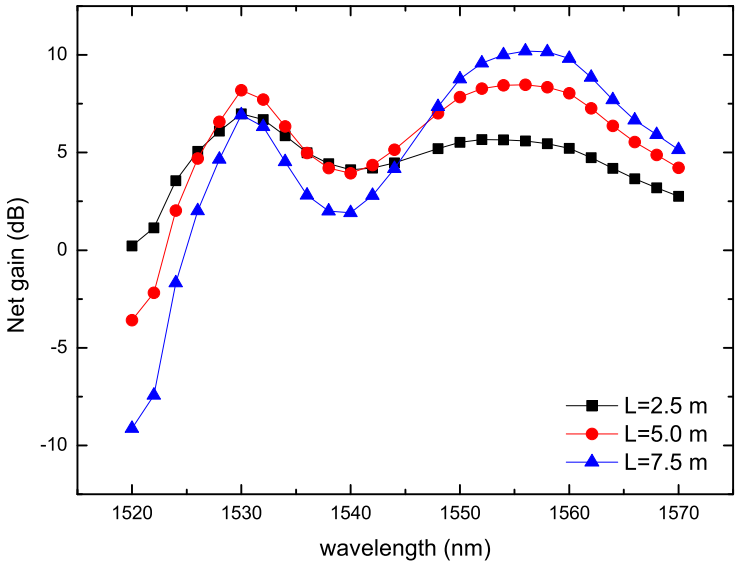

Figure 5.16: Net gain spectra at the output of three EDFA with 2.5 m , 5.0 m and 7.5 m, respectively. The pump is a 1480 nm diode laser with 100 mW of power forwardly injected into the EDF.

demonstrate that an unpumped EDF has its higher attenuation values at wavelengths around 1535 nm but the high emission cross sections in that spectral region allows for higher gain when strong excitation is provided (higher inversion of population). At longer wavelengths, a lower excitation level is required to have gain, but the maximum gain is smaller. For longer EDF, the pump power decreases as it propagates along the fiber and consequentely the ions in excited state decrease. Wavelengths that require smaller inversion of population to provide gain are more amplified in that context than they would be if smaller lengths of EDF were employed.

5.4.2 EDFA transients

The use of perturbation theory, allows the derivation of the EDFA temporal gain dependency disturbed from the steady state. The approach explained bellow was developed by Sun *et al* [39], [40] for the situation where the number of WDM channels that are inputted in an EDFA vary as a consequence of add/drop. The same procedure can be applied to a single channel with bursty/packeted data by assuming that the idle times corresponde to a steady state with a number of channels equal to zero, disturbed from the equilibrium with the addition of one channel.

We assume N WDM channels and a single stage EDFA with a length L. The powers in this formulation are expressed in units of number of photons per unit time. The

fractional population in the upper state, $N_2(z,t)$ and of the lower state, $N_1(z,t)$, satisfy the relationship $N_1(z,t) + N_2(z,t) = 1$.

The upper state population N_2 can be found from equation 5.5 and substituted into equation 5.4 according to:

$$\tau u_k \frac{\partial}{\partial t}\left(\frac{1}{P_k}\frac{\partial P_k(z,t)}{\partial z}\right) = -u_k\left(\frac{1}{P_k}\frac{\partial P_k(z,t)}{\partial z}\right) - \frac{1}{P_k^{IS}}\sum_{j=1}^{N} u_j \frac{\partial P_j(z,t)}{\partial z} - \alpha_k \tag{5.11}$$

where $\alpha_k = N_t \Gamma_k \sigma_k^{12}$ is the absoption constant. After integration over *z* from 0 to *L* and by naming $P_k^{in}(t)$ and $P_k^{out}(t)$ the input and output powers of the k^{th} channel at time *t*, the following expression is obtained [41]:

$$\tau \frac{d}{dt}\left[\ln \frac{P_k^{out}(t)}{P_k^{in}(t)}\right] = \ln \frac{P_k^{out}(t)}{P_k^{in}(t)} - \frac{1}{P_k^{IS}}\sum_{j=1}^{N}\left[P_j^{out}(t) - P_j^{in}(t)\right] - \alpha_k L \tag{5.12}$$

By introducing the overall gain parameter, $G_k(t) = \ln\left[P_k^{out}(t)/P_k^{in}(t)\right]$; and the total absorption constant, $A_k = \alpha_k L$, equation 5.12 can be rewritten as the following ordinary differential equations:

$$P_k^{IS}\left[\tau \frac{dG_k(t)}{dt} + G_k(t) + A_k\right] = -\sum_{j=1}^{N} P_j^{in}(t)\left[\exp\left(G_j(t)\right) - 1\right] \tag{5.13}$$

The system of ODE stated above can be reduced into a single equation by combination of channels *k* and *j*:

$$\tau \frac{dG_{kj}(t)}{dt} + G_{kj}(t) + A_{kj} = 0 \tag{5.14}$$

where $G_{kj} = P_k^{IS} G_k(t) - P_j^{IS} G_j(t)$ and $A_{kj} = P_k^{IS} A_k - P_j^{IS} A_j$.

The solution is trivial and given by $G_{kj}(t) = \left(G_{kj}^0 + A_{kj}\right)\exp(-t/\tau) - A_{kj}$, being the initial conditions used to determine G_{kj}^0.

The gain in the j^{th} channel is then expressed in terms of the gain in the k^{th} channel, as:

$$P_j^{IS} G_j(t) = P_k^{IS} G_k(t) - \left(G_{kj}^0 + A_{kj}\right)\exp\left(-\frac{t}{\tau}\right) + A_{kj} \tag{5.15}$$

The substitution of equation 5.15 in equation 5.13 originates the following expression:

$$\tau\frac{d}{dt}P_k^{IS}G_k\left(t\right)+P_k^{IS}A_k= \\ -\sum_{j=1}^{N}P_j^{in}\left(t\right)\left\{\exp\left[P_k^{IS}G_k\left(t\right)\right]-\left(G_{kj}^0+A_{kj}\right)\exp\left(\frac{-t}{\tau}\right)+\frac{A_{kj}}{P_j^{IS}}-1\right\} \quad (5.16)$$

Equation 5.16 is solved to determine the $G_k\left(t\right)$. To determine the gain of the other channels, the solution of 5.16 must be substituted in equation 5.15 using the condition that in steady state EDFA at $t=0$, we have $G_{kj}^0+A_{kj}=0$.

The overall gain parameter introduced above can also be expressed using the gain and absorption per units of length as $G_k\left(t\right)=\bar{g}_k\left(t\right)L$. The parameters $\bar{g}_{kj}^0$ and α_{kj} are defined as:

$$\bar{g}_{kj}^0=P_k^{IS}\bar{g}_k\left(0\right)-P_j^{IS}\bar{g}_j\left(0\right) \quad (5.17)$$

$$\alpha_{kj}=P_k^{IS}\alpha_k-P_j^{IS}\alpha_j \quad (5.18)$$

Thus, equation 5.16 takes the following form:

$$\tau\frac{d}{dt}P_k^{IS}\bar{g}_k\left(t\right)L+P_k^{IS}\bar{g}_k\left(t\right)L+P_k^{IS}\alpha_k\left(t\right)L= \\ -\sum_{j=1}^{N}P_j^{in}\left\{\exp\left[\frac{P_k^{IS}\bar{g}_k\left(t\right)+\alpha_{kj}}{P_j^{IS}}L\right]-1\right\} \quad (5.19)$$

Considering that the time dependent gain, $\bar{g}_k\left(t\right)$, was disturbed from steady state by a small dimensionless perturbation,$\bar{g}_{kt}\left(t\right)$, according to:

$$\bar{g}_k\left(t\right)=\bar{g}_{k0}\left[1+\bar{g}_{kt}\left(t\right)\right] \quad (5.20)$$

According to perturbation theory, the substitution of equation 5.20 in equation 5.19 originates two equations:

$$P_k^{IS}\bar{g}_{k0}L+P_k^{IS}\alpha_kL=-\sum_{j=1}^{N}P_j^{in}\left[\exp\left(\bar{g}_{j0}L\right)-1\right] \quad (5.21)$$

$$\tau\frac{d}{dt}\bar{g}_{kt}\left(t\right)+\bar{g}_k\left(t\right)=-\bar{g}_{kt}\left(t\right)\sum_{j=1}^{N}\frac{P_j^{in}}{P_j^{IS}}\exp\left(\bar{g}_{j0L}\right) \quad (5.22)$$

A saturation factor, γ is defined as:

$$\gamma = -\sum_{j=1}^{N} \frac{P_j^{in}}{P_j^{IS}} \exp\left(\bar{g}_{j0} L\right) = \sum_{j=1}^{N} \frac{P_j^{out}}{P_j^{IS}} \tag{5.23}$$

An averaged saturation factor can be used, given by:

$$\gamma = \frac{\gamma\left(0\right) + \gamma\left(\infty\right)}{2} \tag{5.24}$$

where $\gamma\left(0\right)$ and $\gamma\left(\infty\right)$ are the saturation factors in the initial and final states.
By considering the saturation factor, equation 5.22 can be rewritten as:

$$\tau \frac{d}{dt} \bar{g}_{kt}\left(t\right) + \left(1+\gamma\right) \bar{g}_{kt}\left(t\right) = 0 \tag{5.25}$$

The solution is given by:

$$\bar{g}_{kt}\left(t\right) = \bar{g}_{kt}^{0}\left(t\right) \exp\left(-\frac{t}{\tau_e}\right) \tag{5.26}$$

where τ_e is defined by the following:

$$\tau_e = \frac{\tau}{1+\gamma} \tag{5.27}$$

Therefore, the gain per unit length can be expressed as:

$$\bar{g}_k\left(t\right) = \bar{g}_{k0}\left[1 + \bar{g}_{kt}^{0} \exp\left(-\frac{t}{\tau_e}\right)\right] \tag{5.28}$$

Equation 5.28 can be rewritten as equation 5.29 in order to include the initial and final gains after the perturbation, enhancing its application range.

$$\bar{g}_k\left(t\right) = \vec{g}_k\left(\infty\right) + \left[\bar{g}_k\left(0\right) - \bar{g}_k\left(\infty\right)\right] \exp\left(-\frac{t}{\tau_e}\right) \tag{5.29}$$

Where $g_k\left(0\right)$ and $g_k\left(\infty\right)$ are the gain per unit length of the k^{th} channel before and after the transient, respectively and P_k^{out} is its output power.

To assess the impact of the use of EDFA using burst mode transmission, several experiments were carried on. The latter aim to characterize the transient in terms of gain excursion and time constants. A comparizon with distributed Raman amplifiers was also accomplished [42].

The implemented experimental setup used for the transient assessment consists of an external cavity laser peaking at 1549.32 nm and an optical power of 10.0 dBm, followed by a polarization controller and a Mach-Zehnder optical modulator operating at 2.5 Gb/s. The considered digital data are programmable packets with an approximate duration of $26\mu s$ (pseudo random bit sequence (PRBS) of length $2^{16}-1$) and different idle times (4, 20, 40 and $80\mu s$), produced by a BERT (Agilent N4901B).

After the Mach-Zehnder the optical signal is amplified by an EDFA, attenuated, and then injected into a span of 40.0 km of SSMF. The optical power at the fiber input and output are 10.0 dBm and 0.5 dBm, respectively. To analyze the temporal evolution of the packets, a PIN (HP-11982A) and an (Agilent Infinium 86100A) oscilloscope were used as receivers. The EDFA was previously characterized in order to determine the input optical signal saturation power (-10 dBm for driving current of the pump laser equal to 1.98 A for a threshold driving current of 0.7 A). It must be noted that all the subsequent experiments were carried out with the EDFA in deep saturation (corresponding to a pump power of 26 dBm). The gain excursion of packets was analyzed using the oscilloscope.

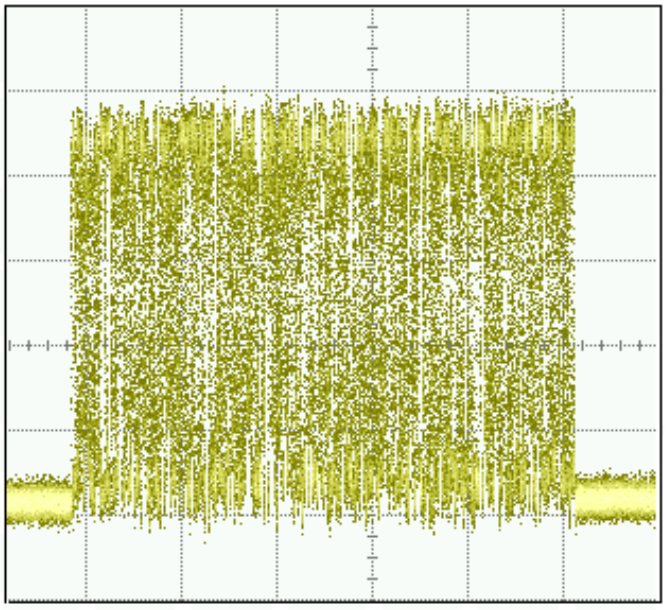

Figure 5.17: $2^{16} - 1$ bit PRBS packet - 50000 bit idle obtained in the oscilloscope at the receiver for a Raman amplification with 40 km of SSMF. The horizontal scale is 5.000 μs/div and the vertical scale is arbitrary.

For the Raman amplification assessment, the implemented experimental setup uses the same scheme as the EDFA but an isolator was inserted after the Mach-Zehnder modulator to protect the signal source. The EDFA and the attenuator were removed and a Raman amplification module from Amonics, model ARA-CL-4B-R-FA, with 4 pumping lasers, peaking at 1426, 1444, 1462 and 1487 nm with a total optical power of 1 W was added to the setup. The experiment was carried out with a span of SSMF fiber with 40 km. The input and output fiber powers are equal to -0.52 dBm and 3.22 dBm, respectively.

The results concerning the Raman amplification scheme are depicted in Figure 5.17,

with the visualized patterns at the oscilloscope. As excepted, the amplifier is unsaturated so transients are not visible. However, when EDFA are used, a distinct decaying on the packet envelope is assessible. The latter exhibit a behaviour that fit an exponential decay, with characteristic time τ_{ch} given by 5.30.

$$P(t) = P_0 \exp\left(-\frac{t}{\tau_{ch}}\right) + P_\infty \tag{5.30}$$

where P, P_0 and P_∞ stands for the instantaneous optical power, the packet initial optical power and the steady state optical power, respectively. Figure 5.18 (a), (b), (c) and (d) display the observed packets and the exponential fitting curves for idle times value equal to 2, 20, 40 and 80 μs, respectively.

The characteristic decay times obtained from the packet envelope fit (τ_{ch}) are also presented in Figure 5.19. Their dependency with the idle time was adjusted by an exponential decay with r^2 value equal to 0.9803.

From these results, we notice that the packet decaying time decreases with the idle time increase, resulting from the increase of the Er^{3+} ions population inversion [43]. The exponential fit depicted in Figure 5.19 demonstrates that there is a stabilization towards $1.35 \pm 0.25 \mu s$ as the idle time increases indefinitely.

The obtained experimental results were also compared to the theoretical model, described above, namely the time parameter τ_e, given by 5.27. In the calculation, we consider an EDF core radius equal to $1.8 \mu m$, a confinement factor of 0.9, being the absorption and emission cross sections are respectively equal to $2.1 \times 10^{-25} m^2$ and $5.5 \times 10^{-25} m^2$ at the pump wavelengths and $5.2 \times 10^{-25} m^2$ and $5.5 \times 10^{-25} m^2$ at the signal wavelength [44]. The packet initial and final optical power were used in 5.29 ($g_k(0)$ and $g_k(\infty)$). The analyzed scenario was the one with the highest idle time ($80 \mu s$) in order to obtain a good inversion of population and thus a situation close to the steady state before the transient regime. The obtained value for the theoretical characteristic decay time, τ_e, given by equation 5.29 was $1.72 \mu s$, which is in very good agreement with the one obtained experimentally (1.71 ± 0.03 μs).

In the EDFA dynamics, the restoration of the initial conditions depends on the idle time. If the latter is high enough to allow a complete inversion of population of Erbium ions, the initial conditions are restored and the next packet will behave as its precedent. However, if the next packet arrives before complete inversion, it will experience less initial gain and consequently less power decay. To assess the amount of gain excursion with variable idle time we need to evaluate how consecutive packets are affected by variable idle time [45].

The experiment was extended in order to evaluate the sequences described in Table 5.5. The patterns of the packets with $2^{12} - 1$ (Sequence A and Sequence B) and $2^{16} - 1$ (Sequence C and Sequence D) were visualized in the oscilloscope as displayed in Figure 5.20 and Figure 5.21, being noticeable that the packets exhibit different gain excursion due to the variable idle time. The initial power difference of consecutive

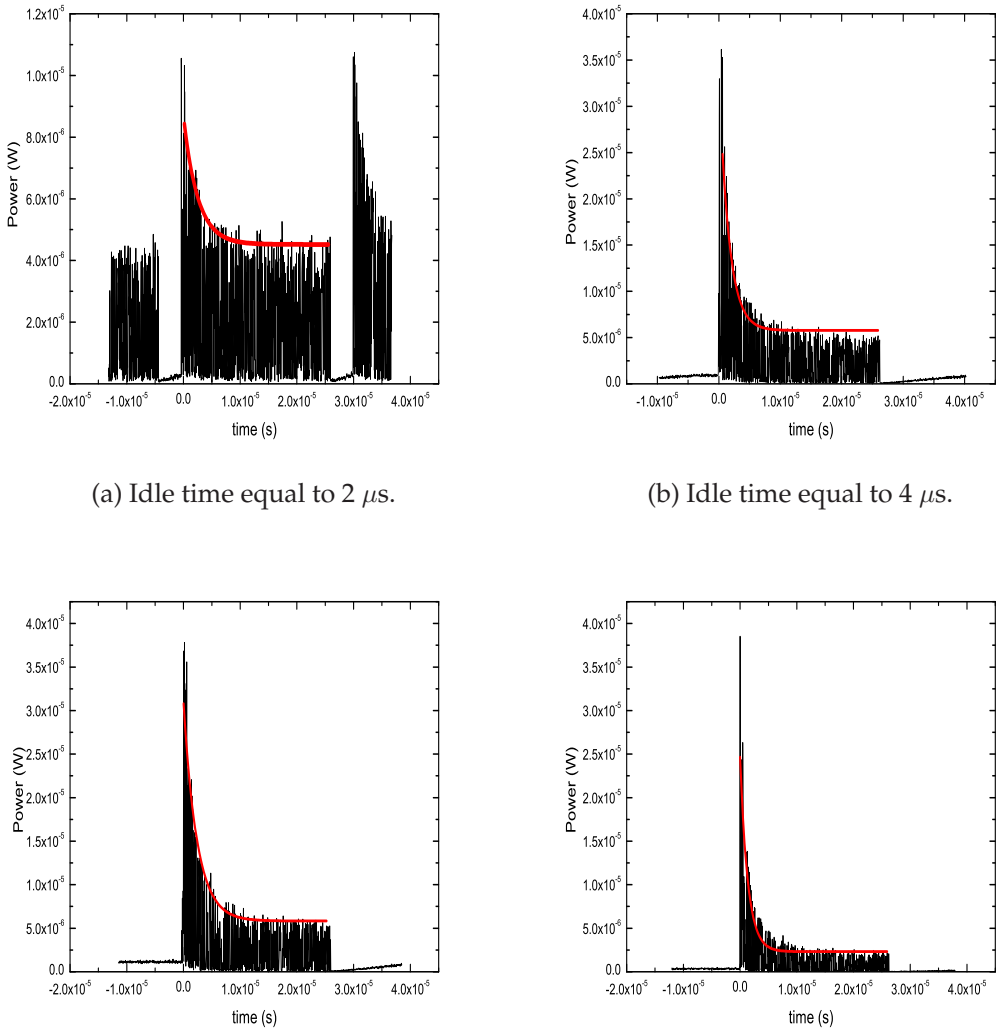

(a) Idle time equal to 2 μs.

(b) Idle time equal to 4 μs.

(c) Idle time equal to 40 μs.

(d) Idle time equal to 80 μs.

Figure 5.18: Visualized packets and their envelope exponential fit.

packets was then computed. For the lower length packets ($2^{12}-1$ PRBS) that difference decreases with the idle time (21.81 μs for Sequence A and 3.76 μs for Sequence B). This result was interpreted by considering that lower idle time situation is not sufficient to obtain a good inversion of population of Erbium ions. The same tendency was also observed for the longer length packets (Sequence C and Sequence D).

To assess the performance of a network in the presence of packet traffic, we have analyzed the Q factor at the receiver and compare its value with the Q factor in the back to back situation. The Q factor difference between the back-to-back and the receiver (ΔQ) was computed as a function of the packet occupancy density, as depicted in Figure 5.22. The used sequences include packets with $2^{16}-1$ intercalated

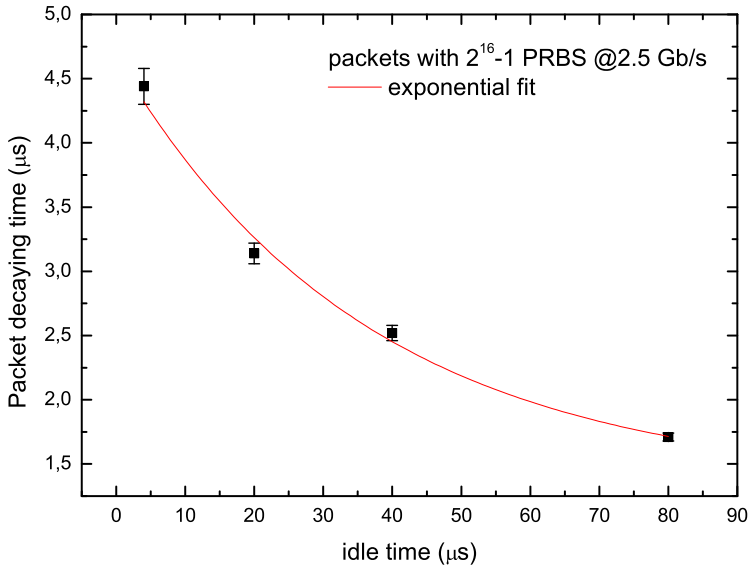

Figure 5.19: Packet decaying time as a function of the idle time. The line represents an exponential fit in the form $A_0 \exp(B_0) + C_0$. $A_0 = 3.32 \pm 0.27\ \mu s$, $B_0 = 36.39 \pm 10.22\ \mu s$, $C_0 = 1.35 \pm 0.25\ \mu s$, $r^2 = 0.9803$.

Table 5.5: Tested bit sequences.

Sequence A	$2^{12}-1$ PRBS	10000 zeros	$2^{12}-1$ PRBS	50000 zeros
Sequence B	$2^{12}-1$ PRBS	100000 zeros	$2^{12}-1$ PRBS	200000 zeros
Sequence C	$2^{16}-1$ PRBS	10000 zeros	$2^{16}-1$ PRBS	50000 zeros
Sequence D	$2^{16}-1$ PRBS	100000 zeros	$2^{16}-1$ PRBS	200000 zeros

with variable idle times in the 2-80 μs range (points 1, 3, 5 and 7 in Figure 5.22) and packet with $2^{16}-1$ intercalated with fixed idle times in the 2-80 μs range. By looking at the plot, we notice that the best situations, the ones in which the ΔQ has a lower value (points 6, 7 and 8), is obtained with a high packet density. This result is due to the increase in the average power at the receiver. We also notice that the ΔQ is quite stable in the $0.3-0.7$ occupancy density range and that the gain excursion due to variable idle time does not seem to be more penalizing than the situation with fixed idle time.

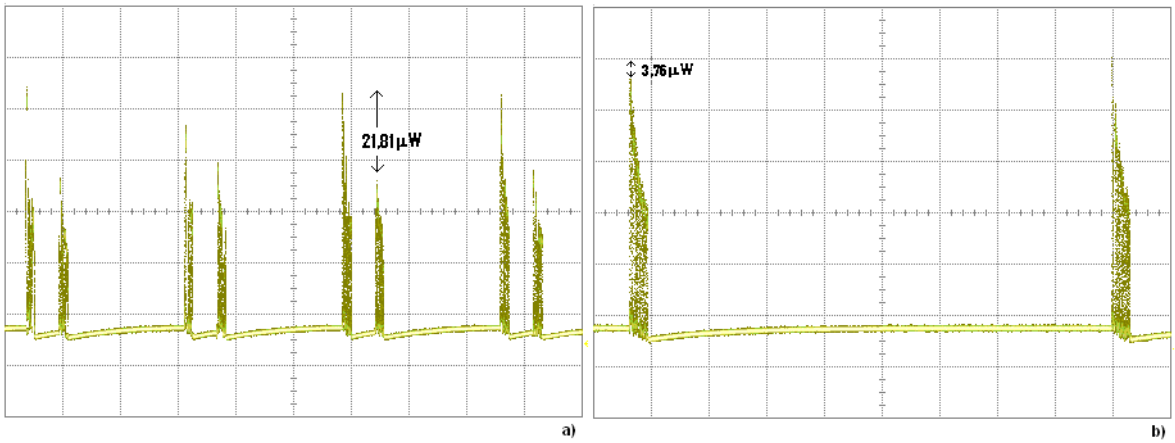

Figure 5.20: Visualized sequences at the receiver: (a) Sequence C, (b) Sequence D. Horizontal scale 20.00 μs/div and vertical scale is arbitrary.

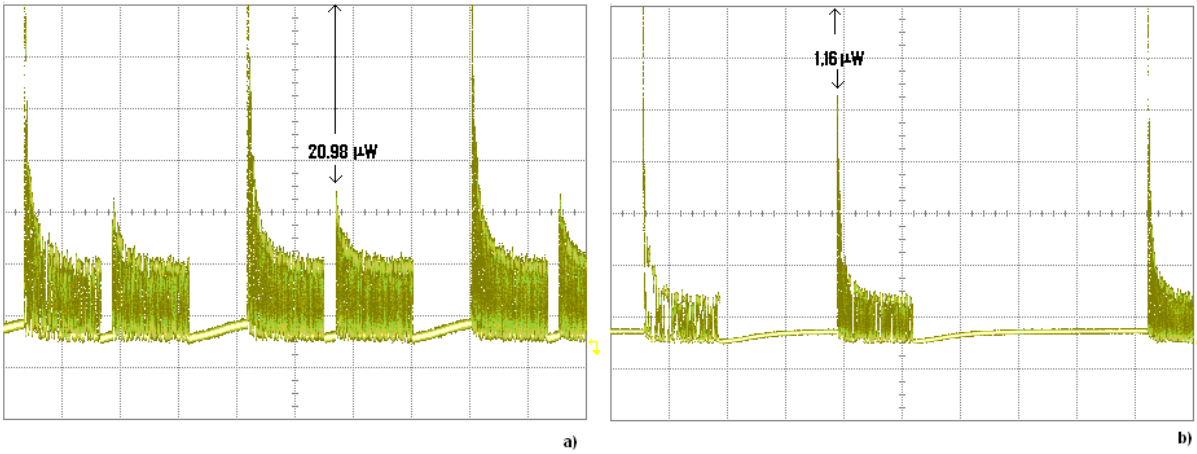

Figure 5.21: Visualized sequences at the receiver: (a) Sequence A, (b) Sequence B. Horizontal scale 5.000 μs/div and vertical scale is arbitrary.

5.4.3 EDFA transient mitigation

Mitigation methods for burst mode amplifiers transients were successfully demonstrated and are based on a combination of techniques such as linear gain control, gain clamping and fast automatic gain control [46], [39]. Additionally, passive mitigation approaches have also been proposed, such as the use of EDF with a large active area of Er^{3+} [47], [48]. In the optical domain, the idea of re-circulating ASE as a clamping mechanism in a feed-back loop was presented in the context of WDM ring networks [49]. The idea of re-circulating ASE using a bandpass filter to select the lasing wavelength, and a variable optical attenuator (VOA) to adjust the feedback cavity loss was presented in [50]. The same principle using FBGs as bandpass filters was demonstrated to flatten and clamp the gain of L-band EDFA for

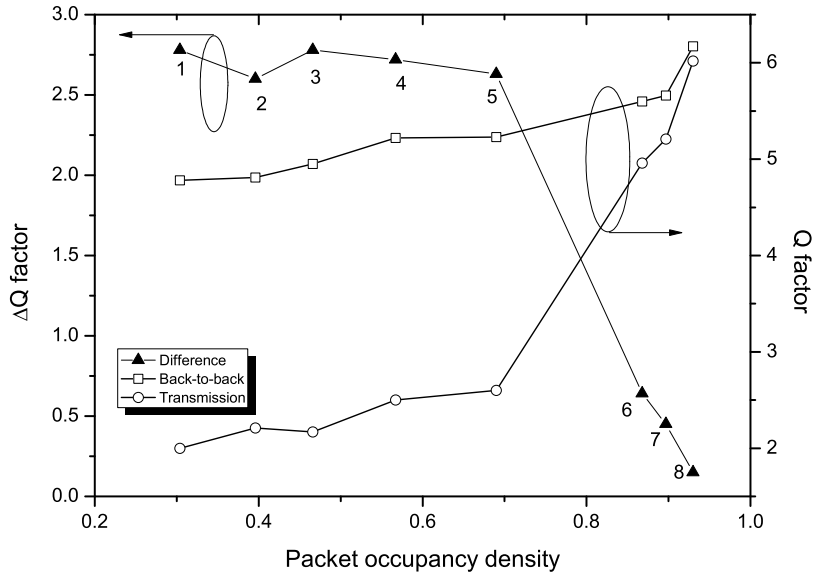

Figure 5.22: Q factor as a function of the occupancy density. The lines are visual guides.

WDM applications [51]. Other approaches based on feed-back techniques make use of a DWDM multiplexer [52]. Published studies in the context of WDM ring PON, such [51] have assessed the stabilizing effect of feedback based gain clamping on cascaded EDFA. Hybrid electronic/optical techniques to achieve transient mitigation are valuable such as the approach presented in [53] in which, the use of a packet envelope technique to generate an inverted modulation on a control signal promotes the mitigation of the transients. The subsequent use of a FBG filters the control signal.

In order to reduce the impairment of transients, we report two mitigations techniques that were developed, based upon the optical clamping. The first method performes clamping using the saturation feedback signal reflected on a FBG. Like the previously reported feed-back methods, it provides constant gain on the packets envelope. The second method uses bidirectional CW clamping as an enhanced method.

Method 1

This solution preserves the passiveness of the access network, clamps the transient of the packets gain and thus improves the performance of the network. The idea of using a CW DFB laser signal in the feed-back loop instead of re-circulating ASE, as fully used in the literature, is valuable because it increases the OSNR. This technique is feasible in the context of hybrid WDM/TDM PON, namely in the TDM tree, by using a small portion of the downstream to clamp the gain of the upstream bursty

channel. The proposed scheme is illustrated in Figure 5.23. It is composed of two

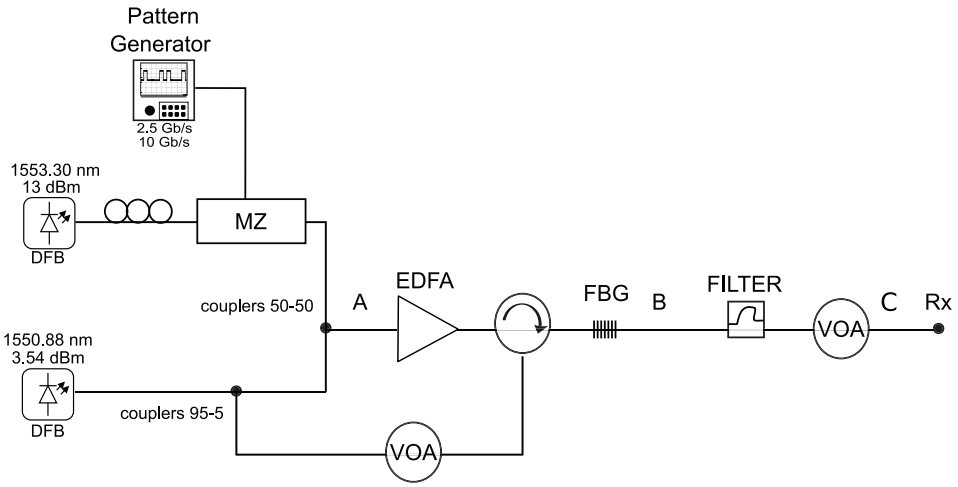

Figure 5.23: Scheme of the experimental setup used for the gain clamping.

distributed feed-back (DFB) lasers peaking at 1553.30 nm and 1550.88 nm, emitting with optical power of 13.00 dBm and 3.54 dBm, respectively. The wavelength of the control laser was previously tuned in order to match the Bragg wavelength of a FBG with a rejection of 27.00 dB and a bandwidth, $\Delta\lambda$, equal to 0.81 nm. The first laser (data) is followed by a polarization controller, modulated by a Mach-Zehnder optical modulator at 2.5 Gb/s, with programmable packets, as described in the previous section, and coupled with the second CW laser. The two copropagating signals are injected into an EDFA pumped with a laser diode at 965 nm. After the EDFA the control signal is reflected by the FBG and re-injected into the EDFA generating a lasing mechanism. The power of the feedback signal is controlled by a variable optical attenuator (VOA) placed in the feedback path. The spectrum images captured by the OSA at the points A and B assigned in Figure 5.23 are displayed in Figure 5.24. Note that in point B, the clamping channel was removed by the FBG. The data signal is then filtered, being its power adjusted by a second variable optical attenuator (VOA), in order to have a constant value of -8 dBm at the receiver (C).

The experiment was accomplished with packets of $2^{16} - 1$ PRBS and idle lengths equal to 50000 bits at 2.5 Gb/s and then repeated at 10.0 Gb/s where the idle length was varied from 50 000 to 200 000 bits. The measurements include the packets gain excursion and the Q factor. For comparison purposes, Q measurements when the packets are replaced by PRBS with lengths equals to $2^{15} - 1$ and $2^{31} - 1$ were also carried out.

For the measurements carried out at 2.5 Gb/s, oscilloscope captions were taken at the receiver for increasing re-injected power (from -30 dBm to 5 dBm) and for the back-to-back situation, as depicted in Figure 5.25. The packet gain excursion and the Q at the receiver were measured being their dependency with the re-injected power

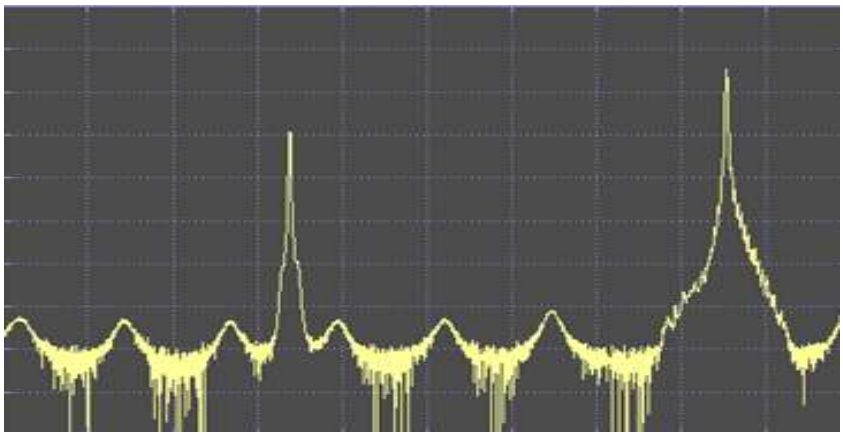

(a) Point A.

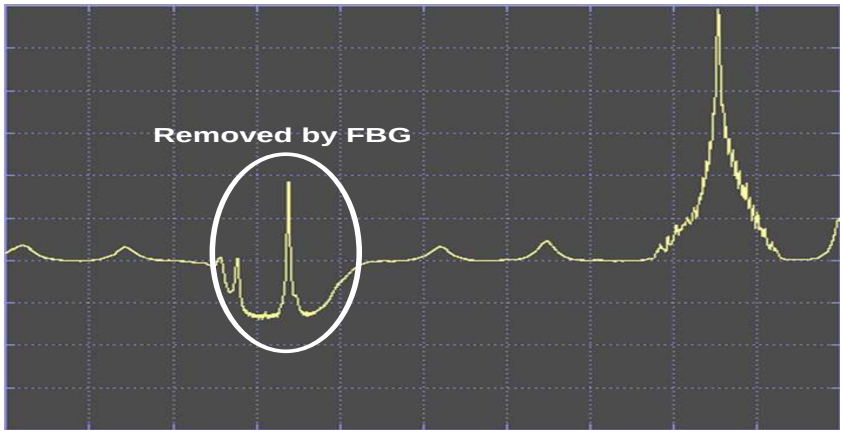

(b) Point B.

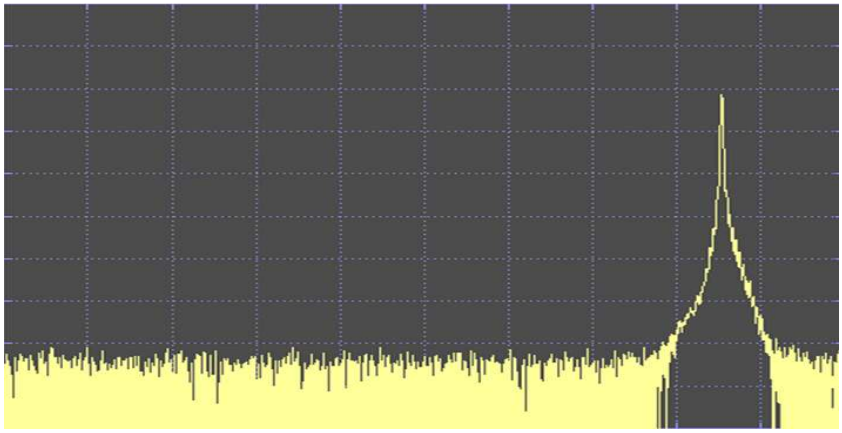

(c) Point C.

Figure 5.24: Spectra captured by the OSA. Horizontal scale 0.47 nm/div, vertical scale 10 dB/div.

displayed in Figure 5.26. The back-to-back has a Q-factor equal to 5.85 dB. The Q-factor obtained when packets are replaced by PRBS with lengths $2^{31} - 1$ and $2^{15} -$

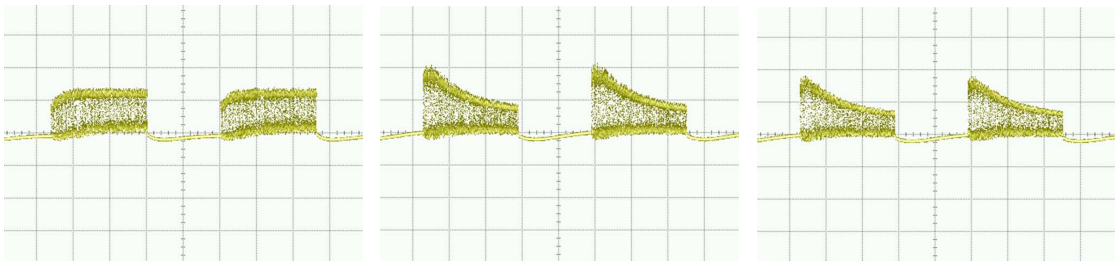

(a) Back-to-back. (b) -30 dBm. (c) -25 dBm.

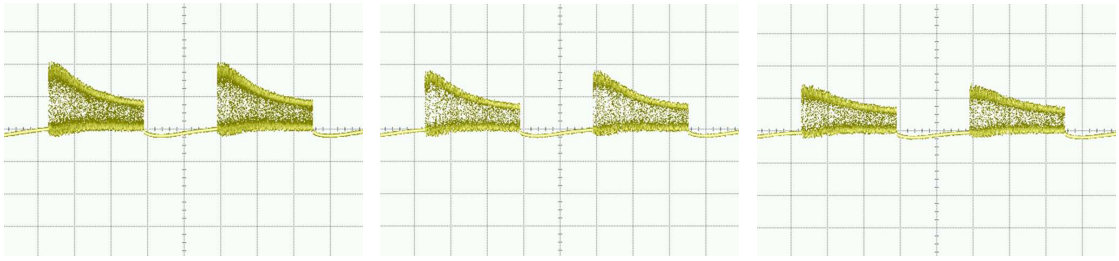

(d) -20 dBm. (e) -15 dBm. (f) -10 dBm.

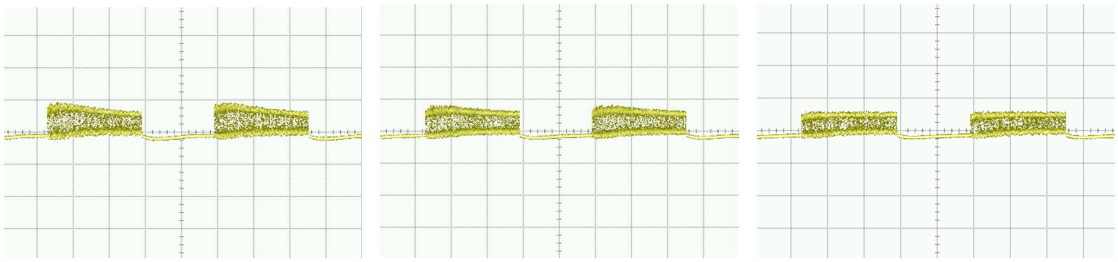

(g) -5 dBm. (h) -2 dBm. (i) 5 dBm.

Figure 5.25: Spectra captured by the OSA. Horizontal scale 0.47 nm/div, vertical scale 10 dB/div.

1 are also displayed. On analyzing those results, we notice that by increasing the power of the feed-back signal, the clamping is enhanced and consequently, the gain excursion of the packets decreases. From the Q-factor results, we also observe that the clamping improves the performance of the system. This effect observed in packets is not observed in PRBS where the Q is almost constant.

For the measurements carried out at 10 Gb/s, a similar behaviour is also observed: the gain excursion decreases with the feedback signal power and consequently, the system performance is also enhanced. Measurements with different idle lengths (corresponding to 5, 10 and 20 μs) were also accomplished. The results concerning the gain excursion as a function of the measured reinjected power are displayed in Figure 5.27. For longer idle times (20 μs, 200000 bits), the variation of gain excursion, when the feedback signal power is varied from -30 dBm to -10 dBm, is higher and the packet still exhibit transient when the packets with lower idle times (5 μs and 10 μs)

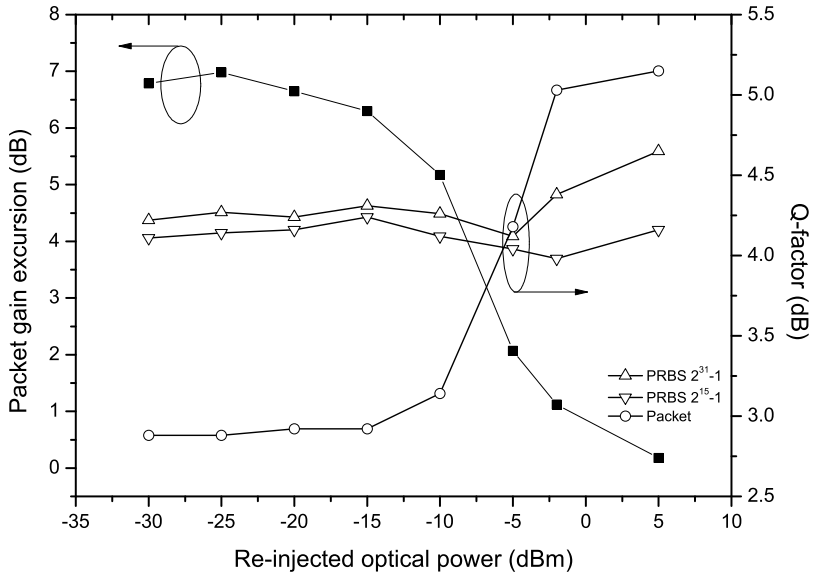

Figure 5.26: (left) Packets gain excursion as a function of the re-injected signal power. (right) System signal-to-noise ratio as a function of the re-injected signal power with traffic based on packets and PRBS of length $2^{31}-1$ and $2^{15}-1$. The receiver power is kept constant equal to -8 dBm.

are already fully clamped. This result is explainable by considering that the increase in the transient is due to an increase in the Er^{3+} ions population inversion. The system performance is assessed with the Q-factor results depicted in Figure 5.28. The results are consistent with the gain excursion, showing that the Q-factor is improved when the gain excursion is decreased.

The transients in EDFA arise due to the modulation in time, namely the packets. As the packets bit rate approaches the frequency with which the erbium gain dynamics can respond, the transients become more relevant. In both situations (2.5 Gb/s and 10 Gb/s), the packets have the same lengths ($2^{15}-1$) but they have different durations (26.21 μs and 6.55 μs) which corresponds to different dynamics with the Erbium. The input with the longer duration will quickly deplete the reservoir by causing a very fast power transient in a way that is more noticeable to the packet with shorter duration. The idle time is also important because it is concerned with the recovery time of the Erbium dynamics. The longer the idle time the higher is the inversion of population of Erbium ions when the next packet arrives and the stronger the transient. Thus the situation that we can compare is the one with the same idle time (20 μs). The results at 2.5 Gb/s in Figure 5.26 were obtained with idle time equal to $20\ \mu s$ while the results at 10 Gb/s (Figure 5.27 and Figure 5.28) were obtained with idle times equal to 5, 10 and 20 μs. To assess the influence of the packet duration on the EDFA transients, only

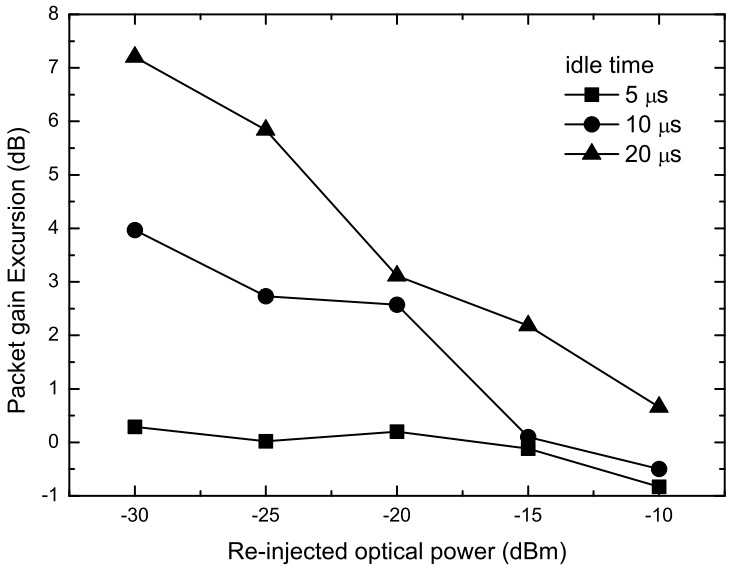

Figure 5.27: Gain excursion as a function of the feedback signal power for packets with idle time equal to 5 μs (50000 bits), 10 μs (100000 bits) and 20 μs (200000 bits) at 10 Gb/s. The receiver power is kept constant equal to -8 dBm.

the 20 μs idle time situations can be compared. Hence it is expectable that the longer packets present stronger transients measured by higher gain excursion and lower Q factor. On looking at Figure 5.18, we verify that the characteristic decay times for idle time equal to 20 μs is approximately 3.5 μs. Since each of the packets (at 2.5 Gb/s and 10 Gb/s) have a duration superior to that time, we can conclude that both the packets are affected in the same way by the transients. The results on Figure 5.26 and Figure 5.27 demonstrate a gain excursion of 6.51 dB and 6.54 dB respectively, being the packet at 10 Gb/s mitigated with lower re-injected power. On looking at Q factor, we notice that it the same trend is observed at both bitrates. At 10 Gb/s the Q-factor stabilizes with lower re-injected power.

Method 2

The idea of this technique is to use the intrinsic characteristics of bidirectional traffic existing in PON as a transient mitigation mechanism for the packeted / bursty upstream traffic. In such architecture, instead of using re-circulating ASE that degrades the OSNR, the downstream channel itself acts as a clamping signal. Since we presume that its power is possibly low due to the PON operation and that by this reason the clamping on the EDFA transient could be insufficient, a FBG was inserted in order to enhance the clamping. Unlike conventional clamping mechanisms, the proposed method does not use feed-back. The principle of operation is summarized

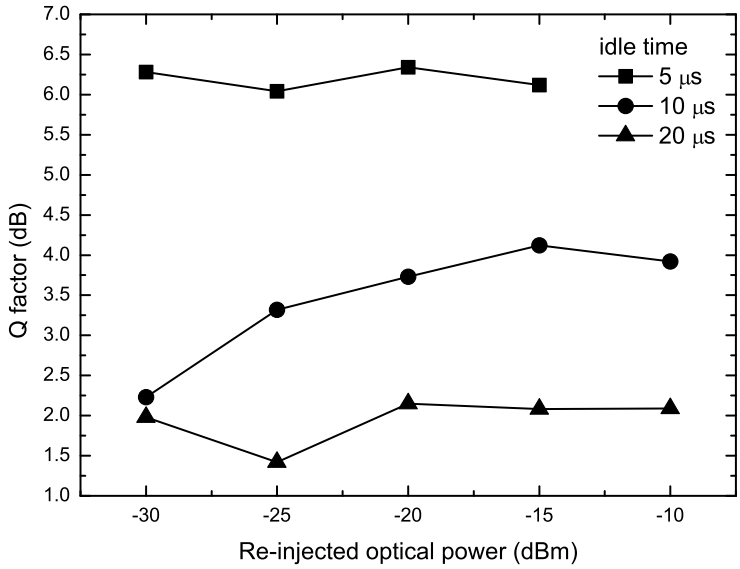

Figure 5.28: Signal-to-noise ratio as a function of the feedback signal power for packets with idle time equal to 5 μs (50000 bits), 10 μs (100000 bits) and 20 μs (200000 bits) at 10 Gb/s. The receiver power is kept constant equal to -8 dBm.

in Figure 5.29, where a remote node is schematized. In such a configuration, two channels are dropped (and added) using the 200 GHz and 100 GHz add/drops. The 90/10 power splitters are used to select the downstream channel power so that it can be used to clamp the EDFA. A FBG tuned with the clamping channel is inserted in the opposite side of the EDFA to provide the bidirectional clamping.

Although the scheme suggests backward clamping for a matter of simplicity, forward clamping is also feasible. To infer the efficiency of forward and backward clamping, some simulations were carried on. They compute the packet gain excursion by implementation of Bononi et al dynamical model for EDFA [43]. The results obtained for a span of 15 m of EDF using 20 μs packets are plotted on Figure 5.30.

On looking at the results, it is noticeable that despite the forward clamping is more efficient on mitigating the transient, the method converges when the clamping power is increased. To demonstrate experimentally the proposed mitigation approach, we implemented the setup depicted in Figure 5.31 that provides forward clamping. Although, some of the used equipments are not cost efficient for PON, the experiments serves the purpose to demonstrate the technique in a laboratorial environment.

It consists of two DFB lasers peaking at 1554.92 nm and 1550.80 nm with optical powers of 13.0 dBm and 3 dBm, respectively, followed by polarizations controllers. The laser at 1554.92 nm works as the upstream data signal and is optically modulated by a Mach-Zehnder operating at 2.5 Gb/s with an extinction ratio of 14.4 dB. The data

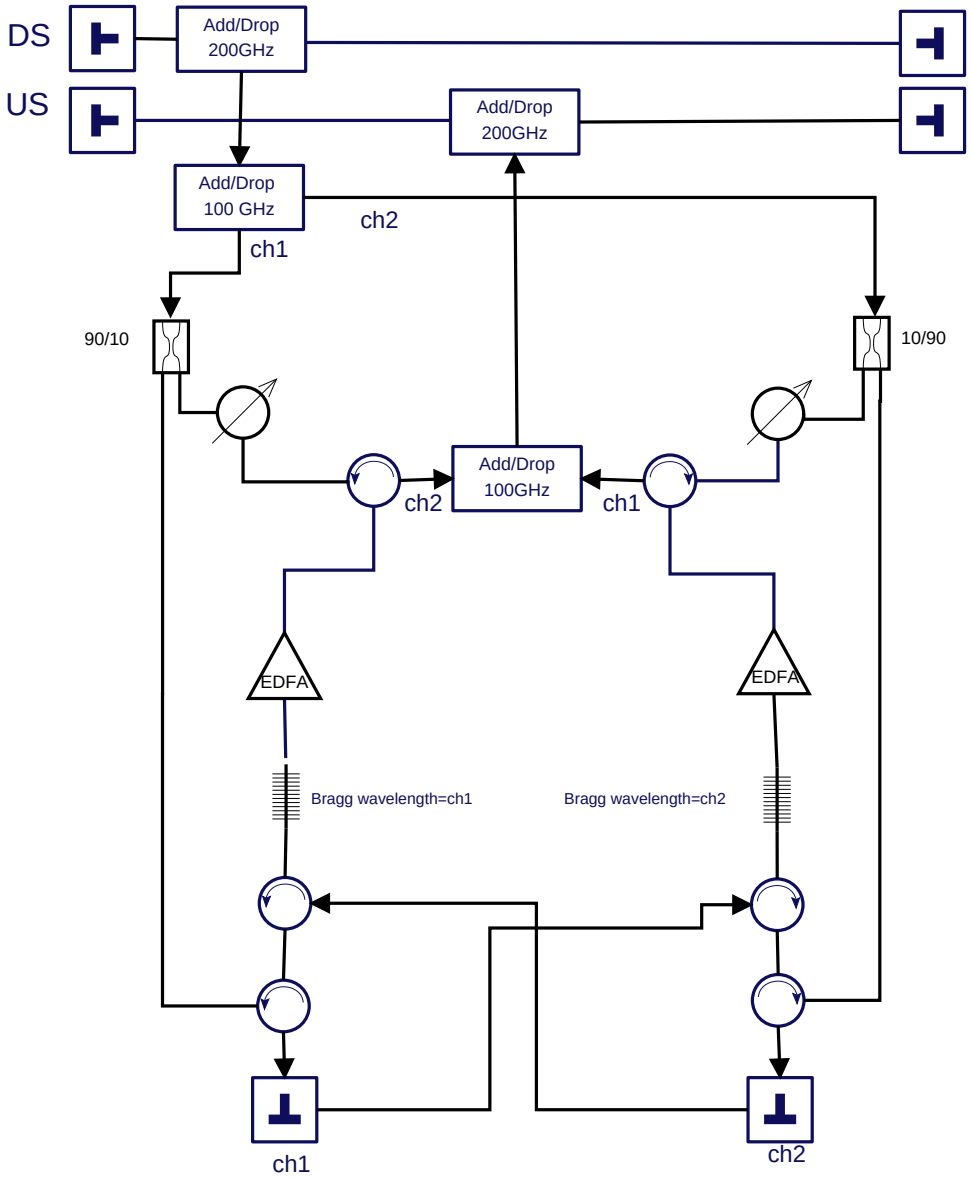

Figure 5.29: Generic clamping scheme feasible in a WDM/TDM-PON remote node (RN) in which two channels are dropped / added.

are programmable packets with a duration of 26 μs (pseudo random bit sequence-PRBS of length $2^{16} - 1$) and an idle time equal to 20 μs (50000 bits), produced by a bit error rate tester (BERT) (Agilent N4901B). The signal at 1550.80 nm works in continuous wave (CW) and represents the clamping control signal, being its power adjusted by a VOA. The two signals are brought together by a 50 / 50 coupler and injected into a bidirectionally pumped highly EDF (Thorlabs ER-4/125) with a span of 22.5 m. The average inputted power of the data signal is -7.0 dBm. The EDF pumps are three diode lasers peaking at 1470 nm, 1480 nm and 1490 nnm with a total injected power of 24.0 dBm. Two WDM couplers are used to join signals and

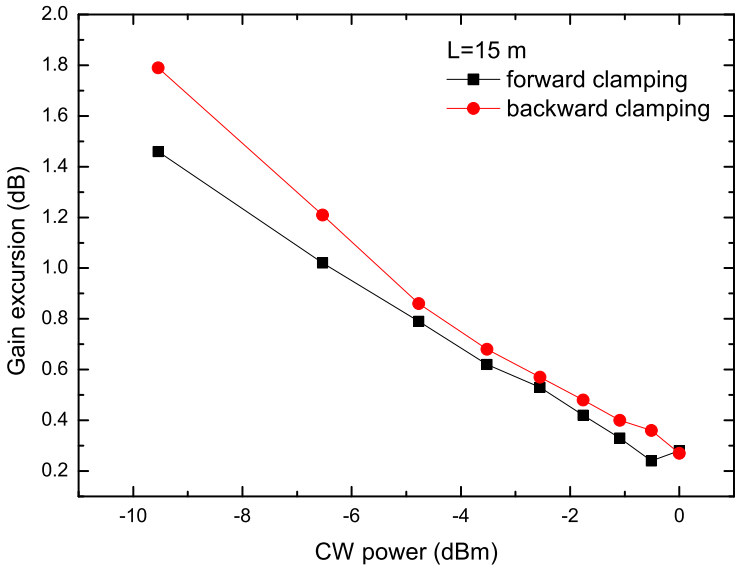

Figure 5.30: Packet gain excursion as function of control signal power for an EDF with 15 m. (black squares) fForward clamping, (red circles) backward clamping.

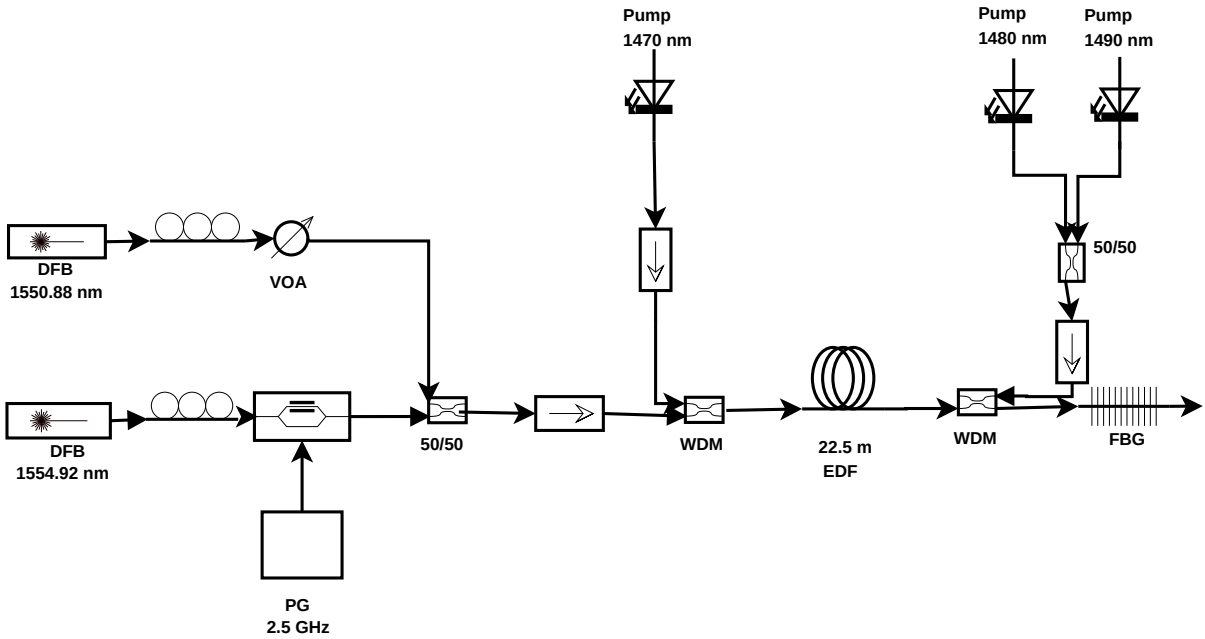

Figure 5.31: Scheme of the implemented experimental setup.

pumps as well as three isolators to protect the sources. After the amplification stage, a FBG with a rejection of 27.0 dB and an optical bandwidth, $\Delta\lambda$, equal to 0.81 nm is inserted in order to reflect the clamping control signal backwardly into the EDF. To analyze the temporal evolution of the upstream data packets, a PIN (HP-11982A) with

responsivity of 0.7 A/W and an oscilloscope (Agilent Infinium 86100A) oscilloscope were used. The gain excursions of packets as well as the Q factor were experimentally analyzed.

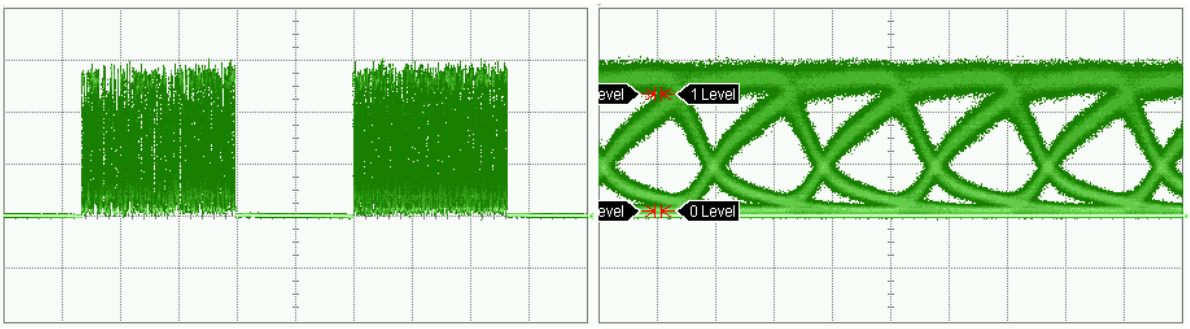

Figure 5.32: Back-to-back. (Left)-Pattern- horizontal scale 10.00 μs/div, vertical scale 30 mV/div. (Right) eye diagram- horizontal scale 200 ps/div, vertical scale 30 mV/div.

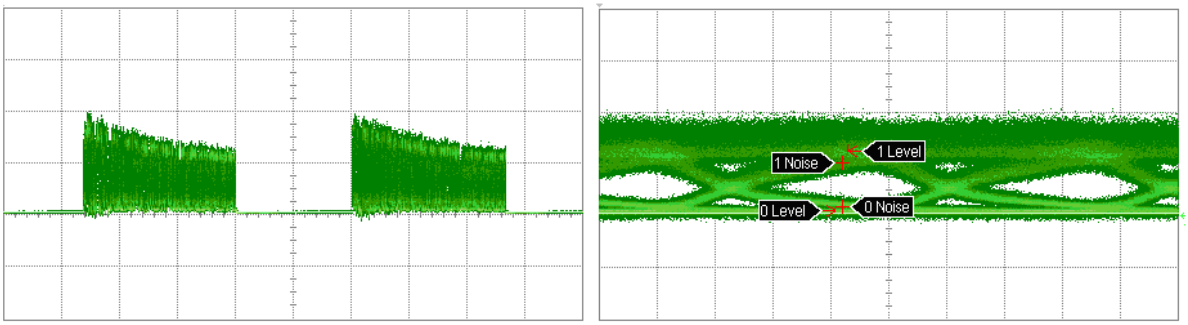

Figure 5.33: Receiver output with the CW signal off. (Left)-Pattern- horizontal scale 10.00 μs/div, vertical scale 100 mV/div. (Right) eye diagram- horizontal scale 100 ps/div, vertical scale 100 mV/div.

Firstly, the experiment began with the visualization of the back-to-back performance. Thus, with the CW signal off, the patterns and eye diagrams were visualized on the oscilloscope, being the extinction ratio and Q-factor measured. After that, the same procedure was applied at the system receiver. The measured Q factor are 4.83 dB and 2.63 dB for back-to-back and receiver respectively. The captured patterns and eye diagram on back-to-back and receiver are depicted in Figure 5.32 and Figure 5.33, respectively.

In order to emphasize the effect of the FBG in the proposed mitigation setup, we compare the results obtained with FBG (enhanced clamping) and without FBG (simple clamping) the FBG and varying the clamping control signal power -25.74 dBm to -1.67 dBm, being the Q-factor measured.

The use of a control signal is able to clamp the gain whenever its power is high enough, as stated from the square plot on Figure 5.34, where the gain excursion

is plotted as a function of the clamping control input power for the implemented situations: simple clamping and enhanced clamping. Hence, a decrease on the gain excursion is observed when the control power is increased. However, the use of a FBG with Bragg wavelength coincident with the control signal is able to re-inject it backwardly into the fiber, enhancing the clamping while keeping the same amount of power. A decrease on the gain excursion is observed, when the control power is increased. Both results were linearly fitted. For the simple clamping, the linear fit provides a slope equal to -0.047 dB/dBm, the enhanced clamping data has a slope equal to -0.036 dB/dBm. In the latter case, the gain excursion decreases 1.12 dB, when the control power is equal to -25.7 dBm.

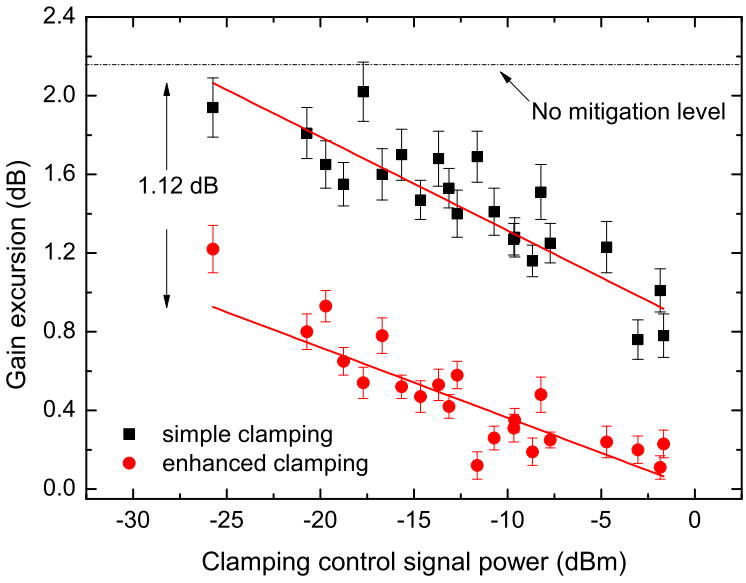

Figure 5.34: Packet gain excursion as function of control signal power. Continuous lines are linear fits. (squares) - Simple clamping, adjusted *r* square= 0.79; (circles) enhanced clamping, adjusted *r* square = 0.73. The dashed line stands for the gain excursion level for the unclamped situation.

The clamping effect is also visible in the Q-factor that exhibits an improvement with the control signal power. These results are displayed in Figure 5.35, where the Q-factor as function of the control signal power is plotted for simple clamping and enhanced clamping.

On looking at the results, we verify that the simple clamping shows two distinct regimes. The first one, observable for low powers (until -15.7 dBm), demonstrates that the Q-factor remains stable and the clamping is not assessable. However, from that power value the Q-factor starts to grow linearly with the clamping control signal power. The interpretation of this behavior is based on the idea that, bellow

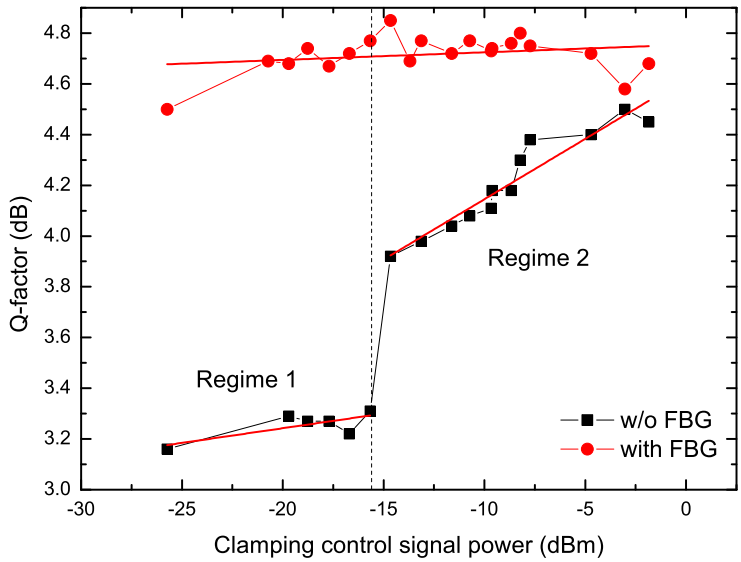

Figure 5.35: Q factor at the receiver as a function of the clamping control signal power. (squares) - Simple clamping and (circles) enhanced clamping. The dashed line stands for the Q-factor level for unclamped situation.

a predefined value of power, the effect of the clamping signal is negligible. Above this value, the clamping has an effect on decreasing the gain excursion and the Q-factor increases. The same behavior is not observable for the enhanced clamping in which the Q factor remains almost constant with an average value of 4.71 dB in the range of the inputted control powers. By decreasing the gain excursion over a threshold value the Q-factor was definitely increased. It must be noted that, the use of the FBG was able to improve the Q-factor to a value close to that of back-to-back values.

The dynamics in terms of gain excursion are determined by the packet duration and idle times. By increasing idle times, the EDFA restores the initial conditions more effectively and thus the gain excursion on the next packet envelope that income the EDF is larger. By increasing the packet duration, the depletion effect on the excited Erbium ions population is also more significant. If the system is not given enough time to restore the initial conditions, the next incoming packet will experience less gain and consequently less gain excursion. So, the results in terms of gain excursion are a combination of these factors. However, the exponential dependency of the filling and depletion effects of the Erbium excited state population impose a stabilization effect [43] so asymptotic behaviors can be settled.

Hence, although, the method was analyzed by considering a specific situation of packet and idle times, it is expected that the results complying other traffic characteristics will only differ in terms of the necessary clamping powers. Thus, the

mitigation technique can be seemingly extrapolated to different types of packet traffic.

5.4.4 Transmission at 10 Gb/s

In this work, we assess the dynamic effect of adding/dropping channels in a 30 km, 10×10 Gb/s WDM system using a hybrid Raman/EDFA amplification scheme. To reproduce the addition and dropping, the channels power function is given by a square wave with low frequency. The hybrid amplification scheme is composed by a multi-backward pumped Raman amplifier and an EDFA acting as preamplifier [54].

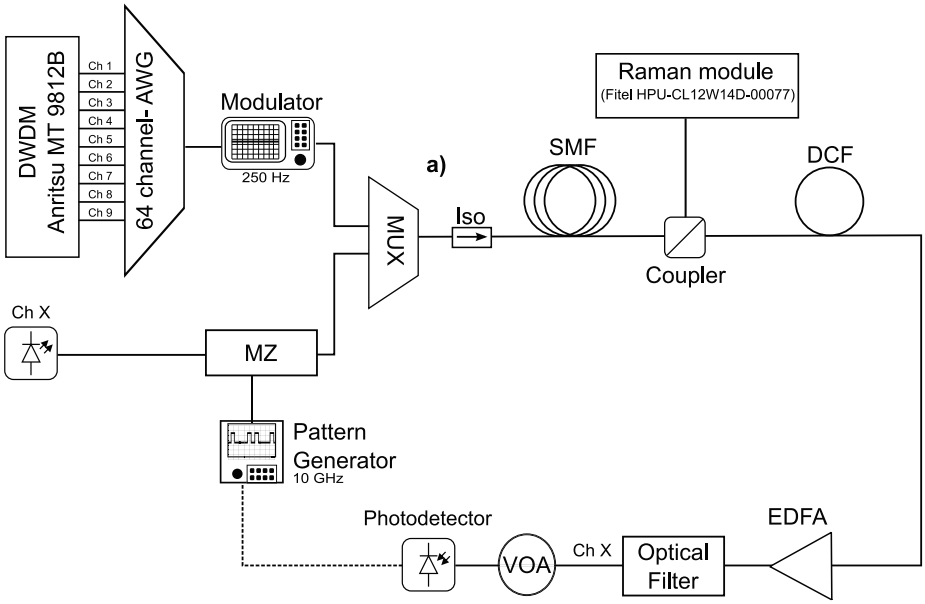

Figure 5.36: Scheme of the implemented experimental setup.

The experiment follows the setup depicted in Figure 5.36. Channel X (test channel) is provided by a tuneable laser (Net Test Tunics) centred at 1546.71 nm with an input power of 5 dBm, whereas the other DWDM channels are provided by nine DFB lasers (Anritsu MT 9812B) comprised between 1547.72 nm and 1554.15 nm (100 GHz spaced) and with an input power equal to 9.3 dBm. Each channel is followed by a polarization controller with attenuator. The test channel is modulated at 10 Gb/s, while the nine channels are modulated at 250 Hz by two Mach-Zehnder external modulators (Fujitsu FTM+174M-5208-J155). The imposed modulation is a pseudo random bit (PRBS) sequence of length $2^{33} - 1$, provided by a pattern generator (Anritsu MP1761B). The 10 channels are then coupled and injected into the 30 km of SSMF fiber. The polarizations of the channels as well as the bias voltage of the modulators were adjusted to keep all the channels approximated with the same optical power and signal to noise ratio, measured before the coupler. An isolator was placed after the coupler to protect the signal lasers from the backward propagated high-power Raman pumps. The Raman

pump module (Fitel HPU-CL12W14D-00077) was placed after the transmission fiber and has a total of 14 pump diode lasers, [1410.0, 1410.2, 1416.9, 1417.3, 1452.1, 1458.1, 1465.5, 1472.6, 1494.8, 1502.4 nm] with a maximum pumping power of 1.175 W. The power of each laser was tuned individually to keep the spectral gain region equalized.

To prevent the effect of chromatic dispersion on channel X a negative dispersion fiber module (11268 m) was used before the receiver, this fiber length compensate completely the dispersion of the SSMF link. In this scenario, the fiber attenuation is controlled by the Raman amplifier module and the chromatic dispersion is compensated by the additional fiber. The receiver is composed by an EDFA, a filter centred in the channel X, a photodetector and an error detector (Anritsu MP1762A). The signal electric and optical signals at the receiver were analyzed using an oscilloscope (Agilent Infinium 86100A) and an Optical Spectrum Analyzer (OSA Advantest 8384), respectively. After the optical filter a tunable attenuator (VOA) was inserted, to change the optical power injected into the receiver. The considered acquisition time for the BER measurement was 30 s, resulting in a BER floor of 10^{-13}. Each BER measurement was repeated three times and an average value was estimated. Initially, we identify an error free regime (BER <10^{-12}) and then successively decrease the output power, using the attenuator, to obtain lower BER values. To appraise

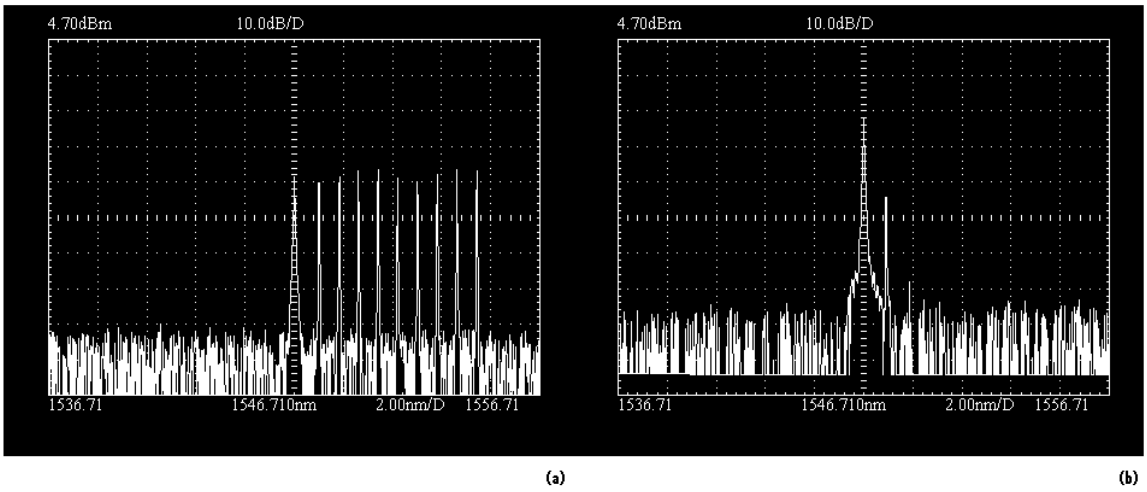

Figure 5.37: Optical spectrum at the output of (a) the negative dispersion fiber and (b) the receiver. The vertical and horizontal scales are 10 dB/div and 2.00 nm/div, respectively.

the impact of the addition and the dropping of channels, we set initially all the nine channels on and then turn them off with the test channel always kept active. In the off situation, only the test channel is amplified and consequently the transience because of the other channels is not present. With the nine channels, the effect of transience on the test channel is observed since the low frequency modulation reproduce the behavior of the addition and dropping of channels in the system. The back-to-back

measurement was also accomplished.

The optical spectra obtained at the DCF fiber output, and the photodiode input are displayed in Figure 5.37. These images show that the 10 DWDM channels are equalized in terms of optical power. However, in the receiver is observed the channel X and also a secondary peak not completely eliminated by the optical filter but with a 25-dB suppression.

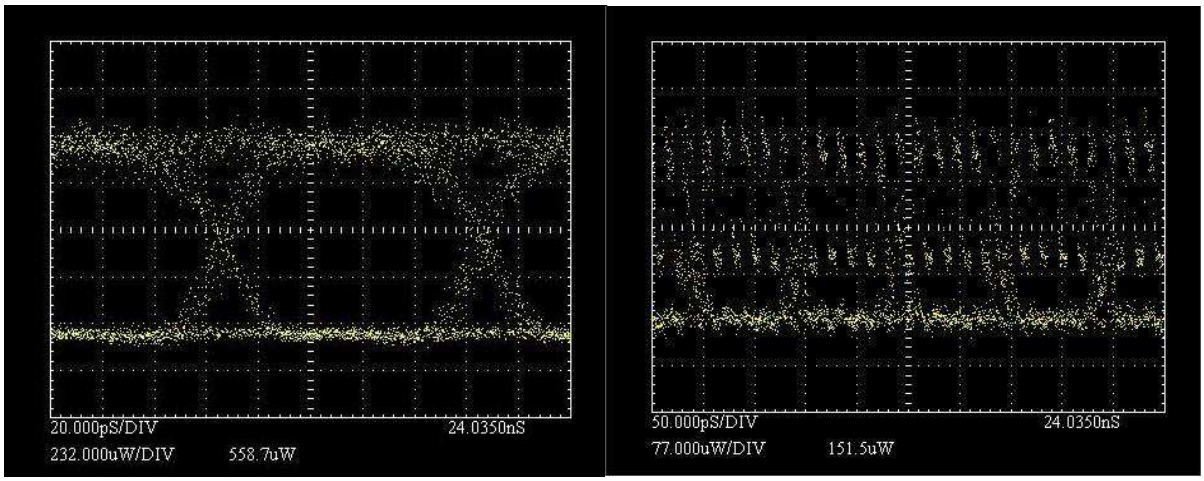

Figure 5.38: Eye diagram at the receiver when all the low frequency modulated channels are (left) off and (rigth) on.

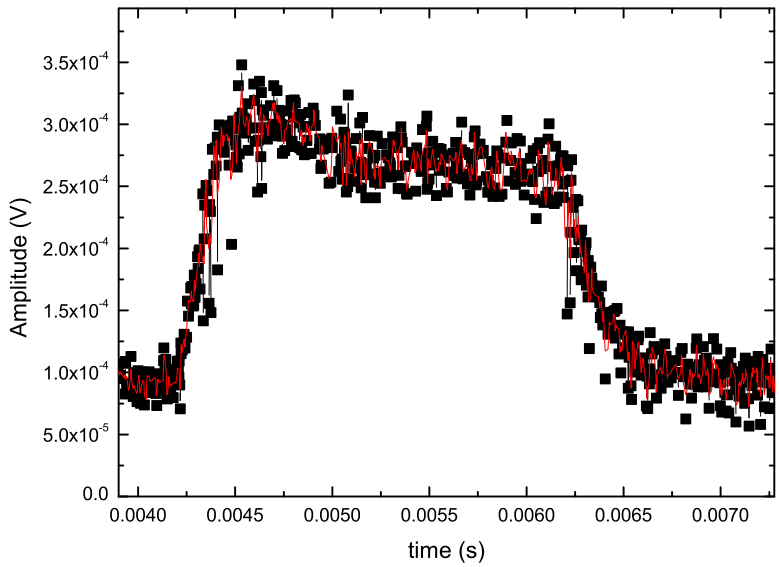

Figure 5.39: Signal pattern, of the test signal, in the presence of add/drop function. The vertical scales are arbitrary.

The eye diagrams at the receiver output obtained with the low frequency modulated channels off and on are depicted in Figure 5.38. The test signal pattern in the presence of the low frequency modulated channels is also depicted in Figure 5.39. The osciloscope image file was edited and smoothed using the Savitzky-Golay method. The transient effect is clearly visible. The results concerning the BER measurements as a function of the received power are shown in Figure 5.40. From these results, it is noticeable that the power penalty for a BER of 10^{-9} is 8 dB. It is also noticeable that the back to back curve and the channels off curve are coincident. In the latter situation, we can conclude that the transmission channel do not introduce any power penalty at this bitrate. However, with the add/drop of channels, the observed penalties are due to the inexistence of power transients. Those transients will enhance the degradation imposed by nonlinearities and amplified spontaneous emission. In the worst case scenario with 9 drop-add channels, the power increase due to channel dropping, degrades the performance of surviving channel because of self-phase modulation in single mode fiber. The channel re-adding will result in the degradation of all the channels because of cross-phase modulation and four-wave mixing, which is enhanced when the chromatic dispersion is compensated.

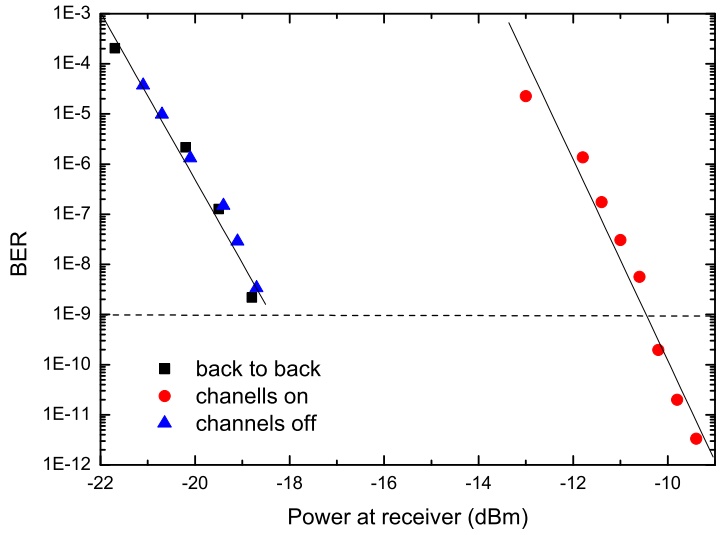

Figure 5.40: BER versus the optical power at the receiver. The squares represent the back-to-back, circles represent all the channels on and triangle shown the situation where only channels X is on. Lines are guides for the eyes.

A second experiment was carried on at 10 Gb/s in order to assess the impact of single channel Raman transients on the system performance [55].

The signal emitted by the tuneable laser (NetTest Tunics) is centred at 1546.71 nm with input power equal to 10 dBm. The receiver is composed by a packet receiver,

an error detector (Anritsu MP1704A), a demultiplexer (Anritsu MP1802A) and an oscilloscope (Agilent Infinium 86100A). The bit data are generated at 9.95328 GHz. A packet with a 192 bits header (Preamble: 64, Frame: 64 and Sequence field size: 64), a 8840 bits payload and a gap length with 524288 bits (that corresponds to approximately to 53 μs) is generated. The transmission medium is a SSMF fiber - two different spans were used with 29425 m (fiber1) and 28816 m (fiber 2) respectively. The Raman module (Fitel HPU-CL12W14D-00077) was used with the 14 lasers on maximum power (1.2 W) and 11268 m a negative dispersion fiber was included to prevent the penalties dues to chromatic dispersion. The patterns of the packet and eye diagram visualized on the oscilloscope at the end of transmitter and the receiver for each fibre are depicted in Figure 5.41.

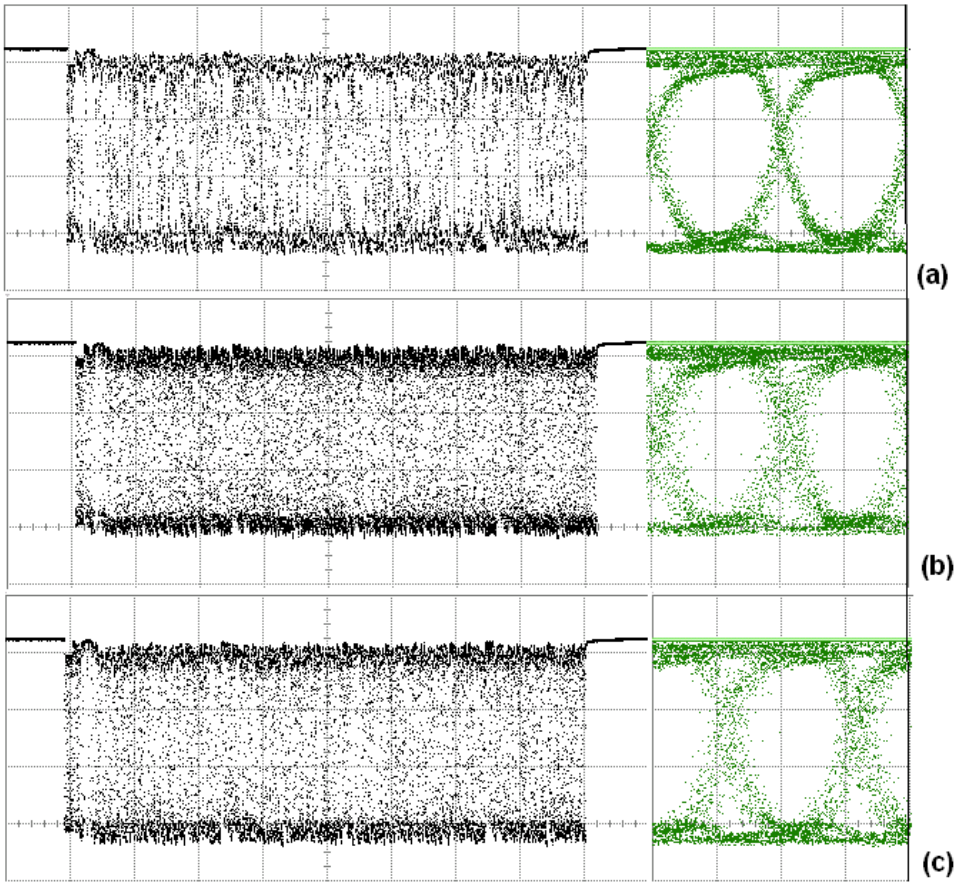

Figure 5.41: Pattern and eye diagram at the end of the: (a) Tx, (b) Rx with fiber 1 and (c) Rx with fiber 2.

To obtain the BER curves as a function of the power at the receiver an attenuator (Agilent 8156A) was added to the experimental scheme. The power penalties obtained for both fibers are approximately equal to 2.42 dB, as displayed in Figure 5.42.

The results obtained from this experiment infer that contrarily to EDFA that were characterized, Raman amplification did not present any power transients.

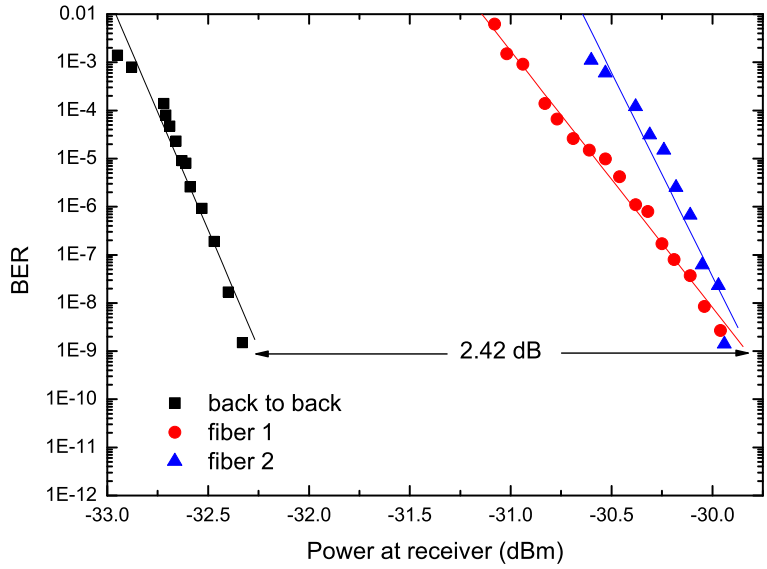

Figure 5.42: BER curves for back to back, fiber 1 and fiber as a function of the power at receiver.

However, both theory and experiments have demonstrated that a single channel Raman amplifier can exhibit transients under saturation conditions [22]. Therefore, we can conclude that the tested Raman amplifier was still unsaturated, despite the high amount of injected pumping power.

We will now return to the WDM ring part the SARDANA network and analyze hybrid Raman/EDFA amplification schemes for transmission at 10 Gb/s. The scenario studied is simular to the one described in section 5.3. WDM ring 80 km long with 8 equally spaced nodes conceived for rural scenario in normal operation mode. In the central office (CO), a bidirectional laser emitting at 1480 nm is used to pump 16 channels spaced by 400 GHz (8 C band + 8 L band) comprised between 192.5 THz to 186.3 THz. The channels leave the central office with 0 dBm of optical power. The transmission has accounted for that the bypass losses are 0.53 dB for channels and 1.01 dB for the pump, being the attenuation of channels and pump are 0.20 dB/km and 0.25 dB/km, respectively. The channels drop losses are 3 dB. In the above described frame, two situations are analyzed, one with Raman amplification and the other with a hybrid amplification scheme composed by in line EDF with Raman. Hence, an optimized span of Erbium Doped Fiber (EDF) is inserted in the mid length of each link according to the dropping channels powers. This procedure was performed with total pumping power equal to 1 W (500 mW in each direction). The results are compared in terms of gain ripple and total amount of EDF span, being their suitability for practical PON analyzed [56].

The 16 analyzed channels with the exception of the last two rely on the maximal

bandwidth of Raman gain efficiency; see Figure 5.43 where the Raman gain efficiency spectrum is plotted for a SSMF pumped at 1480 nm, being the C and L channels represented by black and red arrows, respectively.

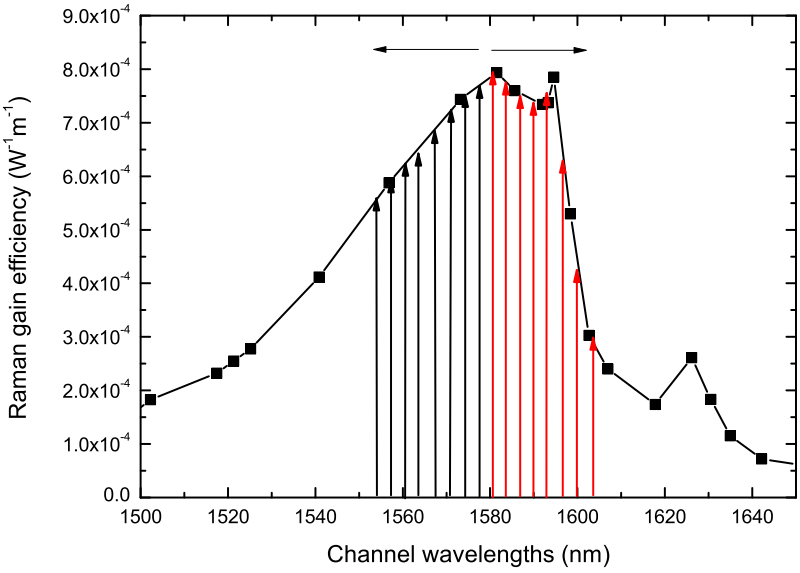

Figure 5.43: Raman gain efficiency for pumping at 1480 nm. The channels are represented by arrows (black-C band and red-L band). The curve was obtained by interpolation of experimental data [57].

The strategy followed for the optimization is the following: (i) drop the channels with the higher gain firstly to settle a maximal gain level and decrease the effect of pump depletion, (ii) whenever the channel power reduction surpasses a predefined value, try several span of EDF fiber in the mid-link to minimize the gain ripple. This method is simple because it is based on the optimization of only one variable, the EDF length. The Raman amplification is maximized in the first links by the settings on the dropping order.The obtained optimized results were also compared with simple Raman amplification. The simulation is based on the implementation of Raman propagation equations [33] and the Saleh [37] model for EDFA using the semi-analytical average power analysis method [58] [38]. This method enables us to obtain quick and accurate solutions.

The optimal dropping order is listed in table 5.4, which corresponds by dropping firstly the channels in the maximal Raman gain efficiency and then move outwardly, as assigned in Figure 5.43. The results for total pumping at 1 W (500 mW for each direction) are depicted in Figure 5.44. The top graph displays the power after dropping spectra for optimized hybrid Raman/in line EDFA and simple Raman, being the middle graph the optimized EDF span and their position in the ring (in relation

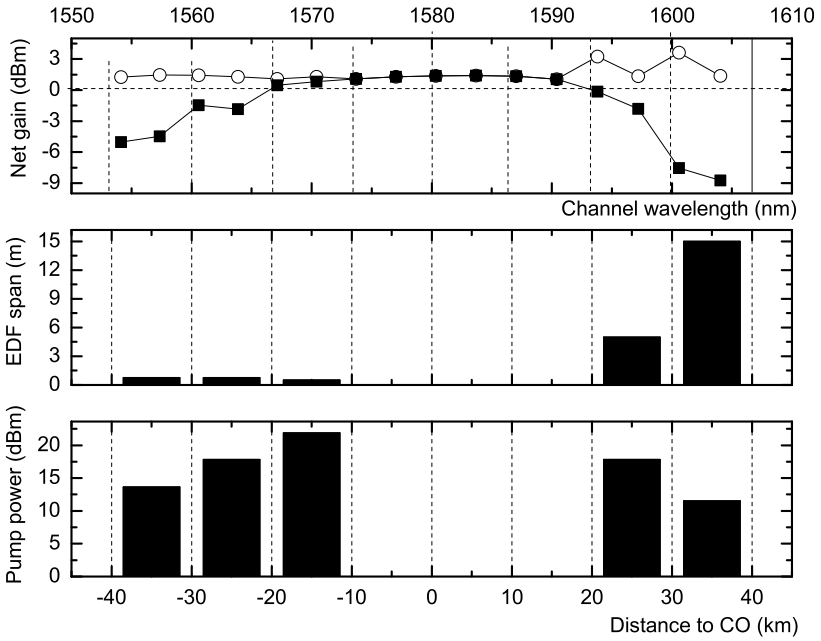

Figure 5.44: (Top)- Net gain dropping spectrum after dropping. Squares- simple Raman. Circles- optimized hybrid Raman/ in line EDFA. The horizontal dashed line settles a detection threshold. (Middle)- Optimized spans of EDF and their positions along the ring. The vertical dashed lines are used to place the dropped channel wavelength along the ring. The total pump power is equal to 1 W. (Bottom) - Available power to pump the EDF along the ring.

to the central office CO). The bottom graph displays the power available to pump the spans of EDF. On looking at the simple Raman results, we verify that just by choosing a dropping order compliant with the maximal Raman gain efficiency, the power is considerably flat in the [1567-1590] nm range and then decreases as the channels wavelength move away from the maximal gain efficiency. On those aparted links, the insertion of span of EDF fiber is able to increase to power above the 0 dBm threshold. It must be noted that in order to provide gain in L band higher spans of EDF are used. On looking at the pump power results, we notice that due this methodology, the available pump power in distant links is still high enough to pump the EDF spans. Hence, in the hybrid approach a total span of EDF equal to 22 m is used (2 m for C band amplification and 20 m for L band amplification) to attain a ripple of 2.54 dB over a bandwidth of 50 nm.

5.5 Chapter summary

This chapter described the work that was carried out concerning applications of optical amplifiers in access networks. It starts with an overview of passive optical networks, namely their principles of operation and transmission techniques (TDM-PON, WDM-PON). The topic of extended reach PONs is also addressed, presenting state of the art achievements and research challenges. Hybrid WDM/TDM PONs, such as SARDANA used to metro and access are then presented and discussed. We remark that most of the work developed in the frame of this chapter was planned for this kind of architecture. Although SARDANA was initially planned for operation in the C band, the possibilibity of extending the transmission to L band in C+L applications is discussed and amplification issues are analyzed. By implementing simple Raman amplification for the WDM ring part of the SARDANA network, it was concluded that this amplification scheme was not suitable for C+L transmission. Thus, hybrid Raman/EDFA amplification was considered.

The second part of this chapter is about hybrid amplifiers. An introduction to EDFA theory is presented. Their numerical implementation and dynamical behaviour is also approached. Since the upstream traffic in SARDANA network is bursty/packeted, issues related to the used of amplifiers, Raman, EDFA and both are studied. Experimental work was carried on to evaluate their impact, and, for EDFA, dynamic behaviour was inferred from the theory. Besides that, mitigation techniques based on optical clamping were presented and implemented experimentally. The chapter ends with an analysis on 10 Gb/s transmission systems, where the impact of combined Raman/EDFA transients are assessed on system the performance. Hybrid amplification is also addressed for the WDM ring of SARDANA and an optimization strategy is presented to optimize the channel gain in an extended C+L band transmission scenarios.

References

[1] J. Lazaro, J. Prat, P. Chanclou, G. Tosi Beleffi, A. Teixeira, I. Tomkos, R. Soila, and V. Koratzinos, "Scalable extended reach pon," in *Optical Fiber communication/National Fiber Optic Engineers Conference, 2008. OFC/NFOEC 2008. Conference on*, 24-28 2008, pp. 1 –3.

[2] H. Ueda, K. Okada, B. Ford, G. Mahony, S. Hornung, D. Faulkner, J. Abiven, S. Durel, R. Ballart, and J. Erickson, "Deployment status and common technical specifications for a B-PON system," *IEEE Communications Magazine*, vol. 39, no. 12, pp. 134–141, 2001.

[3] M. McGarry, M. Maier, and M. Reisslein, "Ethernet PONs: a survey of dynamic bandwidth allocation (DBA) algorithms," *IEEE communications magazine*, vol. 42, no. 8, pp. S8–15, 2004.

[4] A. Cauvin, J. Brannan, and K. Saito, "Common technical specification of the G-PON system among major worldwide access carriers," *IEEE Communications Magazine*, vol. 44, no. 10, pp. 34–40, 2006.

[5] C. Lee, W. Sorin, and B. Kim, "Fiber to the home using a PON infrastructure," *Lightwave Technology, Journal of*, vol. 24, no. 12, pp. 4568–4583, 2006.

[6] J. H. Lee, K. Lee, S. B. Lee, and C. H. Kim, "Extended-reach wdm-pon based on cw supercontinuum light source for colorless fp-ld based olt and rsoa-based onus," *Optical Fiber Technology*, vol. 15, no. 3, pp. 310 – 319, 2009.

[7] C.-H. Lee, W. V. Sorin, and B. Y. Kim, "Fiber to the home using a pon infrastructure," *Lightwave Technology, Journal of*, vol. 24, no. 12, pp. 4568 –4583, dec. 2006.

[8] D. Gutierrez, K. S. Kim, F.-T. An, and L. G. Kazovsky, "Success-hpon: Migrating from tdm-pon to wdm-pon," in *Optical Communications, 2006. ECOC 2006. European Conference on*, 24-28 2006, pp. 1 –2.

[9] C. Bock, J. Prat, and S. D. Walker, "Hybrid wdm/tdm pon using the awg fsr and featuring centralized light generation and dynamic bandwidth allocation," *J. Lightwave Technol.*, vol. 23, no. 12, p. 3981, 2005.

[10] G. Talli and P. Townsend, "Hybrid DWDM-TDM long-reach PON for next-generation optical access," *Journal of Lightwave Technology*, vol. 24, no. 7, p. 2827, 2006.

[11] P. Iannone, K. Reichmann, C. Doerr, L. Buhl, M. Cappuzzo, E. Chen, L. Gomez, J. Johnson, A. Kanan, J. Lentz, and R. McDonough, "A 40gb/s cwdm-tdm pon with a cyclic cwdm multiplexer/demultiplexer," in *Optical Communication, 2009. ECOC '09. 35th European Conference on*, 20-24 2009, pp. 1 –2.

[12] R. Davey, D. Grossman, M. Rasztovits-Wiech, D. Payne, D. Nesset, A. Kelly, A. Rafel, S. Appathurai, and S. Yang, "Long-reach passive optical networks," *Lightwave Technology, Journal of*, vol. 27, no. 3, pp. 273–291, 2009.

[13] I. Tafur Monroy, R. Kjær, F.
"Ohman, K. Yvind, and P. Jeppesen, "Distributed fiber Raman amplification in long reach PON bidirectional access links," *Optical Fiber Technology*, vol. 14, no. 1, pp. 41–44, 2008.

[14] B. Zhu and D. Nesset, "GPON reach extension to 60 km with entirely passive fibre plant using Raman amplification," *Proceedings-ECOC 2009*, 2009.

[15] K. Lee, J. Riding, A. Tran, and R. Tucker, "Extended-reach gigabit passive optical network for rural areas using distributed raman amplifiers," in *Optical Fiber Communication - incudes post deadline papers, 2009. OFC 2009. Conference on*, 22-26 2009, pp. 1 –3.

[16] J. H. Lee, Y.-G. Han, S. B. Lee, and C. H. Kim, "Raman amplification-based wdm-pon architecture with centralized raman pump-driven, spectrum-sliced erbium ase and polarization-insensitive eams," *Opt. Express*, vol. 14, no. 20, pp. 9036–9041, 2006. [Online]. Available: http://www.opticsexpress.org/abstract.cfm?URI=oe-14-20-9036

[17] M. Maeda, "Operations and management of WDM optical networks," in *Optical Fiber Communication Conference*, vol. 2, 1996.

[18] M. Karásek and M. Menif, "Channel addition/removal response in Raman fiber amplifiers: modeling and experimentation," *Lightwave Technology, Journal of*, vol. 20, no. 9, pp. 1680–1687, 2002.

[19] P. Krummrich and M. Birk, "Experimental investigation of compensation of Raman-induced power transients from WDM channel interactions," *IEEE Photonics Technology Letters*, vol. 17, no. 5, 2005.

[20] C.-J. Chen and W. S. Wong, "Transient effects in raman optical amplifier," in *Optical Amplifiers and Their Applications*. Optical Society of America, 2001, p. OMC2. [Online]. Available: http://www.opticsinfobase.org/abstract.cfm?URI=OAA-2001-OMC2

[21] C.-J. Chen and W. Wong, "Transient effects in saturated raman amplifiers," *Electronics Letters*, vol. 37, no. 6, pp. 371 –373, 15 2001.

[22] A. Bononi, M. Papararo, and M. Fuochi, "Transient gain dynamics in saturated Raman amplifiers," *Optical Fiber Technology*, vol. 10, no. 1, pp. 91–123, 2004.

[23] R. Stolen, J. Gordon, W. Tomlinson, and H. Haus, "Raman response function of silica-core fibers," *J. Opt. Soc. Am. B*, vol. 6, pp. 1159–1166, 1989.

[24] P. Andre, R. Correia, L. Borghesi, A. Teixeira, R. Nogueira, M. Lima, H. Kalinowski, F. Da Rocha, and J. Pinto, "Raman gain characterization in standard single mode optical fibres for optical simulation purposes," *Optica Applicata*, vol. 33, no. 4, pp. 559–574, 2003.

[25] A. Atieh, P. Myslinski, J. Chrostowski, and P. Galko, "Measuring the Raman Time Constant (T_R) for Soliton Pulses in Standard Single-Mode Fiber," *J. Lightwave Technol*, vol. 17, pp. 17–2, 1999.

[26] M. Menif, M. Karasek, and L. Rusch, "Cross-gain modulation in raman fiber amplifier: experimentation and modeling," *Photonics Technology Letters, IEEE*, vol. 14, no. 9, pp. 1261 – 1263, sep 2002.

[27] D. Christodoulides and R. Jander, "Evolution of stimulated raman crosstalk in wavelength division multiplexed systems," *Photonics Technology Letters, IEEE*, vol. 8, no. 12, pp. 1722 –1724, dec. 1996.

[28] J. Ferreira, M. Fugihara, and A. Pinto, "Transient Response and Control of Pump-Reflecting Raman Fiber Amplifiers," *Fiber and Integrated Optics*, vol. 29, no. 1, pp. 44–61, 2010.

[29] B. Neto, R. P. Dionísio, A. M. Rocha, C. Reis, S. Chatzi, F. Bonada, J. A. Lazaro, A. L. J. Teixeira, and P. S. André, "C+l band extended reach next generation access networks through raman amplification: assessment in rural scenario," in *OptoElectronics and Communications Conference, 2010. OECC 2010. 15th*, 5-9 2010, pp. 1 –2.

[30] A. Rocha, B. Neto, M. Facao, and P. Andre, "Low cost incoherent pump solution for Raman fiber amplifier," *Optica Applicata*, vol. 39, no. 2, pp. 287–293, 2009.

[31] B. Neto, A. Teixeira, N. Wada, and P. André, "Efficient use of hybrid genetic algorithms in the gain optimization of distributed raman amplifiers," *Optics Express*, vol. 15, no. 26, pp. 17 520–17 528, 2007.

[32] B. Min, W. J. Lee, and N. Park, "Efficient formulation of raman amplifier propagation equations with average power analysis," *Photonics Technology Letters, IEEE*, vol. 12, no. 11, pp. 1486 – 1488, nov 2000.

[33] S.-K. Liaw, L. Dou, A. Xu, and Y.-S. Huang, "Optimally gain-flattened and dispersion-managed cï£¡+ï£¡l-band hybrid amplifier using a single-wavelength pump laser," *Optics Communications*, vol. 282, no. 20, pp. 4087 – 4090, 2009.

[34] E. Desurvire, *Erbium-doped fiber amplifiers: principles and applications*. Wiley New York, 1994.

[35] C. Giles and E. Desurvire, "Modeling erbium-doped fiber amplifiers," *Lightwave Technology, Journal of*, vol. 9, no. 2, pp. 271–283, 1991.

[36] P. Becker, N. Olsson, and J. Simpson, *Erbium-doped fiber amplifiers: fundamentals and technology*. Academic Pr, 1999.

[37] A. Saleh, R. Jopson, J. Evankow, and J. Aspell, "Modeling of gain in erbium-doped fiber amplifiers," *IEEE Photonics Technology Letters*, vol. 2, no. 10, pp. 714–717, 1990.

[38] T. Hodgkinson, "Improved average power analysis technique for erbium-doped fiberamplifiers," *IEEE Photonics Technology Letters*, vol. 4, no. 11, pp. 1273–1275, 1992.

[39] Y. Sun, G. Luo, J. Zyskind, A. Saleh, A. Srivastava, and J. Sulhoff, "Model for gain dynamics in erbium-doped fibre amplifiers," *Electronics Letters*, vol. 32, no. 16, pp. 1490 –1491, 1 1996.

[40] Y. Sun, J. L. Zyskind, A. K. Srivastava, and L. Zhang, "Analytical formula for the transient response of erbium-doped fiber amplifiers," *Appl. Opt.*, vol. 38, no. 9, pp. 1682–1685, 1999. [Online]. Available: http://ao.osa.org/abstract.cfm?URI=ao-38-9-1682

[41] Y. Sun, G. Luo, J. Zyskind, A. Saleh, A. Srivastava, J. Sulhoff, L. Technol, and N. Holmdel, "Model for gain dynamics in erbium-doped fibre amplifiers," *Electronics Letters*, vol. 32, no. 16, pp. 1490–1491, 1996.

[42] B. Neto, C. Reis, A. Rocha, A. L. J. Teixeira, N. Wada, and P. S. André, "Transience response of traffic based on optical packets with optical amplifiers," in *Networks and Optical Communications, 2009. NOC '09. 14th European Conference on*, vol. 1, June 2009, pp. 545–550.

[43] A. Bononi and L. Rusch, "Doped-fiber amplifier dynamics: A system perspective," *Lightwave Technology, Journal of*, vol. 16, no. 5, pp. 945–956, 1998.

[44] B. Pedersen, B. Thompson, S. Zemon, W. Miniscalco, and T. Wei, "Power requirements for erbium-doped fiber amplifiers pumped in the800, 980, and 1480 nm bands," *IEEE Photonics Technology Letters*, vol. 4, no. 1, pp. 46–49, 1992.

[45] C. Reis, B. Neto, R. Dionisio, G. Incerti, G. Tosi-Beleffi, D. Forin, A. Rocha, A. Teixeira, and P. Andre, "Transience analysis of bursty traffic with erbium doped fiber amplifiers," in *Transparent Optical Networks, 2009. ICTON '09. 11th International Conference on*, june 2009, pp. 1 –3.

[46] Y. Fukada, K.-I. Suzuki, H. Nakamura, N. Yoshimoto, and M. Tsubokawa, "First demonstration of fast automatic-gain-control (agc) pdfa for amplifying burst-mode pon upstream signal," in *Optical Communication, 2008. ECOC 2008. 34th European Conference on*, 21-25 2008, pp. 1 –2.

[47] Y. Awaji, H. Furukawa, N. Wada, E. Kong, P. Chan, and R. Man, "Guidelines for amplification of optical packets in WDM environment regarding impact of

transient response of erbium-doped fiber amplifier," *Computer Networks*, vol. 52, no. 10, pp. 2087–2093, 2008.

[48] Y. Awaji, H. Furukawat, N. Wada, P. Chan, and R. Man, "Mitigation of transient response of erbium-doped fiber amplifier for burst traffic of high speed optical packets," in *Lasers and Electro-Optics, 2007. CLEO 2007. Conference on*, 2007, pp. 1–2.

[49] G. Sacchi, S. Sugliani, A. Bogoni, F. Di Pasquale, R. Di Muro, R. Magri, G. Bruno, and F. Cavaliere, "Design and experimental characterization of edfa-based wdm ring networks with free ase light recirculation and link control for network survivability," *Lightwave Technology, Journal of*, vol. 23, no. 3, pp. 1170 – 1181, march 2005.

[50] B. Puttnam, Y. Awaji, and N. Wada, "Supplementary transient suppression in a burst-mode edfa using optical feedback," in *OptoElectronics and Communications Conference, 2009. OECC 2009. 14th*, 13-17 2009, pp. 1 –2.

[51] M. Karasek, M. Menif, and L. Rusch, "Output power excursions in a cascade of edfas fed by multichannel burst-mode packet traffic: experimentation and modeling," *Lightwave Technology, Journal of*, vol. 19, no. 7, pp. 933 –940, jul 2001.

[52] T.-T. Huang, L.-G. Sheu, and S. Chi, "All-optical gain-clamped erbium-doped fiber amplifier using a dwdm demultiplexer," in *OptoElectronics and Communications Conference, 2009. OECC 2009. 14th*, 13-17 2009, pp. 1 –2.

[53] S. Harun and H. Ahmad, "L-band erbium-doped fibre amplifier with clamped- and flattened-gain using fbg," *Electronics Letters*, vol. 39, no. 17, pp. 1238 – 1240, 21 2003.

[54] B. Neto, J. Ferreira, N. Wada, A. Pinto, and P. André, "Evaluation of the effect of channel add/drop impact on power transients on the performance of a 10-GB/S DWDM transmission system with hybrid EDFA/Raman amplification," *Microwave and Optical Technology Letters*, vol. 52, no. 6, pp. 1225–1228, 2010.

[55] B. Neto, C. Reis, A. Rocha, J. P. Girão, R. P. Dionísio, , S. Chatzi, F. Bonada, J. Lazaro, J. A. and, and A. L. J. Teixeira, "Impact of transient response of optical amplifiers operating with burst traffic," in *7th Conference on Telecommunications, 2009. Conftele '09.*, vol. 1, May 2009, pp. —.

[56] B. Neto, A. Rocha, J. P. Girão, R. P. Dionísio, C. Reis, S. Chatzi, F. Bonada, J. A. Lazaro, A. L. J. Teixeira, and P. S. André, "C+l band gain equalization for extended reach wdm-ring pon using hybrid raman/in line edfa amplification," in *Transparent Optical Networks, 2010. ICTON '10. 12th International Conference on*, vol. 1, June 2010, pp. 136–139.

[57] M. Fugihara and A. Pinto, "Low-cost Raman amplifier for CWDM systems," *Microwave and Optical Technology Letters*, vol. 50, no. 2, pp. 297–301, 2008.

[58] B. Min, W. Lee, and N. Park, "Efficient formulation of Raman amplifier propagation equations with average power analysis," *IEEE Photonics Technology Letters*, vol. 12, no. 11, 2000.

Chapter 6

Conclusions

6.1 Conclusions

This thesis has provided a survey of applications of Raman fiber amplifiers in the context of modern communications. Two general topics were addressed:

1. the development of an efficient simulator for Raman amplified links and an optimization algorithm for multipump allocation to obtain enlarged and equalize gain in WDM transmission systems.

2. the use of Raman amplification alone and in hybrid combinations with EDFA in metro and access networks and decurrent dynamic effects.

Concerning the first topic, several issues were surpassed, namely the difficulties associated to mathematical description of Raman amplifiers, a boundary value problem with non-linear ordinary differential equations. Although, several numerical approaches are already known in the litterature to solve this kind of problems, Raman equations present some drawbacks that disable the use of traditional solvers. It was mentioned earlier that simple shooting methods fail due to the instability of the Raman equations with initial conditions. Therefore, the work developed in this thesis began with a study of numerical methods for non-linear ordinary differential equation with boundary value conditions. It was demonstrated that modified shooting and collocation method were suitable approaches but a simulator could benefit from the use of semi-analytical method in terms of efficiency. Thus, the average power analysis was implemented together with an optimization routine for backward or bidirectional pumping architecture. Our mathematical study proceed with the a stability analysis of critical points in order to determine the asymptotic behabiour of Raman equations. It was shown that the only critical point with physical significance is the origin and that this point is a node asymtotically stable. The same conclusion was also obained using Lyapunov second method. A geometrical interpretation of this result is assessible from the representation of solutions trajectories on the phase portrait.

One objective of this thesis is to provide broadband and equalized solutions for the data signals gains. It is known from Raman theory that the use of multipump schemes in both forward and/or backward configurations is able to accomplish this goal as

long as the pumping parameters (powers and wavelengths) are adjusted. Hence, an optimization algorithm to accomplish this objective is imposed. There are several dificulties arising from this problem, namely the ones derived from the multivarible optimization. Aware of this issue, our first approach was to use an heuristic and genetic algorithm was a good candidate because of its robustness and ability to obtain solutions on multivariable, multiobjective problems with constraints. The issues of this method is the required computational effort to obtain solutions, so for the purpose of our problem they can be obtained in a timescale superior to the one needed for networks reconfiguration. To surpass this impediment, we first dimensioned the genetic algorithm in terms of operators (selection, crossover and mutation) and population size to increase its efficiency in solving our problem. Selection itself is a very important operator because it decides how fast the solutions converge to a solution. Stochastic uniform, that we tried to prove to be the more the more efficient selection method for our problem , mimics the statistical results expected for population with a high number of individuals, without expense of efficiency. Dispite our efforts in dimensionsing GA, we verify that a hybrid combination with a local search method, such as Nelder-Mead method could increase significantly the efficiency while keeping the accuracy of the solutions. Thus, using the two methods together, the advantages of both are combined: the convergence of GA and the high accuracy of Nelder-Mead. Dispite that, it was also demonstrated that by chosing properly the rigth moment to switch from one method to the other could also increase the effeciency of the algorithm. For the particular problem of a 5 backward pumped Raman amplifier with 16 data signals speach over a bandwidth of 50 nm, the GA was switched to Nelder-Mead after 17 generations were evolved. This coresponds to a solution obtained in half the time that would be necessary if the hybrid method were run in a normal way. The attained gain ripple was 0.17 dB.

The second part of this thesis is focused on Raman amplication in metro and access networks. The studied applications were focused on a specific network architecture, the hybrid WDM/TDM PON SARDANA network in rural scenarios, where longer distance links are used. Due to the network features, hybrid Raman/EDFA was considered in the WDM ring in order to enhance the gain bandwidth enabling possible solutions in the C+L spectral bands. Thus, several amplification strategies were tried in order to extend the bandwidth to C+L and have an equalized gain of the dropped channels.It was verified that the optimization of the channels dropping order and span lengths of EDF is a good approach for the gain equalization and an optimization strategy was proposed.

The use of amplifiers in WDM ring or remote nodes brings additional issues decurrent from the dynamics effect on amplifiers. The latter arise from the add/drop of channels and the use of bursty traffic in the upstream direction. These effects can be very detrimental, especially in EDFA that have longer timescales. Thus, the

dynamics effects of amplifiers, EDFA, Raman amplifiers and hybrid schemes of both were studied and characterized experimentally for burst mode transmission in the context of WDM/TDM PON. Two mitigation solutions based on optical gain clamping were also proposed. The first one, using the saturation feedback signal reflected on a FBG and the second one using bidirectional CW clamping as an enhanced method. Transients in 10 Gb/s WDM ring PON using Raman/EDFA amplification were also studied experimentally being their impact on the system performance assessed quantitatively.

6.2 Directions for future work

The research topics approached in this thesis are important and the obtained results relevant, but some subjects could be explored more thoroughly. Thus, from this work, several investigations can be conducted.

Regarding the topic of the simulation of Raman propagation equations, our attention was focused on numerical or semi-analytical methods. However, analytical approaches could provide deeper insigths on the solutions dependency. Thus, methods based on the linearization of the nonlinear part of Raman propagation equations using series such as Adomian decomposition method, could be adopted.

Although the work of this thesis used an optimization strategy based the Genetic algorithm to perform the allocation of pumps, other heuristics or combination of heuristics could be approached, namely particle swarm optimization or ant colony among others. The optimization of hybrid Raman/EDFA amplifiers can also be approached using the method that was proposed in this thesis. In such a situation, EDF lengths could be optimized and the number of Raman pumps could be minimized. This topic is quite open to development because, since EDFA are still used in telecommunication operation, solutions of this kind are potentially economically valuable, especially when bandwidth extension is intended.

The work accomplished in this thesis regarding the optical transient mitigation was thought on schemes that use clamping signal to saturate the EDFA, however, dynamically controlable variable optical attenuators could be used to obtain the same results. This topic was approached in this thesis through a joint interaction with Multitel, Belgium, using a Dynamic Gain Equalizer (DGE) prototype. However, communication issues with the device (only possible by serie port) had disabled dynamic application in smaller timescales.

Studies on analytical description of Raman transients using a derivation analogous to the one devoloped by Sun *et al* would extend significantly the results obtained experimentally, namely for Raman amplified bursts. The latter could also be explored more thouroughly especially under saturation.

Finally, the optimization method suggested for WDM/TDM PON for dowstream

traffic (the equalization of the dropped gain) could be extended for upstream. In this situation, the optimization function could be the OSNR. Thus, a complete optimizer for this particular metro-access network could be achieved.